THE GEOPHYSICAL INSTITUTE OF ISRAEL המכון הגיאופיסי לישראל
P.O.B. 182, LOD 71100, ISRAEL, TEL: 972-8-9785888, FAX: 972-8-9208811 - רח' הבעש"ט 6, לוד
www.gii.co.il

EMPIRICAL DETERMINATIONS OF LOCAL SITE EFFECT USING AMBIENT VIBRATION MEASUREMENTS FOR THE EARTHQUAKE HAZARD AND RISK ASSESSMENT TO QRAYOT-HAIFA BAY AREAS

FINAL REPORT

June, 2006 **Report No 595/064/06**

Principal Investigator:

Dr. Y. Zaslavsky

Collaborators:

T. Aksinenko, M. Gorstein, Dr. A. Hofstetter, M. Kalmanovich, N. Perelman, V. Giller, I. Livshits, D. Giller, G. Ataev, I. Dan, and A. Shvartsburg.

Prepared for
The Steering Committee for
National Earthquake Preparedness and Mitigation

TABLE OF CONTENTS

LIST OF FIGURES

LIST OF TABLES

ABSTRACT

In the framework of a microzoning study of the Haifa Bay and Qrayot areas, which is close to a major seismogenic zone of the Dead Sea Rift, a methodology based on integration of H/V microtremor measurements and 1D linear model using SHAKE is applied in order to characterize seismic behavior of sediments.

Major geological features of the study area include sub-parallel horsts and grabens dissected by faults; the absence of a common reflector for the whole area; the presence of five lithological units, which may be considered as potential local reflector; intermediate hard layers in addition to the main reflector at most of the analyzed sites and overall sediment thicknesses varying from 10 m up to 600 m.

From microtremor measurements conducted at 480 locations in an area of about 50 km^2 horizontal and vertical component spectral ratios are derived. The results show two H/V peaks at frequencies related to resonances of deep and shallow structures. Spatial variations of the frequency (0.5-5 Hz for the first peak and 1-8 Hz for the second peak) and H/V amplitude level (2-3 for the first peak and 2-10 for the second peak) reflecting the geological complexity are shown in four distribution maps.

Limited data on sediment thickness and velocities are available from a few refraction surveys and boreholes. Models based on these data are used to validate H/V ratios at corresponding locations and justified their further utilization, by velocities extrapolation, to study other sites, away from refraction lines and boreholes. There, layer thicknesses are sought, yielding calculated transfer functions to match the observed H/V curves, considering two response peaks. The modeling results are represented graphically in the geological cross sections characterizing the study area. In some cases, these models suggest a revision of existing concepts relating to the subsurface structure in the region.

The evaluated subsurface models are introduced using the SEEH procedure of Shapira and van Eck [(1993) Natural Hazards 8, 201-215] to assess Uniform hazard Site-Specific Acceleration Spectra for different zones within the Haifa Bay and Qrayot areas. These evaluations are very important for realistic assessment of the vulnerabilities of all types of existing and new newly designed structures and for urban and land use planning.

1. INTRODUCTION

The study area including the Qrayot and Haifa Bay shore is one of the most densely populated and developed urban areas in Israel. Several facilities are concentrated here like, Haifa port, airport, large-scale chemical industry and a whole infrastructure system of pipelines containing flammable gas or potentially pollutant liquids, dense populated coastal strip of Haifa city and several relative small towns in its vicinity (Qiryat Bialik, Qiryat Yam, Qiryat Mozkin and Qiryat Haim) with overall inhabitants of about 120,000. In recent time multi-storey buildings, different industrial plants, roads and bridges were constructed over that area.

Qrayot and Haifa bay area are situated along the active Carmel Fault. In August 1984 a magnitude 5.2 earthquake occurred about 10 km east of the study area. Prior to this event, there is no record of earthquakes with magnitudes greater than 5.0 along the Carmel Fault, but it has been suggested (Shapira and Hofstetter, 2002) that this fault is capable of producing earthquakes with magnitude up to 6.5. This important area in terms of inhabitants, economic activity and administration is located close to a major seismogenic zone that constitutes the Dead Sea Rift and its branching faults. Several major historical earthquakes occurred (Fig. 1) during the present millennium (Amiran et al., 1994) in the distance of 50-80 km from the investigated area. So, due to the concentration of population and taking into account the historical seismicity, this region, is considered as high seismic risk zone.

Several well known examples of destructive earthquakes during the last three decades like the Mexico City, 1985 (Singh et al., 1988; Reinoso and Ordaz, 1999), Spitak, Armenia, 1988 (Borcherdt et al., 1989), California, Loma Prieta, 1989 (Hough et al., 1990) and Northridge, 1994 (Hartzell et al., 1996), Kobe, Japan, 1995 (Iwata, et al., 1996), Kocaeli (Izmit), Turkey, 1999 (Ozel et al., 2002) and Algeria, 2003 (Hamdache et al., 2004) have clearly shown that local site conditions are an important factor in determining the seismic hazard specific to a given site. This is particularly important for the Qrayot and Haifa bay area because of the sedimentary basin with strong impedance contrast between the soft sediments and the underlying bedrock. In addition, over the area of study the soil conditions vary significantly from one place to another.

Recently, at the request of various clients, a number of sites in the Qrayot and Haifa bay area have been investigated by us to determine the ground amplification (see for example Zaslavsky et al., 1997, 1998, 2000a, 2003a,b, 2004a,b). We observed amplification factors of 3 to 6 at various frequencies of 0.5 – 5.0 Hz.

The detailed lithological information from boreholes (providing thickness of the sediments), together with available geological, geotechnical and geophysical data, were used to construct multi-layer 1D-models from which the expected response functions are consistent with the observed features of the H/V spectral ratio functions are calculated.

Once a subsurface model is constructed, it is possible to calculate the site response functions and apply the stochastic evaluation approach for earthquake hazard assessment (Shapira and van Eck, 1993), to compute the uniform hazard site-specific acceleration spectra for the different zones of Haifa bay in order to estimate vulnerabilities of all types of structures.

The application of this methodology is very important, especially in this region, where the occurrence of strong earthquakes presents a long return period, but might exhibit a high seismic risk, according to historical reports, population distribution and its socio-economic importance.

2. TECHNIQUES USED FOR EXPERIMENTAL ESTIMATION OF LOCAL SITE EFFECTS

Various empirical techniques for site response estimating were summarized and discussed by Field and Jacob (1995), Kudo (1995), Lachet et al. (1996), Satoh et al. (2001) and others. There can be no doubt that the best evaluation of site effect will be based on dense strong motion observations using spectral ratio of seismic records from sedimentary sites with respect to bedrock reference sites, because the nonlinear effect is included (Jarpe et al., 1988, 1989; Darragh and Shakal, 1991; Satoh et al., 1995; Hartzell, 1998; Reinoso and Ordaz, 1999 and others).

In regions where seismicity is moderate as Israel, recording not only strong ground motion, but even a representative sample of weak earthquakes may take a long time. Additionally, it may be difficult to obtain simultaneous recordings on the sediments and on the hard rock. A proposed alternative is to use records of microtremors.

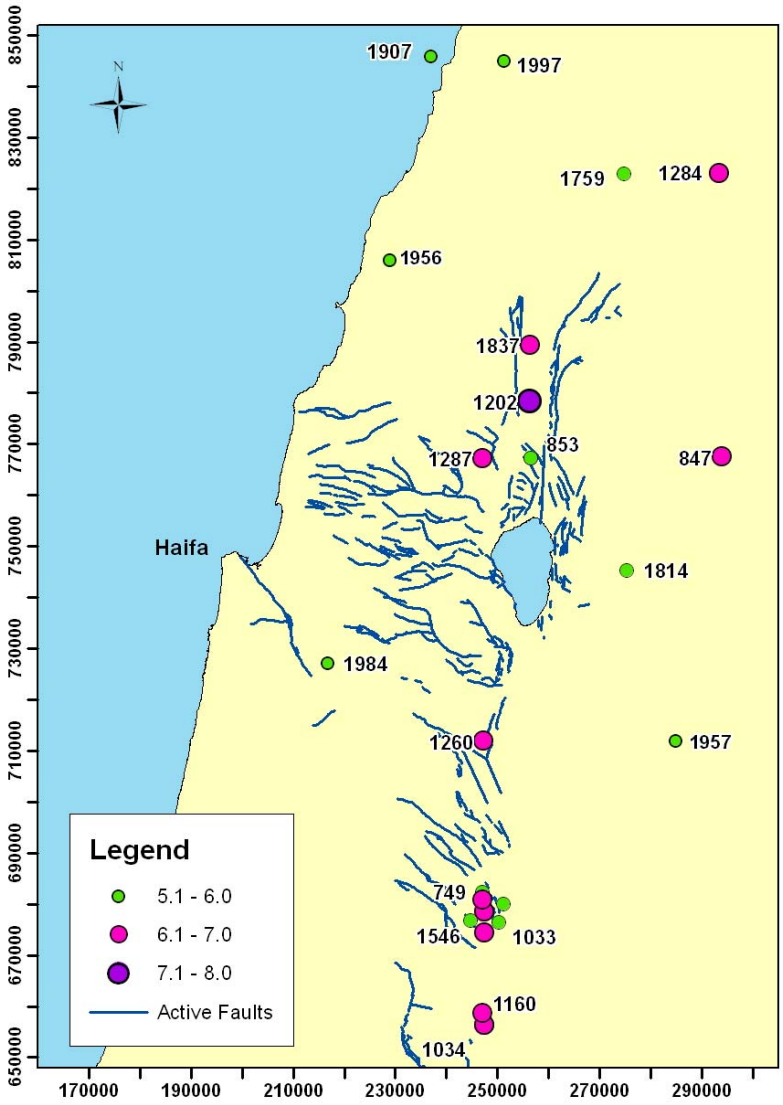

Figure 1. Map of earthquakes (including historical) with magnitude larger than 5.0 at a distance of about 100 km from the area investigated.

Computation of spectral ratios relative to a bedrock reference station widely used to analyze microtremor records with purpose to study site effects. The applicability of high frequency microtremor in site effect studies has been investigated by several studies (Field et al., 1990; Rovelli et al., 1991; Lermo and Chávez-García 1994; Gaull et al., 1995; Zaslavsky et al., 1995, 2005; Ojeda and Escallon, 2000; Horike et al., 2001 and others). However, in urban and suburban areas, microtremors are generated by human activities and intensity of microtremor source may essentially change from place to place. Therefore, this method should be used within limited areas (the distance from the reference station is some hundred meters).

Nakamura (1989) hypothesized that site response could be estimated from the spectral ratio of the horizontal versus vertical components of microtremors observed at same site. Many studies show that the H/V ratio obtained from microtremors coincides with first mode of response function of near surface structures to incident shear wave. The estimation of the amplification of ground motion at resonance frequency using microtremor H/V ratio is controversial, with some authors finding good results while others find significant differences using other methods of site response evaluations. A citation of different literature sources elucidates this problem:

Lermo and Chaves Garcia (1994):

We have applied technique of Nakamura to analyze microtremor records obtained on three cites in Mexico. The results obtained from microtremor measurements were compared with standard spectral ratios of the intense, S-wave part of weak or strong motion records obtained at the same sites. Our results show that microtremor measurements allow for determination of the dominant period of sediment induced amplification with apparently good reliability in the range 0.3 to 5 Hz; with good reliability and rough estimate of amplification level if geological conditions are relatively simple.

Seekins et al. (1996):

This study shows Nakamura's resulting in amplifications that are similar to those derived from the S-wave station-pair ratios.

Malagnini et al. (1996):

The use of microtremors through the application of the Nakamura technique, failed in delineating both the fundamental resonance and the amplification level indicated by the empirical transfer function, equivalent trends were obtained by applying H/V spectral ratios to direct S waves.

Toshinawa et al. (1997):

Weak-motion amplification factors for peak ground acceleration with respect to a rock site correlated well with the peak values of horizontal-to-vertical spectral ratio of microtremors, although there were a limited number of records for some sites, and there was significant scatter in the data. This adds to the growing evidence that the H/V spectral ratio technique can be useful tool for the assessment of ground motion characteristics in alluvia.

Chaves-Garcia and Cuenca (1998):

We show that very coherent results are obtained from different kinds of measurements, and that microtremor records are very useful to interpolate sparse earthquake data.

Mucciarelli (1998):

The set of experiments show that under proper measurement conditions Nakamura's technique provides stable and reliable results, but great care has to be devoted to avoid factors that may significantly and adversely affect the results. It is suitable to use this technique as a low-cost approach to site amplification studies for urban planning and design purposes, provided that great care is devoted to the quality of measurements.

Teves-Costa and Senos (2000):

The application of the Nakamura's technique, using microtremor measurements, is very important, especially in region were big earthquake present a long return period, but which exhibit a high seismic risk, according to historical reports, population distribution and its socio-economic importance.

Enomoto et al. (2000):

H/V spectra from microtremors is much more coincided to the theoretical transfer function due to SH wave propagation in the surface soil layer than the observed transfer function used simultaneous microtremor measurements between the basement and surface.

Mucciarelli and Gallipoli (2004):

Analyzing 608 earthquakes time histories (up to 0.1g) and 1280 triggered noise signals recorded at four different stations, we obtained very similar horizontal-to-vertical spectral ratios for two data sets.

Horike et al. (2001):

The horizontal-to-vertical spectral ratios inferred by the Nakamura method partly reflect site amplification factors, but do not agree with site amplification factors.

Satoh et al. (2001):

In general the frequencies of maximum peaks of H/V ratio for microtremors do not coincide with those of H/V ratios and H/H ratios for S wave. However, if we select H/V ratios with peak frequencies lower than 1 Hz and peak amplitudes larger than three, the peak frequencies of H/V ratios for microtremor roughly coincide with those of H/V ratios for S-wave. Even under these constraints, their amplitudes do not coincide with each other.

Many case studies were devoted to the use of Nakamura's technique for urban microzonation in several cities: Ohmachi et al. (1991) microzonation San Francisco; Alva Hurtado et al. (1991) microzonation of Lima, Kobayashi et al. (1991); microzonation of Mexico City; Peru; Love et al. (1995) microzonation of Adelaide, Australia; Chávez-García at al. (1995) microzonation of Pueblo, Mexico; Ghayamghamian et al. (1995) microzonation of Tehran; Marccellini et al. (1995) Bevento, Italy; Lachet et al. (1996) microzonation of Thessaloniki, Greece; Cardona and Yamín (1997) microzonation of Bogotá, Columbia; Chávez-García and Cuenca (1998) microzonation of Acapulco; Navarro et al. (1998), microzonation of Almeria (Southern Spain); Goulá et al. (1988) microzonation of Barcelona; Ramirez-Centeno (1998) microzonation of Guadalajara, Mexico; Midorikawa (1998) microzonation of Odawara, Japan; Chávez-García and Cuenca (1998); Bouden-Romdhane et al. (2000) microzonation the city of Tunis; Jimenez (2000) mapping soil effects in Barcelona, Spain; Mukhopadhyay et al. (2002) microzonation of Delhi, India; Mirzaoglu, and Dýkmen (2003) microzonation Shin-Yokohama area, Japan; Motamed and Ghalandarzaden (2005) seismic zonation of Bam, Iran.

During the last decade, many sites in Israel have been investigated in an attempt to estimate the possible amplification of the seismic ground motion (Zaslavsky et al., 1995, 2000a,b, 2002, 2003c, 2004a,b, 2005a,b,c; Gitterman et al., 1996; Shapira et al., 2001). All those studies are based on analysing ambient noise and weak motion measurements incorporated with geological and geophysical information about the subsurface. We used various empirical methods to determine the site response functions including reference and non-reference techniques and referring to different sources of excitation – earthquakes, explosions and ambient noise. Most of the studies are based on implementing the so-called Nakamura technique.

However, there are cases where the Nakamura technique failed to yield conclusive results. This often happens when the ratio of the shear-wave velocity of the underlying half space (bedrock) to the shear wave velocity of the soil is smaller than 2 or when we are dealing with a complicated 3D structure of the underlying geology. Other examples are associated with poor excitation of the soil column due to weakness or remoteness of the microtremor sources. In such cases poor performance of the Nakamura method can be foreseen and other methods should be used.

The horizontal-to-vertical spectral ratio technique from microtremor is significantly cheaper than the classical geophysical site investigation, especially in

urban areas. While integrating different types of data from different sources we could use the Nakamura technique to present a systematic picture of the characteristics of the site effects in the investigated region. There is a good agreement between the H/V observations, the subsurface models, the known geological setup and the few geotechnical data. These should add to the credibility of the obtained results. Equally important is a good match between the 1D subsurface models inferred from H/V measurements at nearby grid points. It is definitely the dense grid of measuring sites that eventually enabled us to successfully conclude this microzoning study. We noted that in several cases the Nakamura technique provided estimations of higher harmonics of the soil column resonance.

3. H/V SPECTRAL RATIO TECHNIQUE

Main assumptions of the Nakamura's technique, which has been applied to the microtremor measurements carried out in the present study, may be summarized as follows:

- Horizontal soil layering over a hard bedrock (half-space);
- Ambient noise consists of different types of waves;
- Vertical component of ambient noise displays the characteristics of local noise sources and is relatively uninfluenced by the soft sediment layers overlying a half-space;
- Components of ground motion are equal in all directions at the basement.

If we follow these assumptions the site amplification is defined as

$$S_E(\omega) = H_S(\omega) / H_B(\omega)$$

where $H_S(\omega)$ and $H_B(\omega)$ are the horizontal amplitude spectrum and the ground surface and at the bedrock. In the absence of amplification in the vertical component, microtremor source spectrum can be expressed as ratio of vertical Fourier spectrum at the surface and bedrock, i.e.

$$As(\omega) = Vs(\omega) / V_B(\omega)$$

After normalization by spectrum allowing removing the unknown source effects from the soil amplification we obtain transfer function of the soil layer

$$S_M(\omega) = S_E(\omega) / A_S(\omega) = \left[H_S(\omega) / V_S(\omega)\right] / \left[H_B(\omega) / V_B(\omega)\right]$$

Since according to Nakamura's assumption

$$H_B(\omega)/V_B(\omega)=1$$

The transfer function may be expressed as

$$S_M(\omega)=Hs(\omega)/V_S(\omega)$$

Or, in other words, the vertical component of ambient microtremor on the surface retains the characteristics of horizontal component of the bedrock.

4. GEOLOGICAL SETTINGS

The primary step in every microzonation study is the collection, comparison, validation and mapping of geological and geotechnical information. In the present project it is based on several geological sources. The depths of various geological horizons were compiled from the structural maps of Mero (1983), Fleischer and Gafsou (2003) and Bar Yossef et al. (2003). Borehole information and geological cross sections across the study area (Kafri and Ecker, 1964) are used to determine general subsurface conditions, local site stratigraphy and composition of the soils. In our study we focused, mainly, on the analysis of the geological conditions in terms Vs layering, adequate for site response interpretation and the amplification potential of the seismic movement.

The area studied is located in the part of the Zevulun Plain adjacent to the Haifa Bay shore and is limited by the escarpment of Mt. Carmel to the south-west. The fragment of the geological map showing the study area with measuring sites locations is shown in Fig. 2. Structural blocks occupied by the study area are the Qishon Graben and the Central Horst of the Zevulun Plain.

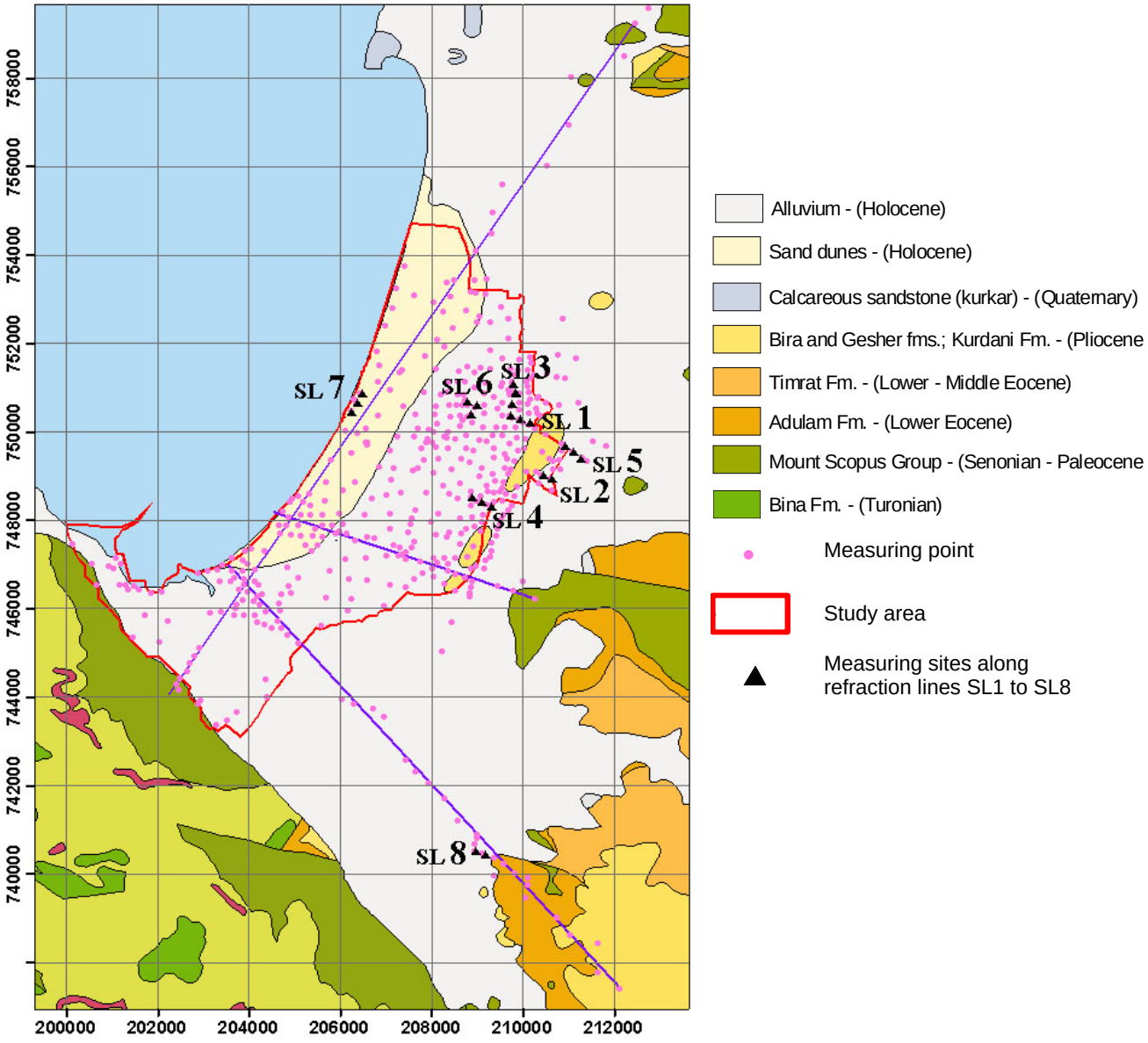

Figure 2. The geological map of the study area showing the locations of microtremor observation sites, refraction lines and profiles designed by request of the Geological Survey of Israel (purple line).

The main lithostratigraphic units of the sedimentary column in the study area are the Judea, Mt. Scopus, Avedat, Saqiye and Kurkar Groups (compiled from Mero, 1983; and Kafri, 1964):

- The Judea Gr. of Turonian-Cenomanian age is represented mainly by the limestone and is not exposed within the study area. Its depth of bedding varies from several meters (point 5, well SH-10) down to 1300-1500 meters at seashore.

- The Mount Scopus Gr. overlaying the Judea Gr., consists of Senonian-Paleocene marly-chalky formations and crops out in the eastern Galilee foothills.
- The Avedat Group of Eocene age consists of chalk and chalky limestone, covers the Mt. Scopus marls and crops out in the southern-eastern part of the Zevulun plain.
- The Saqiye group covers the Avedat and Mt. Scopus Grs. and is subdivided into upper Eocene-early Miocene chalky marl (Beit Guvrin and Lakhish Fms.), upper Miocene limestone and anhydrite with marl (Ziqlag and Mavki'im Fms.) and upper Miocene to Pliocene clays and marls (Yafo Fm.).
- The Kurkar Gr. comprises the Pliocene-Pleistocene rock sequences showing lateral facies changes and represented by sandy limestone to calcareous limestone (Kurdani Fm.) and clay alternated with calcareous sandstone (known as "Kurkar" proper). This part of the column is well known owing to numerous shallow wells, cross sections (Kafri and Ecker, 1964).
- Recent (Holocene) dunes are composed mainly of sand and partly calcareous sandstone separated by clay horizons and distributed along the seacoast.

The structural maps for the most of the mentioned members are available in the studies of Mero (1983) and Fleisher and Gafsou (2003) and they are used for the interpretation goals.

Within the mentioned lithostratigraphic units we presume some reflectors which may produce site effects. From our experience and knowledge, accumulated throughout numerical works carried out in the different places of Israel, we suppose the following lithostratigraphic units to be potential reflectors owing to their geotechnical characteristics. Top Judea Gr. is identified in the Coastal Plain and Hashefela regions as common reflector that may be assumed as the deepest reflector also at the Central Horst. Next reflector is sandy limestone to calcareous sandstone of the Kurdani Fm. dated Upper Pliocene-Lower Pleistocene (Mero, 1983).

We observe different geological situation in the Qishon Graben. In view of the westwards regional dip down to a depth of more than 1000 m, the Top Judea Gr. cannot serve as a reflector any more, therefore we suppose that the next potential reflector from the bottom to the top in the columnar section of the Qishon graben is limestone and gypsum of the Ziqlag and Mavki'im Fm. of Miocene age. Their total

thickness, according to the Mero (1983) data based on information from Canusa 9 well is summed from 180 meters of the Ziqlag limestone and 40 meters of the Mavki'im anhydrite. In fact, besides Canusa-9 well we have no additional data on subsurface extension of the Ziqlag Fm. The impedance contract between sand/sandy loam and calcareous sandstone the Kurkar Gr. or clay of Yafo Fm. may cause additional reflection that we have already fixed in our former investigations at the Coastal plain.

While the geological structure of the study area is rather complex suggesting that complex site effects would be expected, the information contained in the consulted research works is incomplete and sometimes ambiguous that hampers its direct using for site response evaluation. Comparison of two structural maps of Top Judea Gr. constructed by Fleischer and Gafsou (2003) and by Mero (1983) reveals considerable differences in both the surface of Top Judea Gr. and faults locations (see Fig. 3).

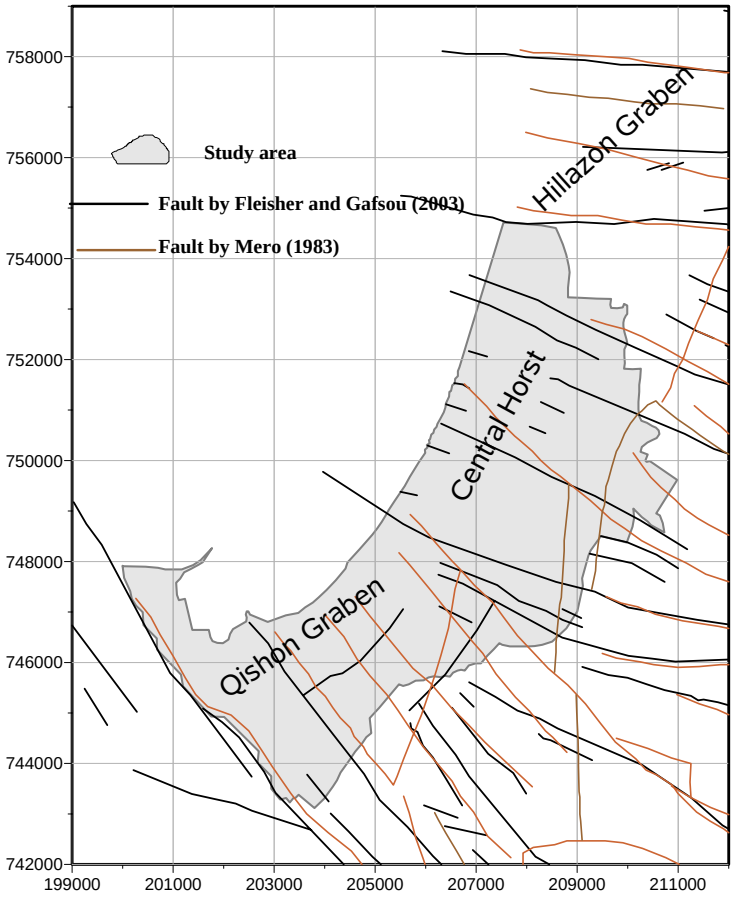

Figure 3. Scheme of faults locations according to different interpretations.

5. INSTRUMENTS AND MICROTREMOR DATA

A single seismic station was used for the microtremor measurements. The acquisition equipment included: an amplifier with 0.2-25 Hz band pass filter, a 16-bit analog-digital converter with GPS time, sampling each channel at 100 samples per second and a laptop computer to control the system and store the data. The GII-SDA, digital seismic data acquisition system is designed for site response field investigations (Shapira and Avirav, 1995). The seismometers used are very sensitive velocity transducers (L4C by Mark Products) with a natural frequency of 1.0 Hz and 70% critical damping. The station is equipped with one vertical and two horizontal seismometers (oriented north-south and east-west). All the equipment: sensors, power supply, amplifiers, personal computer and connectors were installed on a vehicle, which also served as a recording center.

Prior to performing measurements we checked and determined the transfer function of the instrumentation. The individual seismometer constants (free-frequency, damping and motor constant) are determined from sine and step calibration signal. These constants are necessary for procedure "instrument response correction" used in seismology to deconvolve output of seismometer channel and to estimate real ground motion (velocity using micron/sec units in our case). In addition seismometers are placed at the same locations and in the same orientation to record the same waves. These measurements allow assessing the identity of different channels of the entire monitoring system, i.e. transducer, amplifier, filter, and analog-to-digital conversion. After comparison of identity of the channels with and without "instrument response correction" may be seen that removal procedure leads to clear distinctions of channels in the frequency range 0.2-0.8 Hz. Therefore, for the fundamental frequency of site effect less than 1.0 Hz the spectral ratios were calculated without previous instrument correction.

Microtremor measurements were carried out during the period September 2004 to April 2005. The work area is approximately 50 km^2. The distribution of measurement points over the Haifa bay coast is shown in Fig. 2. An important issue that was raised before and during the investigation was how dense the grid of measured points should be. In retrospect, based on many projects in order to estimate site response functions in different towns of Israel, we may state that we obtained

reliable results only because we used a dense grid of measured points. Thus, we start with a large spacing between measurement points (500 m grid) but through lateral variation of the results, density the grid point spacing is increased to 250 m. It should be noted that densely distributed geotechnical information such as S-wave velocities and densities of layers, especially in depth, needed for theoretical estimation of site effect, is not available in Israel. We can compensate for the need of a dense grid of measured points of microtremor by drilling new borehole, conduct many geophysical surveys and monitor strong enough earthquakes at points across the area. These alternatives are by far more expensive, time consuming and may not always provide the necessary information.

Our results indicate significant dependence upon the experimental conditions, for example:

1. What is the required duration of microtremor record to obtain sufficient number of reliable time windows? According to Rovelli et al. (1991), Mucciarelli and Monachesi (1998) and Lebrun et al. (2004) among others the duration of 10-20 minutes is sufficient. We performed an experiment for assessing the optimal operation time necessary for a measurement to be considered a reliable one. A station operates for 6 hours and the microtremor is recorded continuously, creating many data files with a length of 3 minutes each. Fig. 4 illustrates the influence of the recording duration on the reliability of individual and average H/V spectral ratio. It should be mentioned that due to contamination of heavy traffic noise in each file we may select two to three shorter time windows 30-sec each. An important conclusion following Fig. 4 is that in urban areas the high stability and high fidelity H/V ratio estimation is obtained using time windows of 50 to 70 minutes at each point.

2. Another point is how to differentiate a "good" microtremor sample that has been collected from a "bad" one. In urban areas underground piping, construction and soil-structure interaction may seriously change shape of the H/V curves. The effect of underground piping on the microtremor record and the H/V ratios is clearly visible in Fig. 5a. For comparison, Fig. 5b shows microtremor motion and H/V ratios obtained at a station installed about 50 m aside. In the densely built area H/V ratio obtained from microtremor could be influenced by the presence of the structures. We evaluate the site amplification by "free field" station located about 20 m from a four storey building. The individual and average H/V spectral ratios are presented in Fig. 6. The main feature of these spectral ratios is the amplification within two frequency ranges

of 4.0-4.5 Hz and 6.0-8.0 Hz. This building is instrumented by placing the seismometers on the roof. The average Fourier spectra obtained from ambient excitation show that the frequency range 4.0-4.5 Hz is the first translational mode in the EW direction. Hence, the amplification in the frequency range 6.0-8.0 Hz is due to site effect.

It must be mentioned that during the field experiment it is very difficult to assess the conditions only by visual inspection of microtremor waveform. Therefore, in the measurement setup, we carry out not only visual checking quality of time series of microtremors at each site, but also computing H/V ratio several times.

6. DATA PROCESSING

We use for analysis all windows of 60 minutes microtremor recordings, which are unaffected by the traffic noise. Each dataset contains three components. Some examples are shown in Fig. 7. Excluding the short-duration disturbances with large amplitude portions generated by highway traffic near the observation site, the stationary portions were picked out for analysis. To study the spectral character of the microtremor in the study area, we use two different time windows: 30-sec record for sites with resonance frequencies above 1 Hz and 50-sec record for sites with resonance frequencies less than 1 Hz. The selected time windows were Fourier transformed, using cosine-tapering (1 sec at each end) before transformation and then smoothed with a triangular moving Hanning window. The H/V spectral ratio is obtained by dividing the individual spectrum of each horizontal component $S_{NS}(f)$ or $S_{EW}(f)$ by the spectrum of the vertical component $S_V(f)$. To obtain systematic and reliable results from the spectra of microtremor, we use several time windows (60-70 minutes) that yielded a number of spectral ratios that, in turn, are averaged.

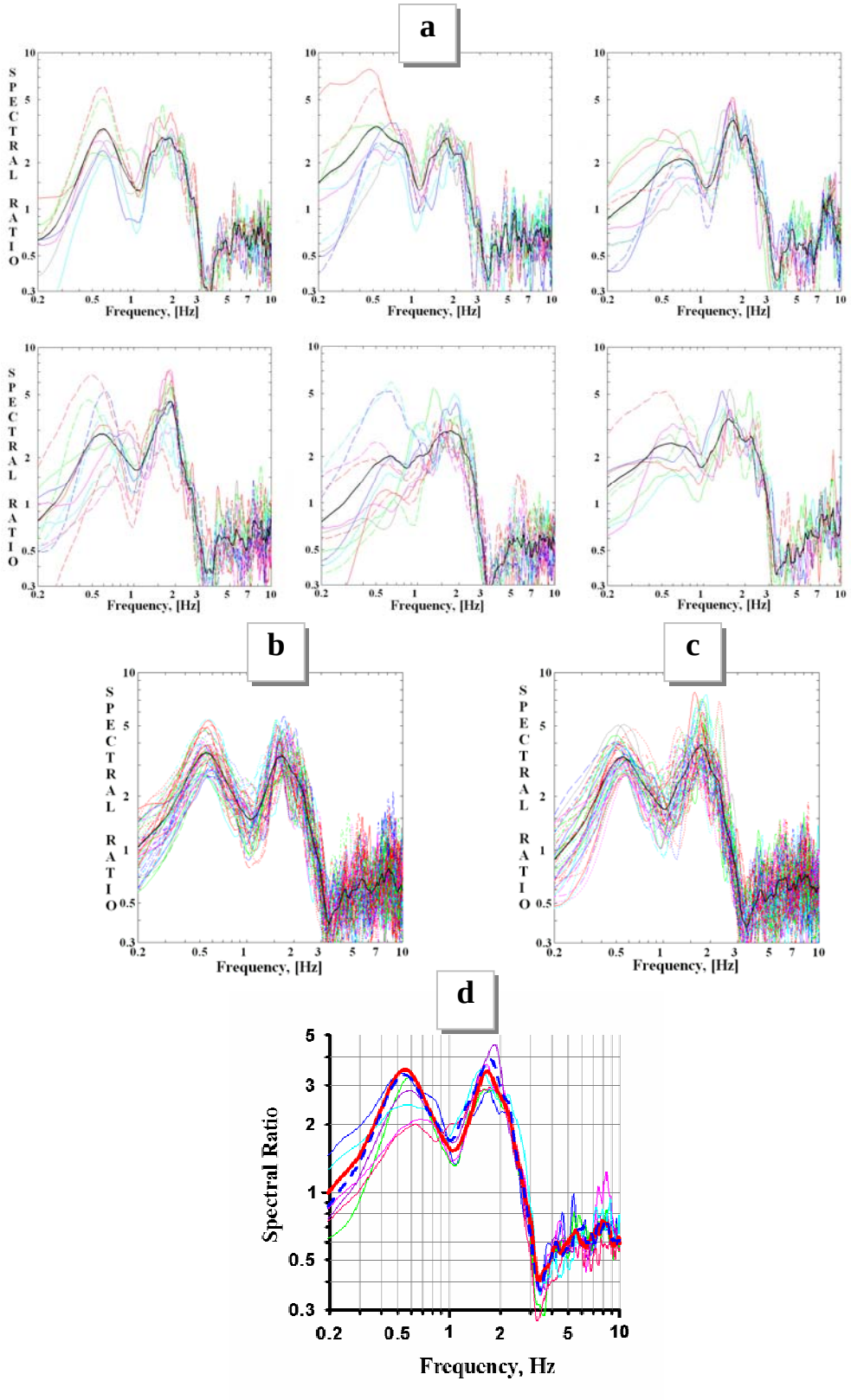

Figure 4. Influence of recording durations on the reliability of individual (colored lines) and average (black line) H/V curves: (a) five minutes of recording every hour, during 6 hours; (b) one hour; (c) six hours; (d) comparison of the average H/V spectral ratios.

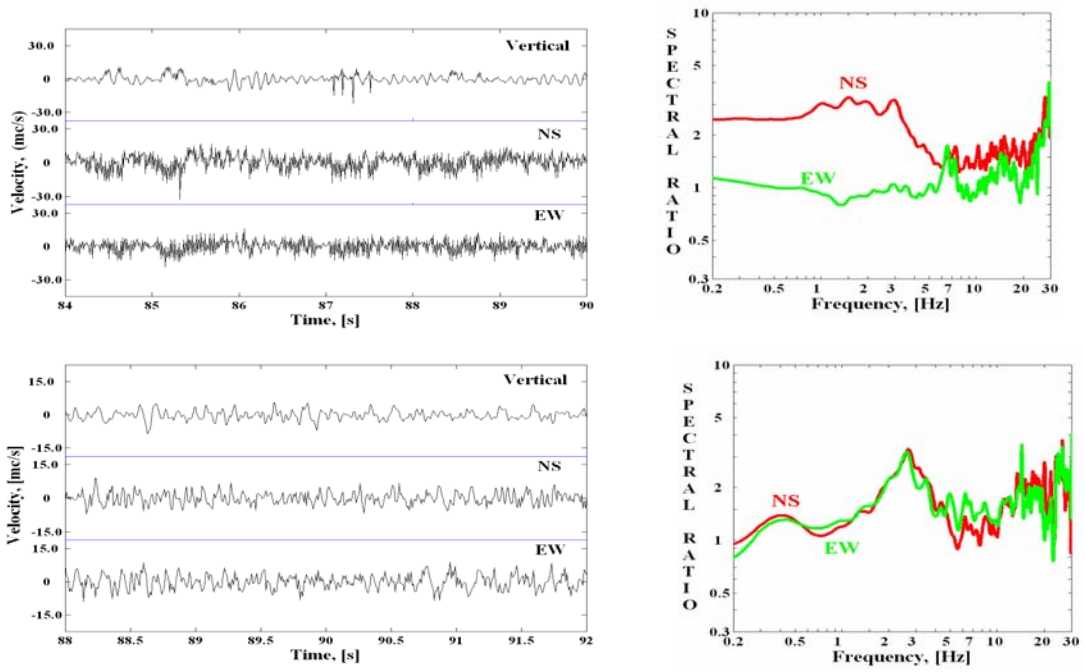

Figure 5. Velocity time history of microtremors and H/V spectral ratios curves obtained (a) near underground pipe and (b) 50 m aside.

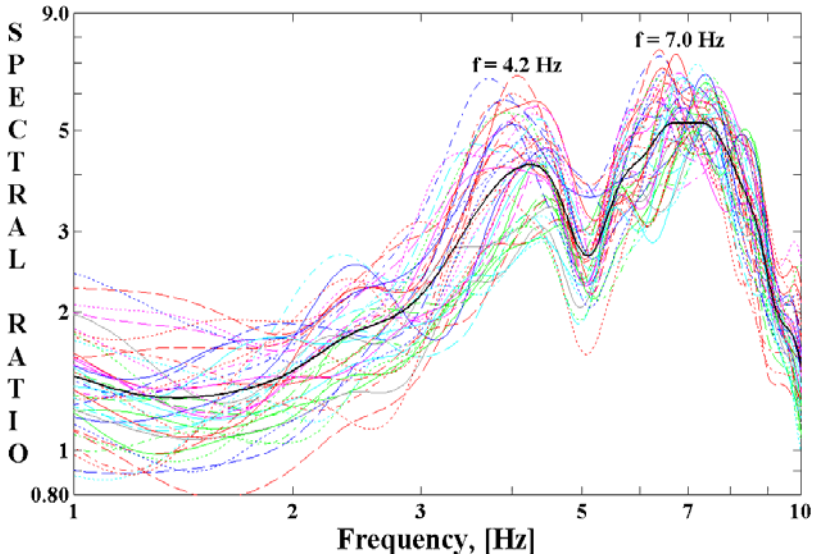

Figure 6. Individual and average H/V spectral ratio from ambient vibration recorded at "free field" seismic stations located about 20 m from a building.

The horizontal-to-vertical spectral ratio $A_{H/V}(f)$ is obtained by dividing the individual spectrum of each horizontal component $S_{NS}(f)$ and $S_{EW}(f)$ by the spectrum of the vertical component $S_V(f)$. If the shapes of $S_{NS/V}$ and $S_{EW/V}$ are similar then the average of the two horizontal-to-vertical ratios is defined:

$$A(f) = \frac{1}{2n}\left[\sum_{i=1}^{n}\frac{S_{NS}(f)_i}{S_V(f)_i} + \sum_{i=1}^{n}\frac{S_{EW}(f)_i}{S_V(f)_i}\right]$$

We have consistently observed that averaging the spectral ratio arithmetically or geometrically does not significantly change the results. Dataset for averaging spectral ratios usually comprises more than 50 curves for each EW and NS components.

Based on wide experience of microtremor data analysis in the last 5 years we recommend using of the manual window selection, because only an appropriate ensemble of carefully selected windows of microtremors can provide the true estimation of site response. We deal with the problem in terms of "signal-to-noise ratio". According to general approach we can consider microtremor recordings, obtained by vertical and horizontal seismometers as "input" and "output" signals of a linear dynamical system observed with unknown signal-to-noise ratio (SNR). This SNR depends on a number of factors responsible for deviation of the 1D model from the true 3D mode determined by the geological and wave velocity structure as well as useful and interfering microtremor sources, their configuration, spectral intensity, remoteness etc. In practice, SNR may vary significantly during short period of time, thus spoiling the H/V results. Evidently, the time periods where signal-to-noise ratio is large are preferable but we have no means to compute SNR from observations. Therefore, the operator involved in data processing is responsible for accurate window selection. Fig. 7 presents an example of selecting appropriate and not appropriate time windows for computing H/V spectral ratio. The influence of automatically and manually selected time windows on the individual and average spectral ratios is apparent in Fig. 8. However, in the present time we do not have formal criteria to choose "appropriate" time windows for automatic processing.

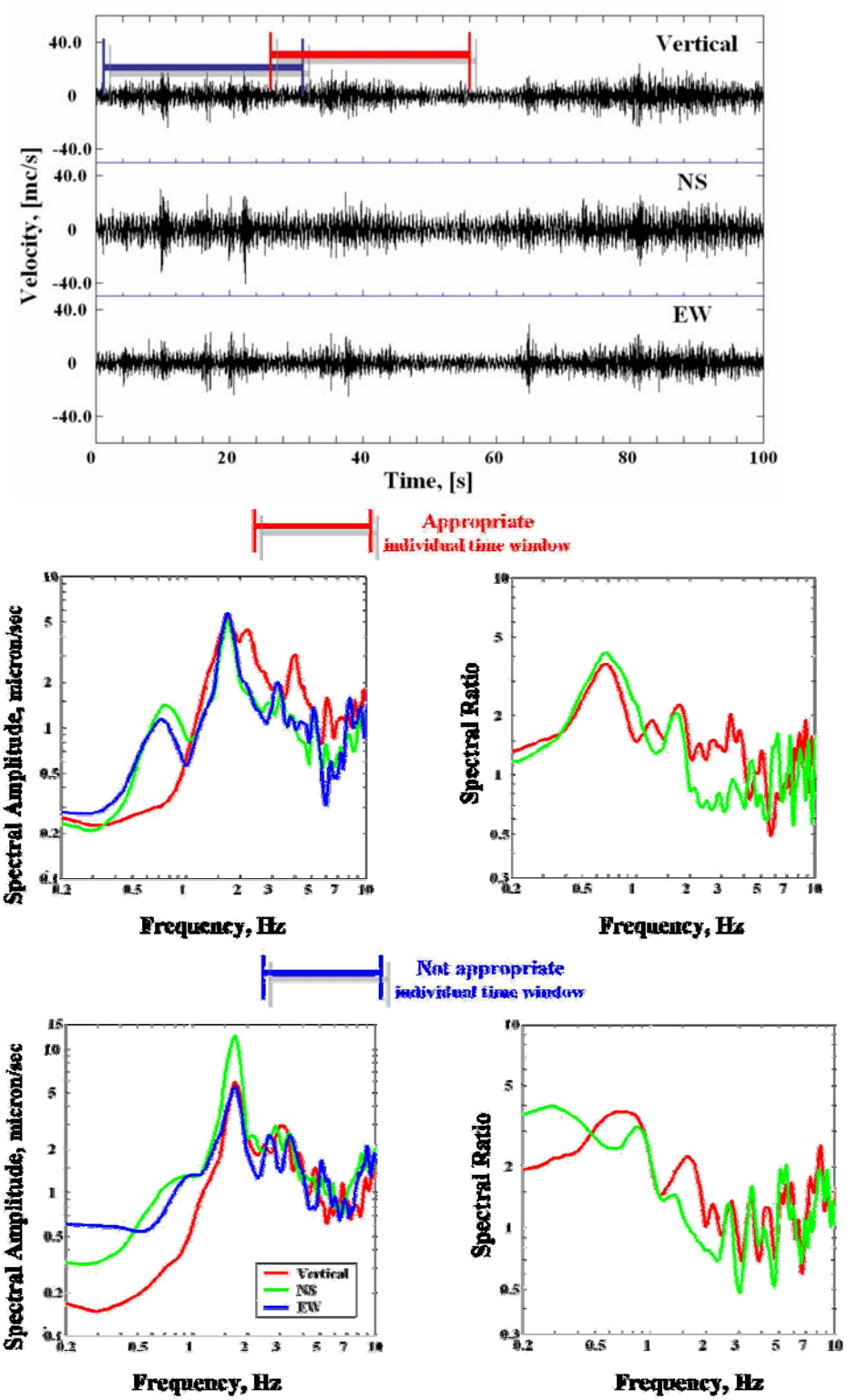

Figure 7. Individual Fourier spectra and H/V spectral ratio for appropriate and inappropriate individual time windows derived from the signal (velocity time history of microtremor) displayed in top of figures.

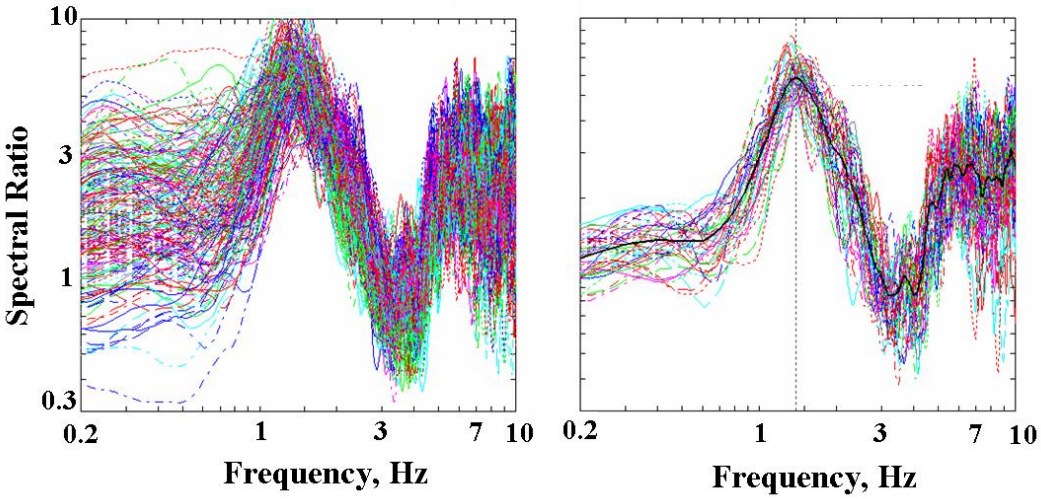

Figure 8. Influence of selected time windows of microtremor on H/V spectral ratio: (a) the automatic window selection; (b) the manual window selection.

7. ESTIMATION OF S-VELOCITY STRUCTURE USING COMPARISON BETWEEN H/V RATIO AND PREDICTED SITE EFFECTS

Analytical assessment of site effects requires as input a model of the site's subsurface. Since geotechnical data on S-velocities are limited in the study area by a few refraction profiles only, we use H/V spectral ratios obtained at borehole locations, where information on layer thicknesses down to reflector is available, in order to constrain possible Vs structure via comparison with analytical models. The geophysical survey provided the shear velocity profiles and thicknesses of shallow sediments (within the accuracy and resolution of the geophysical technique) which were used to develop 1-D multi-layer model of the subsurface, calculate analytical transfer function using SHAKE program (Schnabel at al., 1972) and compare with empirical determinations that is performed by Ezersky (2004).

To demonstrate the way S-wave velocities are estimated, we shall use the example of the location of SH-4 well, columnar section of which is shown in Fig. 10. The depth section of S-waves along the refraction line SL-1 (Ezersky, 2004) is shown in Fig. 9 and the location of the refraction line is in Fig. 2. The lower layer of the section with Vs=1290 m/sec is correlated with limestone of the Kurdani Fm. The H/V spectral ratio obtained at measurement point Q2 located at SH-4 well is shown in Fig. 10 by the red line. The borehole data and velocity model from the refraction survey are given in Table 1. By combining refraction and borehole information we calculated

the theoretical transfer function (black line in Fig. 10) and compared it with the experimental spectral ratio. It should be noted that borehole and geophysical data provide different information on the thickness of the upper soft layer overlying the Kurdani Fm, i.e., 10 meters vs. 18 meters, respectively. We obtained better agreement using velocity model directly from the refraction survey results. Based on this fact, we note that Vs=160 m/sec for the 4-meter upper layer practically does not affect the transfer function and may be disregarded in the modeling. We use S-velocities for marl and limestone of the Judea Gr. obtained from our investigations over the Coastal plain and HaShefela regions (Zaslavsky, 2003d). The final soil column model for point 2 is given in Table 1.

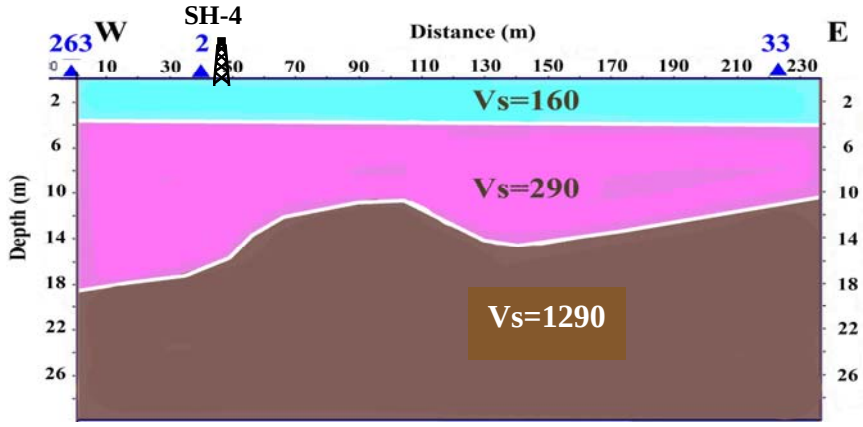

Figure 9. Vs depth section along refraction line SL-1.

The derived model explains shape of the H/V curve with two resonance frequencies, as a result of simultaneous influence of two reflectors. The deep reflector, which is associated with Top Judea Group, is responsible for the first peak at frequency of 1.8 Hz. The shallow reflector, the Kurdani Fm., is related to the second peak at frequency 3.5 Hz. We note that the second peak is considerably higher.

Velocity model derived for point 2 is tested at two additional points in line SL-1: 263 and 33. H/V spectral ratios for these points are shown in Figure 11. The increase in the thickness of the upper layer from point 33 to point 263 observed in the depth section is confirmed by the measurement results. In particular, while the main frequency of the H/V ratios is 2 Hz for both points, the higher frequency for point 33 is 7 Hz vs. 3.5 Hz for point 263.

Table 1. Soil column model for point 2 located at SH4 well derived from borehole and refraction survey data

SH-4 well data		Vs model from refraction survey		Soil column model	
Lithology	Thickness m	Thickness m	Vs m/sec	Thickness m	Vs m/sec
Alluvium	10	4	160	4	160
		14	290	14	290
Limestone	25	Below 18 meters	1290	25	1200
Marl-chalk	60		?	60	750
Limestone and dolomite	-		?		1900

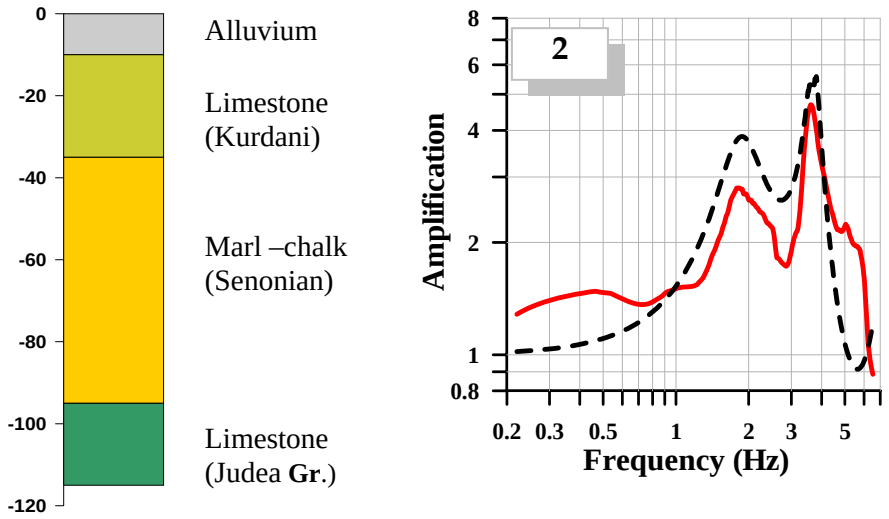

Figure 10. Columnar section of SH-4 well and comparison between average H/V spectral ratio (red line) obtained at point 2 (SH4 well) and analytical transfer function (black line).

Likewise point 2 we try Vs for the upper layers 160 m/sec and 290 m/sec as well as two equal velocity values. A better agreement between theoretical transfer functions and H/V ratios is obtained using Vs=270 m/sec for the both layers above Kurdani Fm. Comparison of average spectral ratios with analytical functions for points 263 and 33 is presented in Fig. 11.

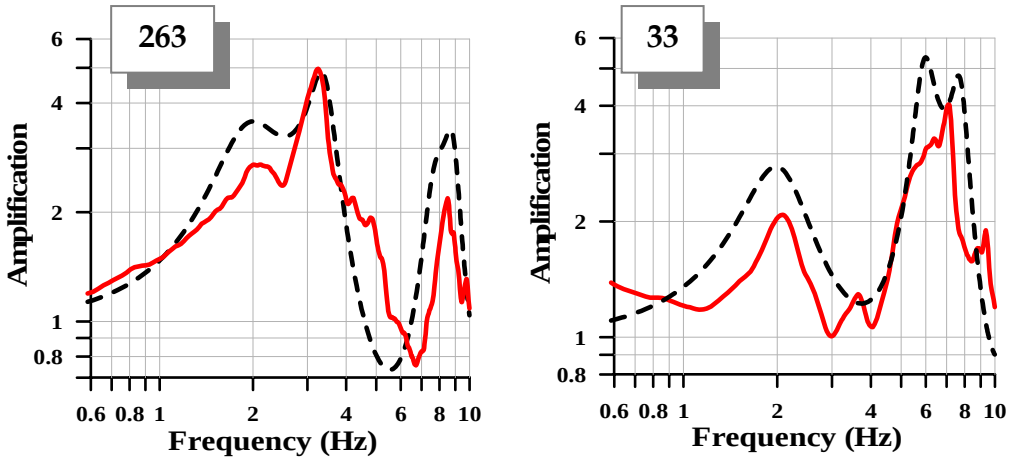

Figure 11. Average H/V spectral ratios (red lines) obtained at points 263 and 33 superimposed with the analytical transfer functions (black lines).

Figure 12 shows a match between the analytical transfer function and H/V spectral ratio for Point Q5 located at well SH10. In this well, the alluvium deposits of 13 m thick overlay the limestone of the Judea Group and the choice Vs values of 160 m/sec and 270 m/sec becomes critical. Vs equals 270 m/sec provides a fairly good fit between the theoretical transfer function and H/V ratio (see Fig. 12a).

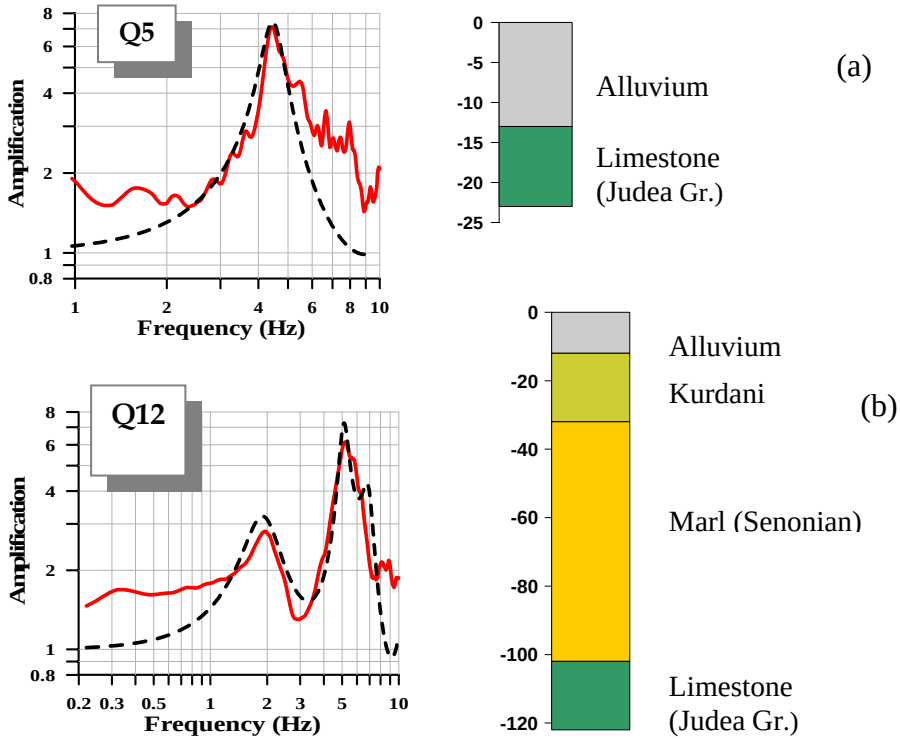

Figure 12. Average H/V spectral ratios (red line) at point Q5 and analytical transfer functions for SH10 well (black line) – (a) and Q12 (SH-6 well) – (b) with corresponding columnar sections.

We continued the validation of Vs model at point Q12, which is situated directly at well SH-6. Its soil column is shown in Fig. 12b. Applying the velocity values from Table 1 we obtain a good fit between the theoretical function and the H/V ratio (see Fig. 12). H/V ratio for point Q3 located at shallow Affec Tazpit well is shown in Fig. 13. Vicinity of this well to the deep SH-4 well allows estimating roughly the thickness of the Kurdani Fm. (about 30 meters) and depth of Top Judea Group, considering its sharp dip as approximately 120-140 meters. Refraction survey (Line SL-3) carried out at this point differentiates two layers of 10 m and 15m thick with S-wave velocities 160-180 m/sec and 480 m/sec, respectively, above the Kurdani limestone (see Fig. 14).

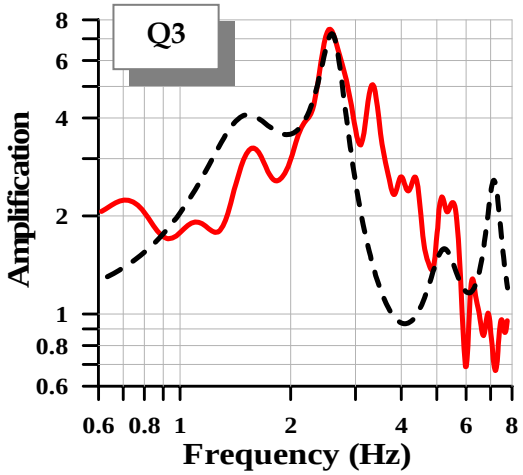

Figure 13. H/V spectral ratio and theoretical transfer function for point Q3 located at refraction line SL-3.

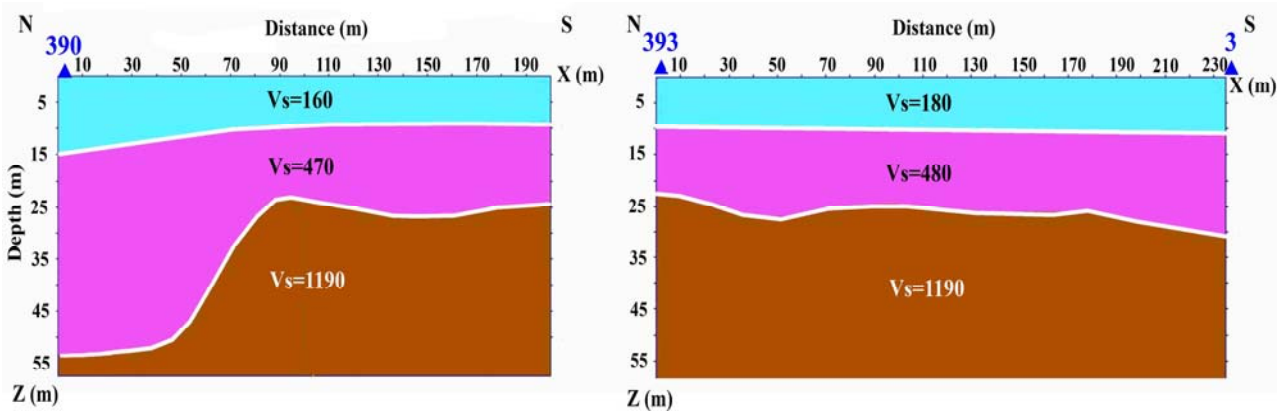

Figure 14. Velocity-depth section along line SL-3.

S-velocity of 480 m/sec was surprising for us in spite of the fact that this value provides fair fit between analytical function and H/V ratio. In Table 2 we collect Vp,

Vs and Vp/Vs values for the second layer in all refraction profiles, which are located relatively close to SL-3 line. One can see that in five out of seven cases the ratio of Vp/Vs is more than 5, i.e. seismic profiles SL-2 and SL-3 are obvious outliers. Therefore, the seismic survey along SL-3 line is used under condition that Vs for the second layer is 280 m/sec. The whole soil column model together with initial data for point Q3 is shown in Table 3. The theoretical transfer function superimposed with H/V spectral ratio is shown in Fig. 13.

Table 2. Vp, Vs and Vp/Vs for the second layer of sediments overlying the Kurdani limestone.

Seismic profile	Vp	Vs	Vp/Vs
SL-1	1860	290	6.4
SL-2	1030	550	1.8
SL-3	1870	470	4.0
SL-4	2260	310	7.3
SL-5	1950	270	7.2
SL-6	1570	290	5.4
SL-7	1660	320	5.2

Table 3. S-velocity model from borehole and refraction survey data and soil column model for point Q3 (SL-3 refraction profile).

<table>
<tr><td colspan="2">Affec Tazpit and SH-4 wells data</td><td colspan="2">Vs model from refraction data</td><td colspan="2">Soil column model</td></tr>
<tr><td>Lithology</td><td>Thickness, m</td><td>Thickness, m</td><td>Vs, m/sec</td><td>Thickness, m</td><td>Vs m/sec</td></tr>
<tr><td>Sand and sandy loam</td><td rowspan="2">15</td><td>5-12</td><td>160-180</td><td>12</td><td>160</td></tr>
<tr><td>Sand and sandy loam</td><td>12-15</td><td>480</td><td>13</td><td>250</td></tr>
<tr><td>Limestone of the</td><td>30</td><td>Below 25 meters</td><td>1190</td><td>25</td><td>1200</td></tr>
<tr><td>Marl-chalk</td><td>70-90</td><td rowspan="2">?</td><td rowspan="2"></td><td>75</td><td>750</td></tr>
<tr><td>Limestone and dolomite</td><td></td><td></td><td>1900</td></tr>
</table>

Ambient vibrations recorded at point Q199 located at Canussa-9 well and results of interpretation of the seismic surveys carried out along SL-7 refraction line,

at Haifa Power Plant and Nesher Industrial Zone sites (Ezersky, 2003) are used to estimate shear velocity for Mavqi'im-Ziqlag Fms. and Pliocene clay within the Qishon graben. Columnar section of Canusa-9 well in our interpretation corresponding to the analytical function and H/V ratio for point 199 is shown in Fig. 15. The best fit between the analytical transfer function and H/V ratio is obtained assuming Vs for the Pliocene clay layer equal to 850 m/sec. Table 4 summarizes all S-velocities derived from the joint analysis of the microtremor records and refraction survey data.

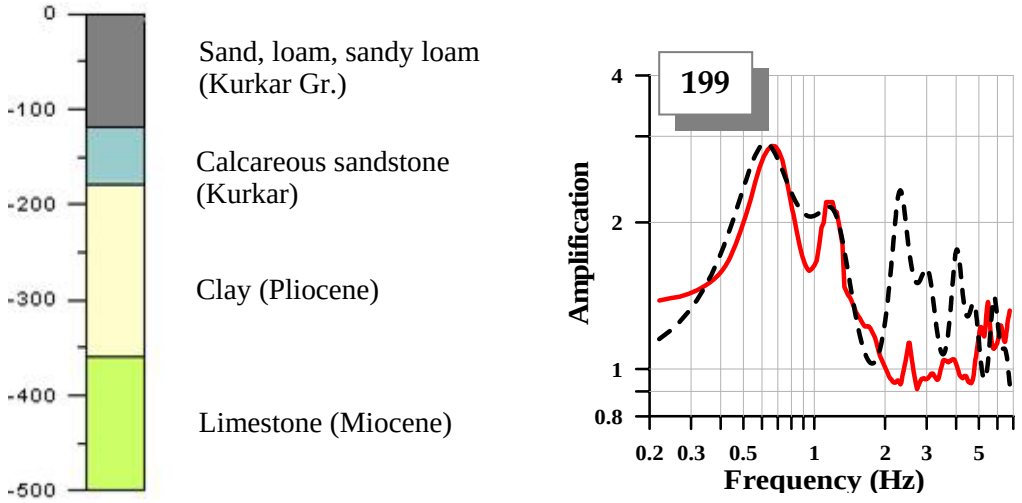

Figure 15. Lithostratigraphic column for Canusa-9 well and H/V spectral ratio compared with theoretical transfer function for point 199 recorded at this well.

Table 4. Shear-wave velocity for lithological units represented in the study area. SL- refraction lines in the Qrayot area (Ezersky, 2004); HaShefela – Zaslavsky et al. (2003d).

Lithological unit	V_s m/sec	Source
Silt	160-180	SL-1, SL-3
Sand and Sandy loam (Kurkar Gr.)	250-350	SL-1,2,3,4,5,6,7
Calcareous sandstone (Kurkar Gr.) and clay (Pliocene)	650	SL-6
	850	Canusa-9 model
Limestone (Kurdani Fm.)	1100-1300	SL1,2,3,4,5,6
Gypsum and Limestone (Miocene age)	1500	Canusa-9 model
Marl-chalk (Senonian)	750-850	HaShefela
Chalk (Eocene)	950-1000	SL-8
Limestone and dolomite (Judea Group)	1900	HaShefela

8. VARIATIONS OF VERTICAL COMPONENT OF MICROTREMOR THROUGHOUT THE STUDY AREA

The horizontal-to-vertical spectral ratio (Nakamura's method) states that the amplification produced by a surface layer can be obtained by evaluating the ratio between the horizontal and vertical Fourier amplitudes spectra of microtremors recorded at the site. In other words, in Nakamura method the input and output to the soil sites are vertical and horizontal motions respectively. However, the characteristics of noise sources change from one site to another, even over short distances, and especially in the short period range. As already mentioned, the Qrayot and seashore of Haifa bay are urban and densely populated areas. Sources of cultural activity are distributed over coastal strip of Haifa city, the towns of Qiryat Bialik, Qiryat Motzkin, Qiryat Yam, Haifa port and airport, and many different heavily used highways and roads. Difficult recording conditions like proximity of highways, roads and other unidentified sources of transient vibrations in combination with complex geological conditions such as the grabens alternating with horsts, great number of faults, different reflectors and different cover sediment thickness etc. is a background of our investigations. Nevertheless, it is of interest to check stability or, on the contrary, variability of vertical component of the ground motion caused by different sources and path effect.

Analysis of five hundreds vertical Fourier spectra showed that the study area can be divided into four zones based on the shape and amplitude level of spectra. Spatial distribution of the zones is presented in Fig. 16. Fig. 17 depicts average spectral amplitude for different zones. For zone 1 is characterized by flat shape of the vertical spectrum in the frequency range 0.5-2.0 Hz and wide maximum in the range from 2.0 Hz up to 7.0 Hz. This zone is represented by the lowest spectral amplitude. The average Fourier spectrum for zone 2 has amplitude three times higher than that in zone 1. Spectrum of the vertical component for Zone 3 gradually increases within the frequency range of 0.5 Hz to 10.0 Hz. The average vertical component of spectra for Zone 4 has the amplitude level significant higher than the other zones. The spectral curve shows broad two-peak maximum from 4 Hz up to 8 Hz and the slope is up to 8 Hz. We understand provisional disposition of our division since microseism spectral amplitude may vary significantly during day of measurements and spectral variations may change considerable from one day to another. Nevertheless, since microtremor

measurements were carried out for a long time (September 2004-April 2005), we believe that our division reflected basic spectral characteristics of vertical components of microtremors. Thus, distribution of the vertical spectral component over the study area revealed correlation between features of geological structure and spectral shape.

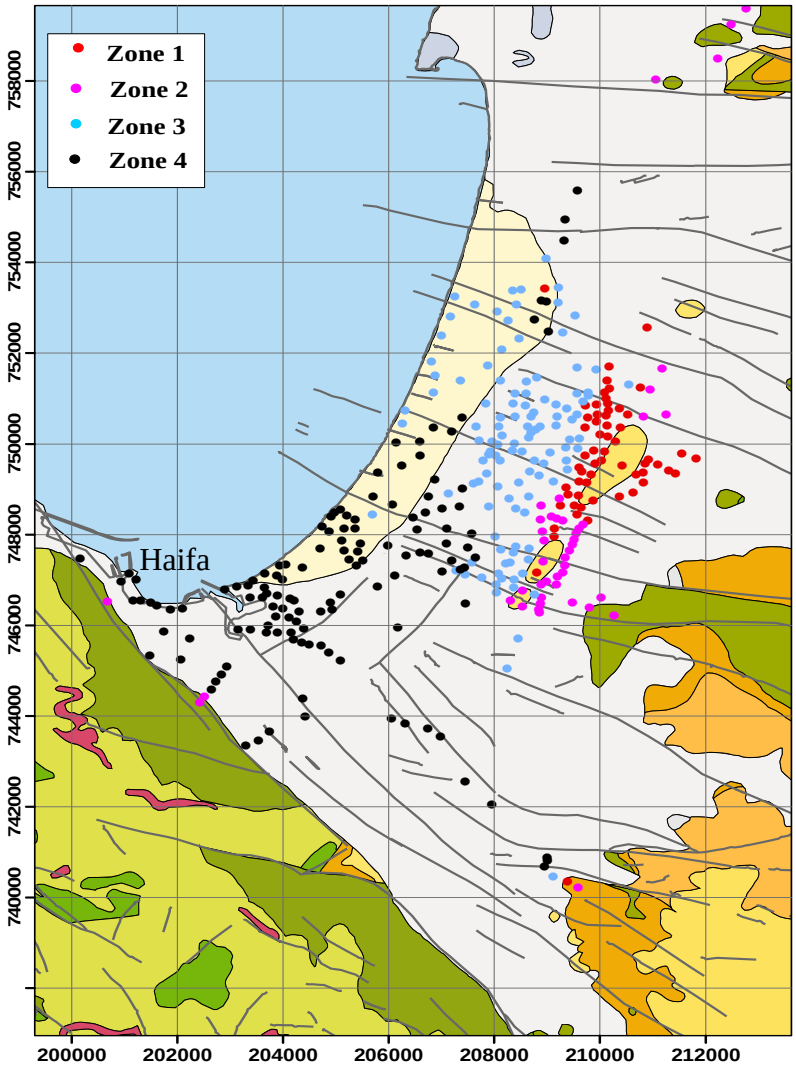

Figure 16. Map showing zones selected by Fourier spectrum shape of the vertical motion of microtremors.

These features generalized for each zone may be described as follows:

Zone 1. The deep reflector (Top Judea Gr.) lays at depths of less than 150 meters. The shallow reflector (the Kurdani Fm.) crops out or underlies the alluvium layer and has thickness of less than 20 meters.

Zone 2. The deep reflector (Top Judea Gr.) lays at depths of more than 150 meters. The shallow reflector (the Eocene and Senonian chalk) or crops out or

underlies the alluvium layer. The Kurdani Fm., if exists, has a thickness of less than 20 meters.

Zone 3. The deep reflector (Top Judea Gr.) occurs at depths of more than 150 meters. Thickness of the shallow reflector (Kurdani Fm.) is more than 50 meters.

Zone 4. Such type of vertical spectra is found in graben. The Top Judea Gr. is deeply located and is not considered as reflector any more and the limestone (sometimes together with gypsum) of Miocene age is assumed as deep reflector. The shallow reflector is sandstone of Kurkar Gr. together with clay of the Yafo Fm.

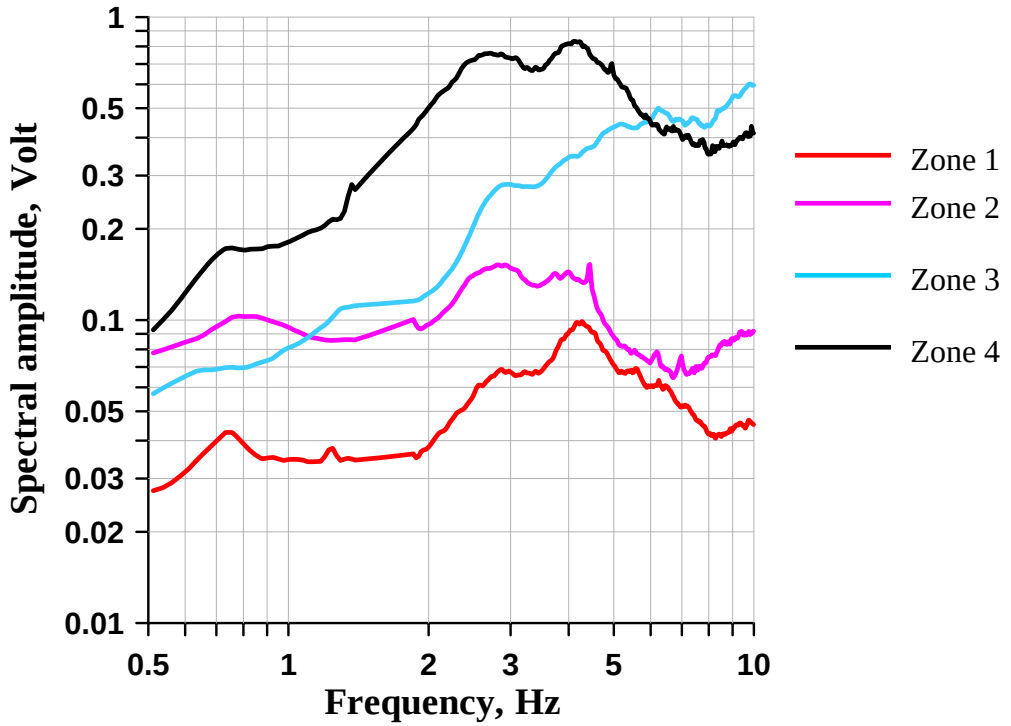

Figure 17. The average Fourier spectra of vertical components for four zones.

9. SUBSOIL STRUCTURE USING MICROTREMOR MEASUREMENTS ALONG PROFILES

Given the observed resonance frequencies across the investigated area and the shear wave velocity values presented in Table 4, we can use this information to construct a subsurface multilayer model and estimate the thickness of the sediments at most of the measurement sites where no well information was available.

The essence of the procedure applied is to match the H/V spectral ratios with an analytical response function, computed by using program SHAKE for a specified

subsurface model. Such subsurface model is constructed by combining available geological information and S-wave velocities for the different soils and rock types. As is above mentioned, the needed geological information is mainly taken from the studies of Kafri and Ecker (1964), Mero (1983), and Fleischer and Gafsu (2003). The program based on the stochastic optimization algorithm (Storn, 1995) is applied in order to approximate the spectral ratio by theoretical function in the best way, considering the dominant frequency, its level and the shape of the H/V curve. Within the chosen frequency interval $[w_1, w_2]$ we look for thickness (h_i) and S-velocity (v_i) that minimize the misfit function

$$F = \sum_{k=1}^{N} (f_{SHAKE}(\omega_k) - H/V(\omega_k))^2 ,$$

where ω_k are points from the frequency interval $[w_1, w_2]$, $f_{SHAKE}(\omega)$ is 1-D theoretical transform function calculated by SHAKE program; and $H/V(\omega)$ is H/V spectral ratio. Velocity and thickness are limited:

$V_{1i} \le v_i \le V_{2i}, i = \overline{1, M+1}$ and $H_{1i} \le h_i \le H_{2i}, i = \overline{1, M}$.

where M is number of layers in 1-D model. Since we apply the stochastic optimization method practically independent of number of parameters in question, an exhaustive search of the model is computationally quite reasonable.

We illustrate the practical relevance of our investigations by means of cross sections, constructed using results of the microtremor analyses. The positions of the presented profiles are indicated in Fig. 18. Microtremor measurements along three of 13 reconstructed profiles were carried out by request of the Geological Survey of Israel. They are profile 1 along the Qishon graben in NW-SE direction, profile 2 extending from the Qishon graben to the Hillazon graben in SW-NE direction and profile 3. As seen from the map in Fig. 2 the measurements along those parts of the profiles, which exceed the boundaries of the study area, are strongly tied to the profiles. Within the Qrayot and Haifa bay area we present 7 representative profiles illustrating our concept of determining the subsurface structure. Practically in all presented cross sections we show for comparison the depth of Top Judea Gr. according to the structural maps of Mero (1983) and Fleischer and Gafsou (2003).

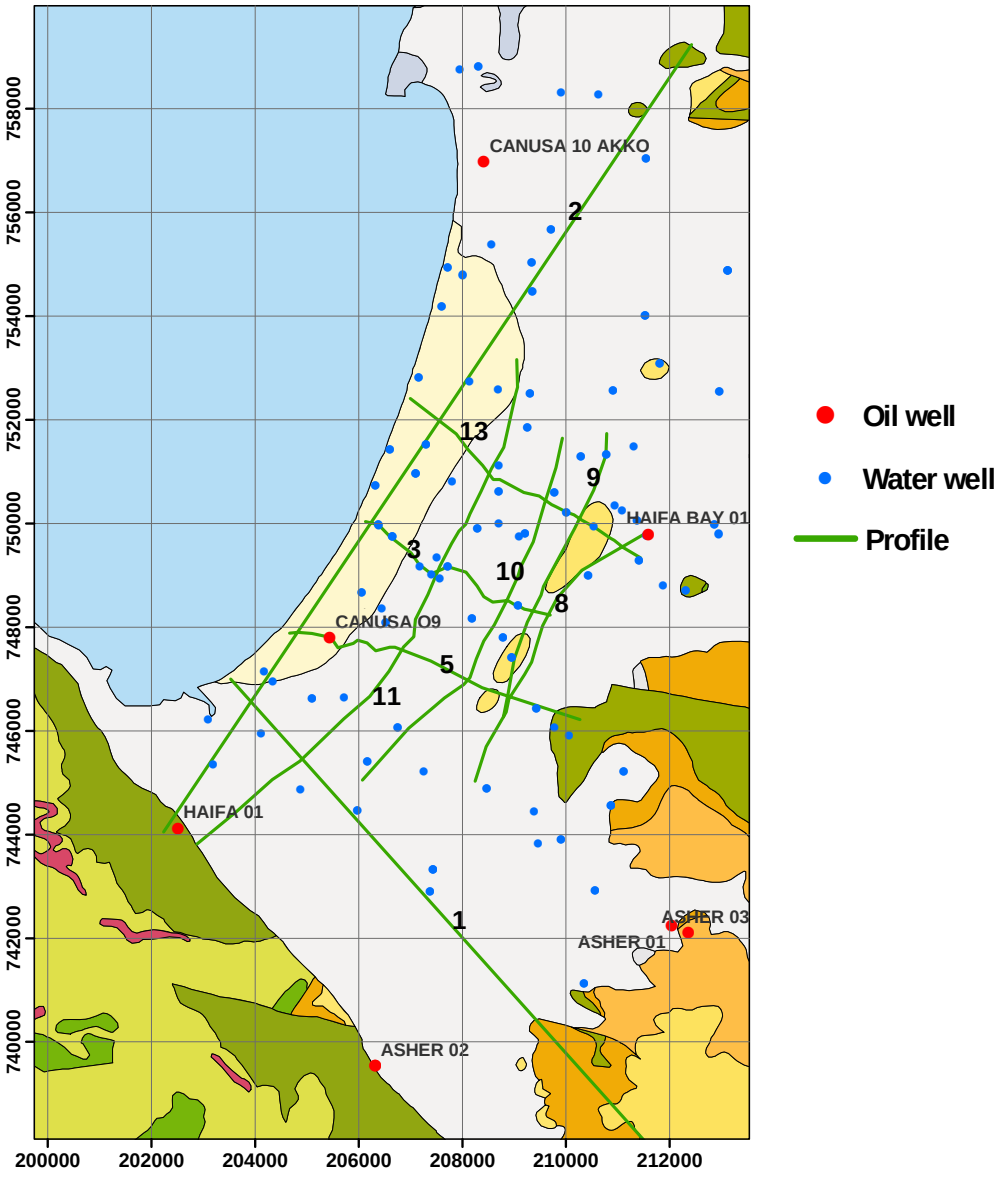

Figure 18. Map showing relative positions of the profiles chosen to illustrate application of H/V method for reconstructing subsurface structure. For legend of the geological map see Fig. 2.

9.1. Profile 13

Cross section along profile 13 is shown in Figure 19. The variations of the Fourier spectra along profile 13 are shown in Fig. 20a. The Fourier spectra for point 4 exhibit a broad area (3-6 Hz), where the horizontal components are higher than the spectral amplitude of the vertical component. This feature, clearly visible looking at the spectral ratios (Fig. 20b) relates to amplification of ground motion. Two close peaks at frequencies 3.2 and 5 Hz are observed on the H/V ratios. They are associated

with Top Judea Gr. and Kurdani Fm. respectively. The soil model for point 4 constructed on the base of SH3 well information and refraction data (SL-5 line) consists of 15 m of alluvium overlying Kurdani Fm. and Marl-chalk of Mount Scopus Gr. Depth of the lower reflector (Top Judea Gr.) derived from the measurements in compilation with the refraction data is 15 meters more than that given in SH3 well. It is explained by sharp relief of Top Judea Gr. at even short distance from the well. Further in the northwest direction the measurements were carried out at point 1 located at SH1 well. The amplitude spectra look different showing trough in the vertical spectra at frequencies of about 1.7-2.2 Hz. The H/V ratio for point 1 shows a low amplitude peak at frequency 2.2 Hz. According to SH1 well, the thickness of the Kurdani Fm. outcropping in this place is 20 meters. Below lies the marl of the Mount Scopus Gr., which overlays the Top Judea Gr. at a depth of 80 meters. The theoretical model derived is in agreement with the borehole data. One can see that at point 33 the second peak appears again on H/V ratio at frequency of 6 Hz, while the first frequency correlated with Top Judea Gr. is not changed. Point 22, which is located at SH-4 well and refraction profile SL-1 was analyzed previously (see Fig. 10). H/V ratio for point 276 is characterized by maximum amplitude level of the second peak of 8 that is confirmed by refraction profile SL-3, which detects the upper layer of 10-20 m thick with Vs=160 m/sec. This point falls into zone of higher amplitudes of the second H/V peak, which is stretching from the NNE to SSW of the study area and is distinguished in all the cross-sections directed NW-SE. Between points 266 and 276 we observed significant decrease of the fundamental frequency from 1.5 Hz down to 1 Hz, that corresponds to an increase of reflector depth from 140 m to 220 m, followed by the fault reaching the Kurdani Fm. Fault in the Top Judea Gr. is marked on the structural map of Mero (1983) as well as Fleischer and Gafsou (2003). Decrease in the amplitude level of the first peak corresponds to increase of the Kurdani thickness by 20-30 meters. We note that up to this point the estimations of the reflector depth by measurements and depth of Top Judea Gr. practically coincide. It is interesting to note that in order to get a good fit between the theoretical function and H/V ratio for this point we increased S-velocity for chalk layer underlain the Kurdani Fm. from 750-800 m/sec up to 950-1000 m/sec. The geological data confirm that marl-chalk deposits of Mount Scopus Gr. are substituted in this area by Eocene chalk-limestone. Further to the northwest along the profile the general trend of the reflector to dip is retained. Point 313 is characterized by an increase of Vs of the upper layer up to 350 m/sec. At

point 389 and more clearly at 385 we observe the third H/V peak at frequency of 5 Hz, which is correlated with the Kurkar sandstone according to the information from NH6, NH29, NH14 and NH34 wells.

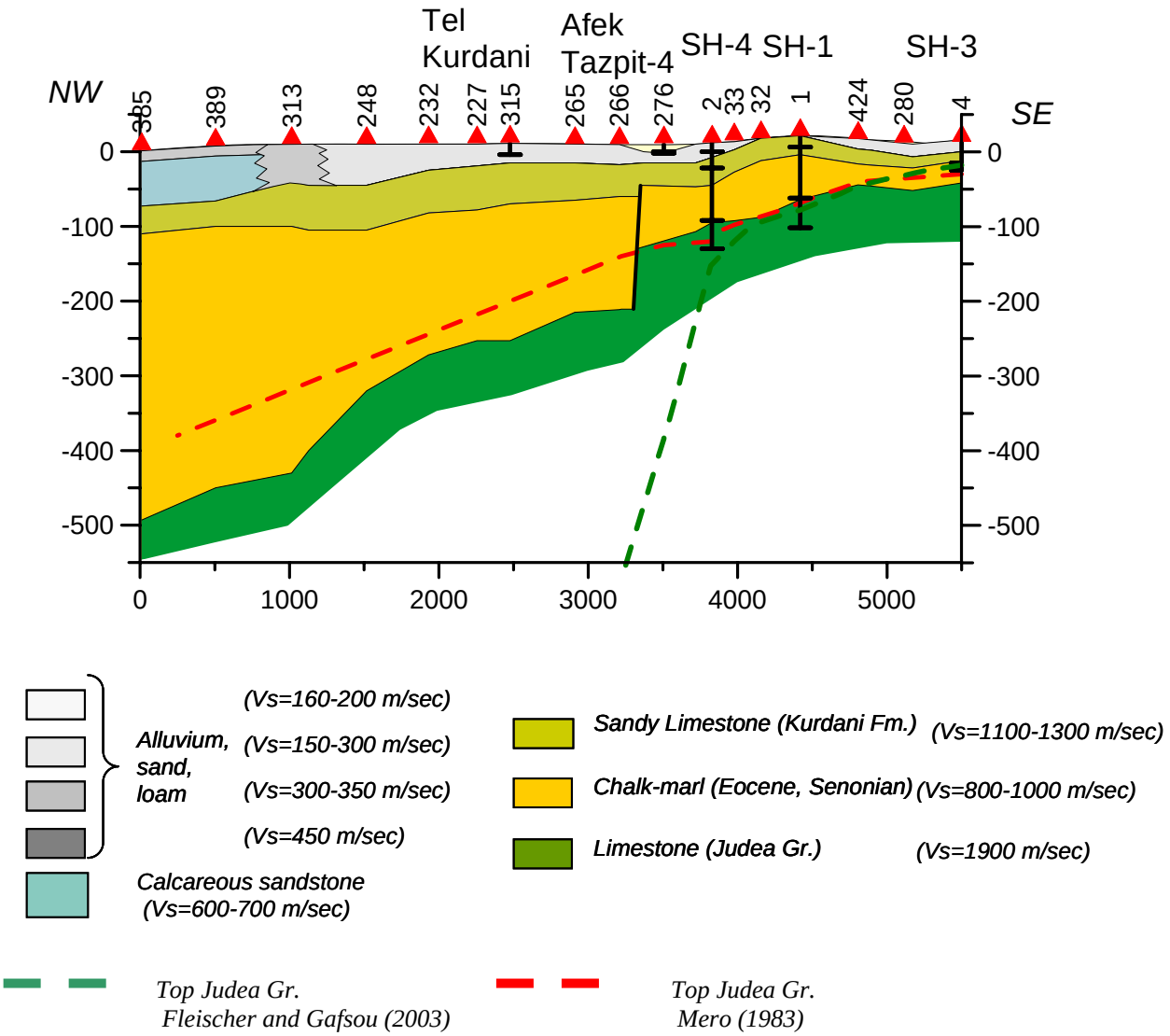

Figure 19. Geological cross section along profile 13.

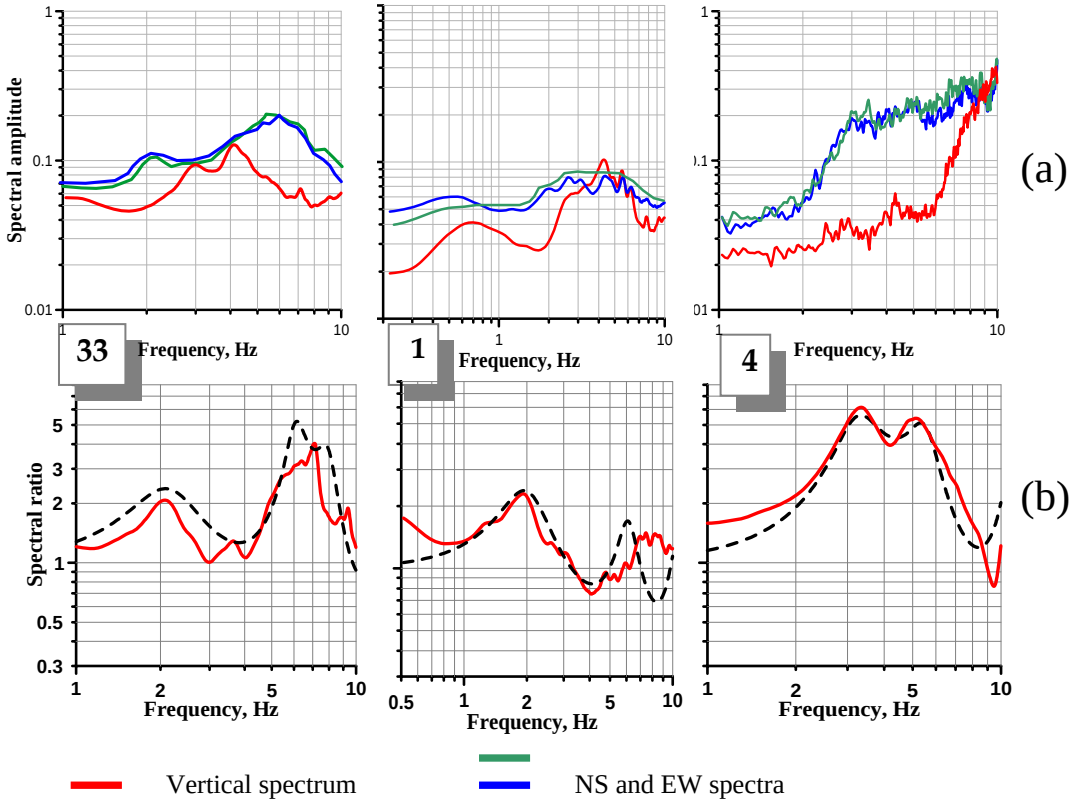

Figure 20. Average Fourier spectra- (a), H/V spectral ratios (red line) and analytical transfer functions (black dashed line) – (b).

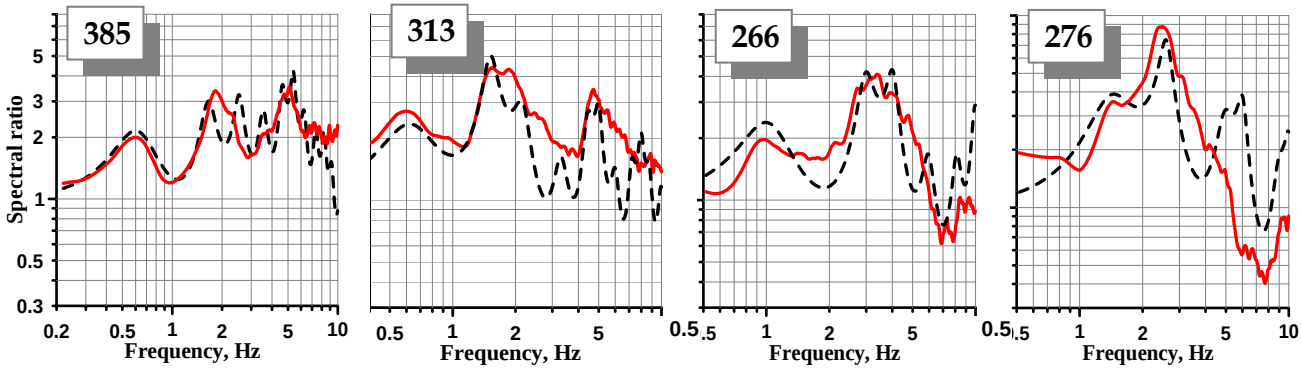

Figure 21. H/V spectral ratios (red line) and analytical transfer functions (black dashed line).

9.2. Profile 3

Figure 22 presents the simplified sketch of subsurface structure along profile 3. Figure 23a shows two horizontal and vertical components of the Fourier spectra obtained at points 408, 394, 396 and 398 located in the southeastern part of the profile 3. The common prominent feature of these graphs is the similarity of all spectra, and especially identity of the vertical components, which are almost flat in a wide

frequency range. Two areas of resonance motions, formed by two increases in the spectral level of the horizontal components at frequencies near 0.55 Hz and 3.5 Hz are distinguished in the spectra and H/V curves and indicate presence of resonance motions from two reflectors. Based on the geological map and cross sections (Kafri and Ecker, 1964) we suppose that for points 64 and 408 the Eocene-Senonian chalk and Top Judea are the shallow and deep reflectors, respectively. Ezersky (2004) using refraction survey along line SL-8 obtained Vs for the Eocene chalk layer of 950-1050 m/sec. For the alluvium layer we use the value of refraction survey SL-4 of 270-300 m/sec. Using the H/V ratios as constrains for the possible subsurface models we calculated the theoretical transfer functions matching well with H/V curves (Fig. 23b). The frequency of the first peak at points 394-396 is 0.6-0.65 Hz, which points out to decreasing depth of Top Judea Gr. from 430 m (point 64 and 408) to 390 m and is accompanied by a fault. This fault is mapped in the structural map of Mero (1983). Another fault between points 396 and 398 is detected by the shift in the first frequency from 0.6 Hz up to 0.75 Hz. The Kurdani layer appearing in the cross section already at point 396 is incorporated in the model in accordance with Hanotea-1 well. Its thickness is small and does not influence the transfer function. At point 398 the low velocity alluvium layer again appears forming a zone of the higher amplitude of the H/V second peak stretching in NNE-SSW direction over the study area (see Fig. 46). While the first resonance frequency for points 398 and 341 is the same, the second frequency is different. This difference is equivalent the change of the Kurdani thickness by 40-50 meters. Change of the first frequency from 0.75 Hz down to 0.6 Hz occurs between points 341 and 343 and corresponds to the increase in depth of Top Judea Gr. of 40 m. We relate these observations with a fault, which is identified between points 341 and 343 and is also mapped by Mero (1983) and is shown in the cross section VIII of Kafri and Ecker (1964). Analytical transfer functions that are fitted to the H/V ratios yield models, which explain the decrease of both the second resonance frequency and its amplitude by increase of alluvium layer thickness up to 40-45 meters and its S-wave velocity up to 300-350 m/sec. Theoretical model for point 90 located at Kiryat Motskin well, shown in the cross section, yields fair agreement with the well description. Approximating the H/V ratio by the theoretical function for point 478 we conclude that the reasonable match may be obtained only assuming the thickness of the upper sand and calcareous sandstone layer at least 70

meters that exceeds more than twice the thickness indicated in cross section VIII of Kafri and Ecker (1964).

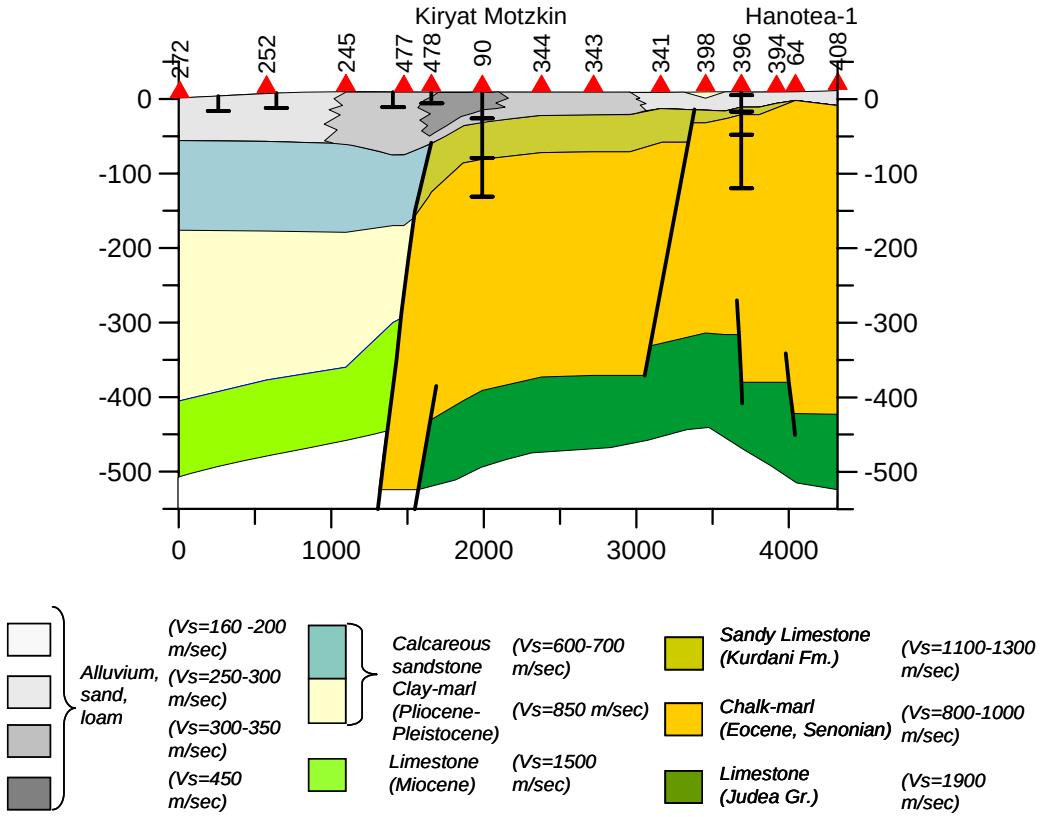

Figure 22. Cross section along profile 3.

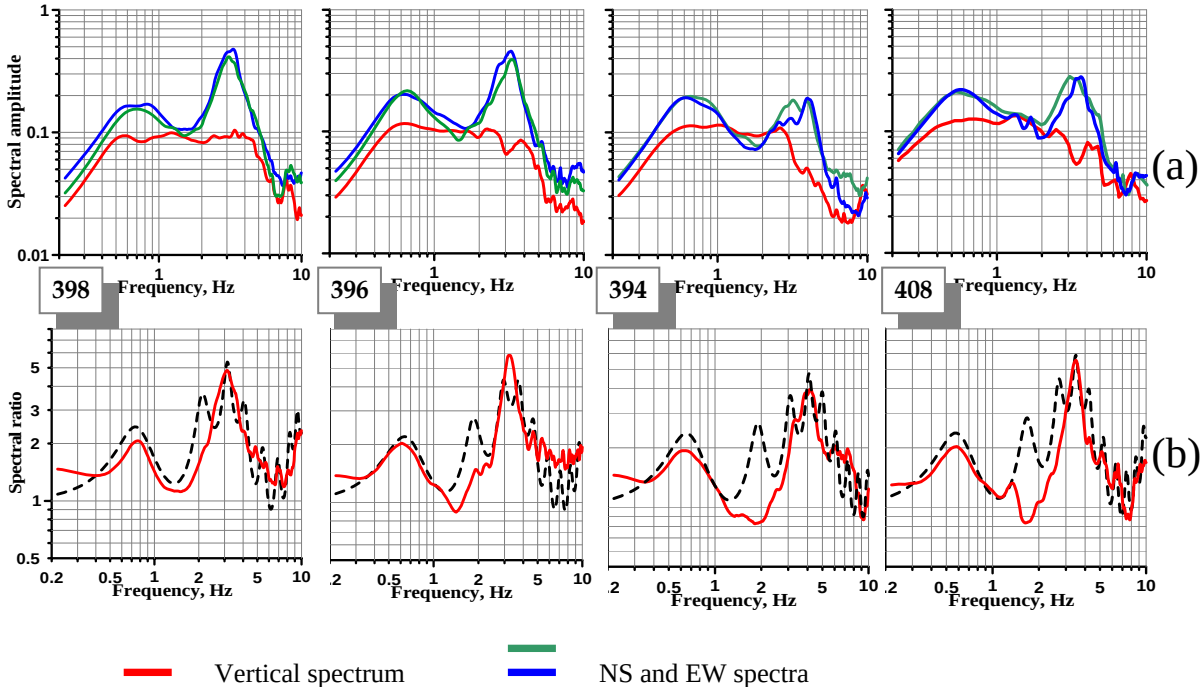

Figure 23. Average Fourier spectra (a) and H/V spectral ratios -red and analytical functions – black dashed (b) for points located in the southeastern part of the profile 3.

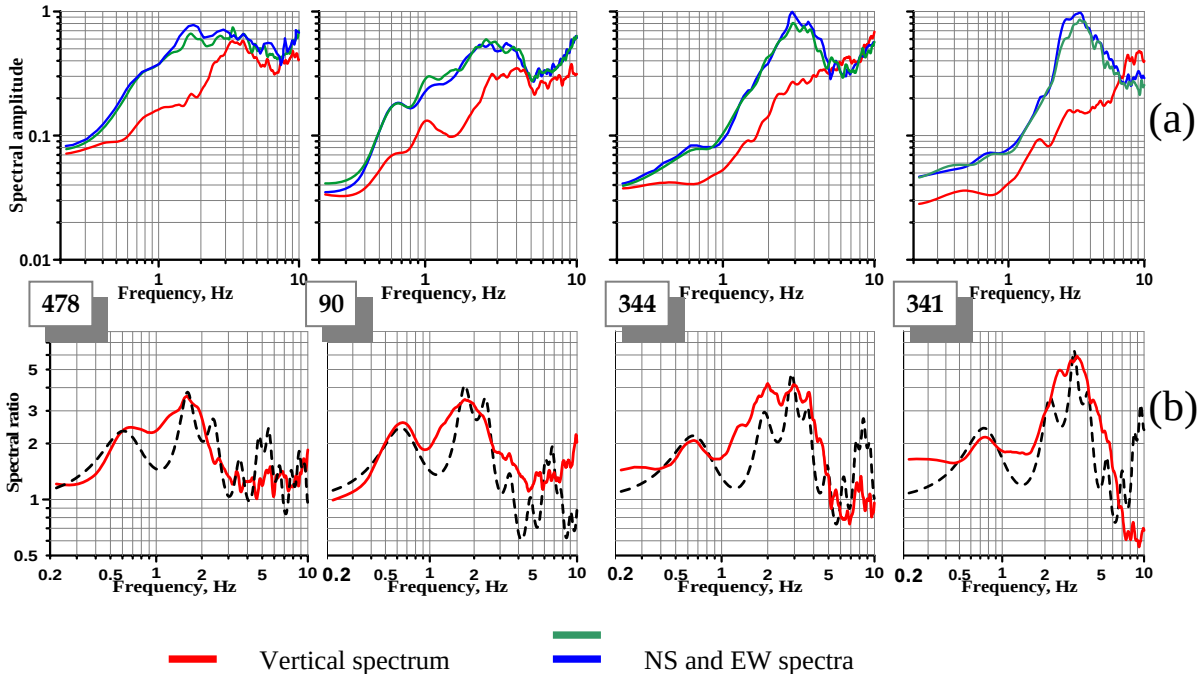

Figure 24. Average Fourier spectra (a) and H/V spectral ratios (b) for points located in the central part of the profile 3.

Point 477 is located at Motskin 4 well, which penetrates 15 meters of the sand and calcareous sandstone. The first attempt to calculate the theoretical transfer function is based on the model derived for point 478. As seen in Fig. 25 the second peak of the H/V curve is not fitted. The analytical function calculated on the basis of velocity structure like in the Qishon graben yields too high amplitudes. Trials to match the theoretical function are not successful until we reach the conclusion, that Top Judea Gr. is too deep to be considered as a reflector, and the reflector is probably the Lakhish Fm. together with underlying Avedat Gr. The optimal transfer function is shown in the same figure by the black line. Analytical functions for points 245, 252 and 477 are calculated based on the assumption of the velocity structure typical for the Qishon graben (Fig. 26) and obtained by modeling at Canusa-9 well.

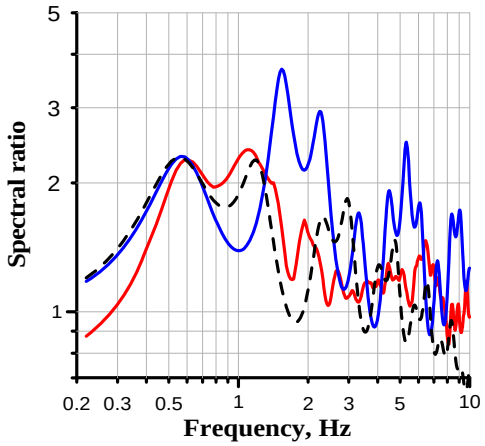

Figure 25. Trial (blue line) and optimal (black dashed line) analytical transfer functions compared with H/V spectral ratio (red line) for point 477.

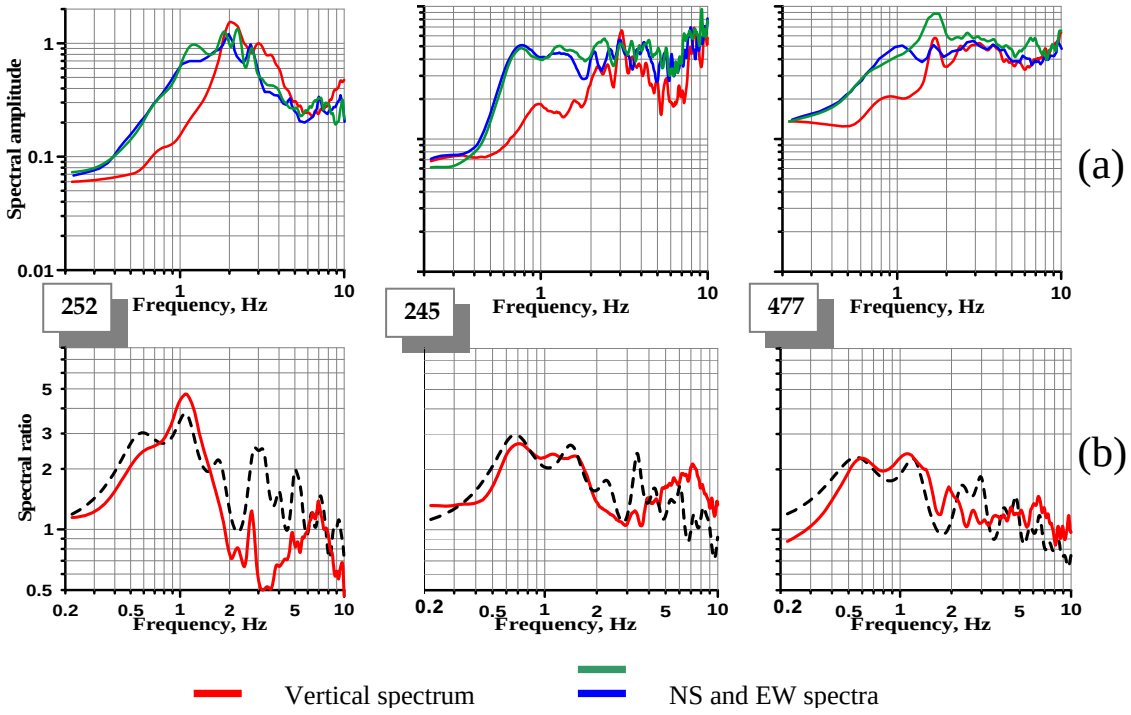

Figure 26. Average Fourier spectra (a) and H/V spectral ratios – red and analytical functions – black dashed (b) for points in the northwestern part of the profile 3.

9.3. Profile 5

Starting-point of profile 5 is located on the outcrop of the Senonian chalk (Fig. 27). In Fig. 28 one can see H/V spectral ratio obtained at point 163, which exhibits single low amplitude peak at frequency 0.55 Hz. According to our calculations the depth of reflector represented by limestone of Top Judea Gr. is about 400 meters.

Point 149 is characterized by two peaks. First one is located at frequency 0.6 Hz and is related to the Top Judea and the second one appears at frequency 4.5 Hz owing to alluvium layer of 15 meters thick overlying the Senonian chalk. Point 148 exhibits the low frequency of 0.5 Hz that indicates dipping of Top Judea Gr. at a depth of approximately 450 m. According to the geological data points 148 and 460 are located on the Kurdani outcrop. However, while the single peak on the H/V ratio for point 148 confirms the presence of only one reflector- the Top Judea Group, the second peak at frequency 6-7 Hz (point 460) indicates an alluvium layer of 10 meters thick. The frequency of the first peak, meanwhile, increases from 0.5 up to 0.75 Hz for point 148 and 460 respectively. We presume a fault between these points. It should be noted that the fault with uplifted eastern side is detected in this place by Mero (1983), while results of microtremor measurements yielded the opposite picture, i.e. the eastern side is downcast. Similar picture we observe on Profile 3 (see Fig. 23; points 394 and 396). According to the structural map of Top Judea Gr. there is no fault in this location.

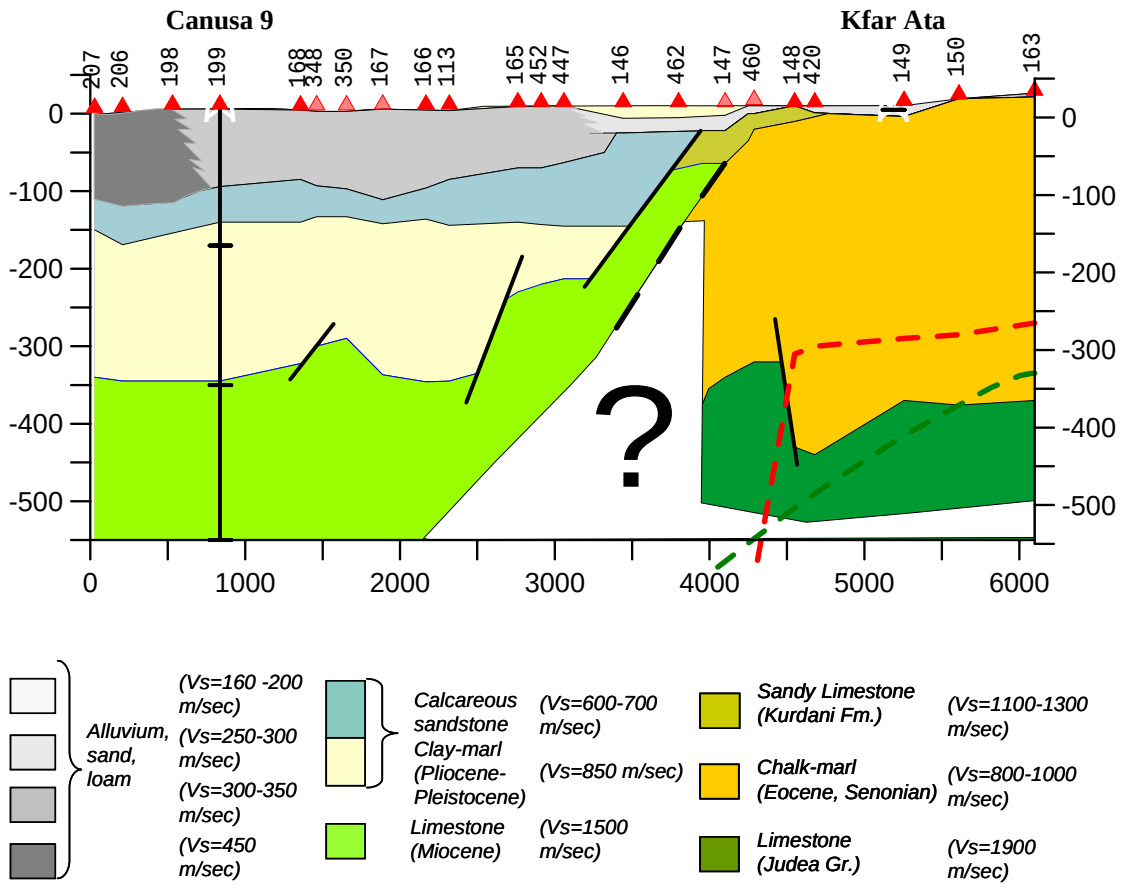

Figure 27. Cross section along profile 5.

Amplitude 7 for the second H/V ratio peak at point 147 supports the idea about presence of low velocity layer providing high amplitude zone that was already mentioned in Profile 3. Considering this layer in the theoretical model we obtain good agreement between the H/V ratio and calculated transfer function. Thickness of the Kurdani Fm. reaches 45 meters.

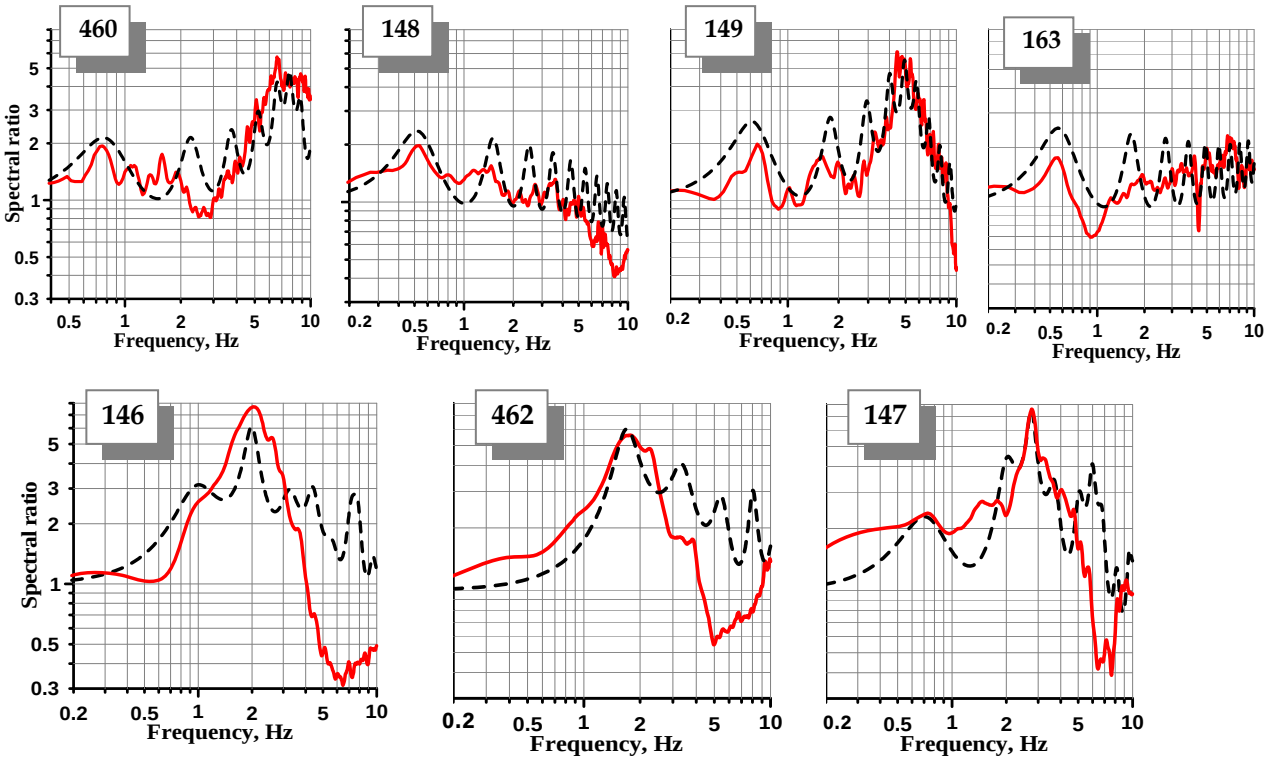

Figure 28. H/V spectral ratios and analytical transfer functions along profile 5.

If we look at H/V ratio of point 462, we see a single peak at frequency of 1.7-2 Hz with amplitude of 5. It is obvious that the Top Judea Gr. cannot be considered as a reflector for this point. We suppose that the geological structure at sites in question is similar to structure in cross section X of Kafri and Ecker (1964), at Usha 9 and Usha 11 wells. Gravels and calcareous sandstone of the Kurkar Gr., found here according to Mero (1983), overlay the Kurdani Fm. and below the Neogene deposits, while the Judea Gr. is too deep. Modeling this situation we obtain a fair agreement between the H/V ratio and theoretical function. However, bearing in mind that the problem of model selection in multi-layer system especially in case of one peak does not have a simple solution, we put on the cross section "question-mark". Another solution is, for example, using Ziqlag Fm. as a reflector. H/V ratio for point 146 can be hardly approximated by one-peak model, and therefore we consider two-peak-model. The

first indistinct peak is at frequency 1 Hz and the second at frequency 2 Hz. The soil column model explaining these peaks consists of sand and sandy loam layer overlying the Kurkar Gr., thickness of which increases up to 120 m. It is assumed as a shallow reflector. We note that our estimate of upper reflector depth coincides with estimate of Mero (1983). The deep reflector is the Ziqlag Fm. of Neogene age. Thus, our subsurface model suggests that close to points 147, 460 and 462 there is a fault with downthrown west wall. H/V ratios of points 447, 113, 206 and 348 (Fig. 27) are approximated by the model based on the velocity structure of the Qishon Graben. While the first resonance frequency at point 447 is 0.75 Hz (Fig. 29), at point 113 it decreases down to 0.6 Hz. We suppose here a fault. It is detected also by Mero (1983). Moving to the west along the profile we observe closing in two resonance frequencies owing to increase of the upper low-velocity layer thickness. Some decrease in the amplitude value at point 206 located at the seacoast is likely connected with increasing velocity of the upper layer.

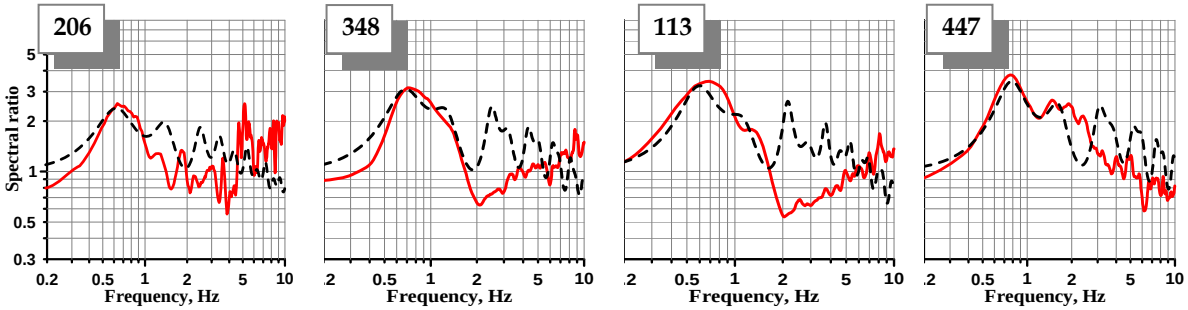

Figure 29. H/V spectral ratio and analytical transfer functions.

9.4. Profiles 8 and 9

Profile 9 directed NNE – SSW begins in the Central Horst is shown in Fig. 30a. The horst location one can see in Fig.3. H/V spectral ratio for point 7 shown in Fig. 31 demonstrates two resonance peaks: the first one, low-amplitude, is observed at frequency 0.9 Hz and the second one is at frequency 2.5 Hz with amplitude 5. Lithological section which generally characterizes the profile 13 from top to bottom is composed of alluvium, the Kurdani limestone, Senonian marl-chalk overlying the limestone of Top Judea Gr. The theoretical transfer function calculated taking into account SH-5 well data yield good agreement with the H/V ratio. H/V ratio at point 38 exhibits a first peak frequency of 1.7 Hz. In accordance with our models, the depth

of the Top Judea Gr. decreases from 230 m down to 120 meters. Between points 438 and 38 we assume a fault, which is confirmed by both structural maps of Mero (1983) and Fleischer and Gafsou (2003). We observe another fault with vertical displacement of 40 meters between points 32 and 94. Point 67 having the fundamental frequency of 0.8 Hz is a point of intersection of two faults (see Fig. 30b). The first one is directed NW-SE and the second one is directed NNE-SSW. Points 409, 95 and 413 are located on the uplifted east side of the NNE-SSW fault. In order to clear these explanation we resort to the map of distribution of the first resonance frequency, which is presented and analyzed in details in section 10. As one can see in Fig. 30a, seismic reflection survey along profile GP-0206 (Medvedev, 2004) traces faults at the same locations. In accordance with our models point 394 is located in graben. At this point the first resonance frequency sharply decreases, that corresponds to increase of the Top Judea depth up to about 400 m. The faults between points 422 and 421 are fixed also in the structural map by Fleischer and Gafsou (2003).

The cross section along profile 8 is shown in Fig. 30c. As we can see in the location map (Fig. 18), big part of this profile is located nearby profile 9. They diverge in their northern edges only. We analyze this profile due to very complicated geological conditions and different geological interpretations of fault locations in this area. It is interesting, that in the common part of these profiles all structural elements in the relief of the Top Judea Gr. that are distinguished in profile 9 are confirmed in profile 8. As was already mentioned, the northern part of the profile 8 does not coincide with profile 9. It begins at point 5 located at well SH-10 and crosses at this point profile 5.

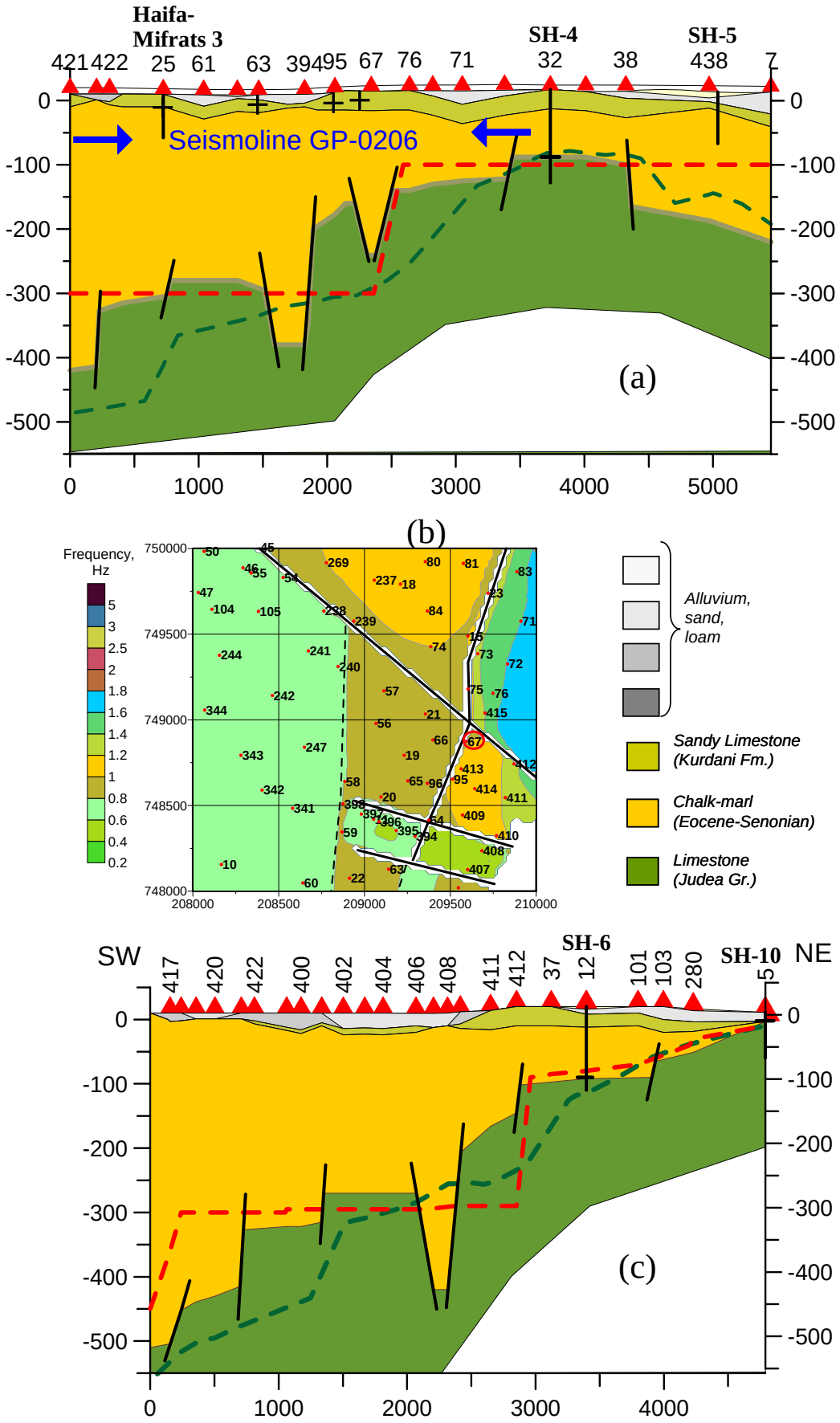

Figure 30. Cross sections along profiles 9 (a) and 8 (c); fragment of the first resonance frequency map (b).

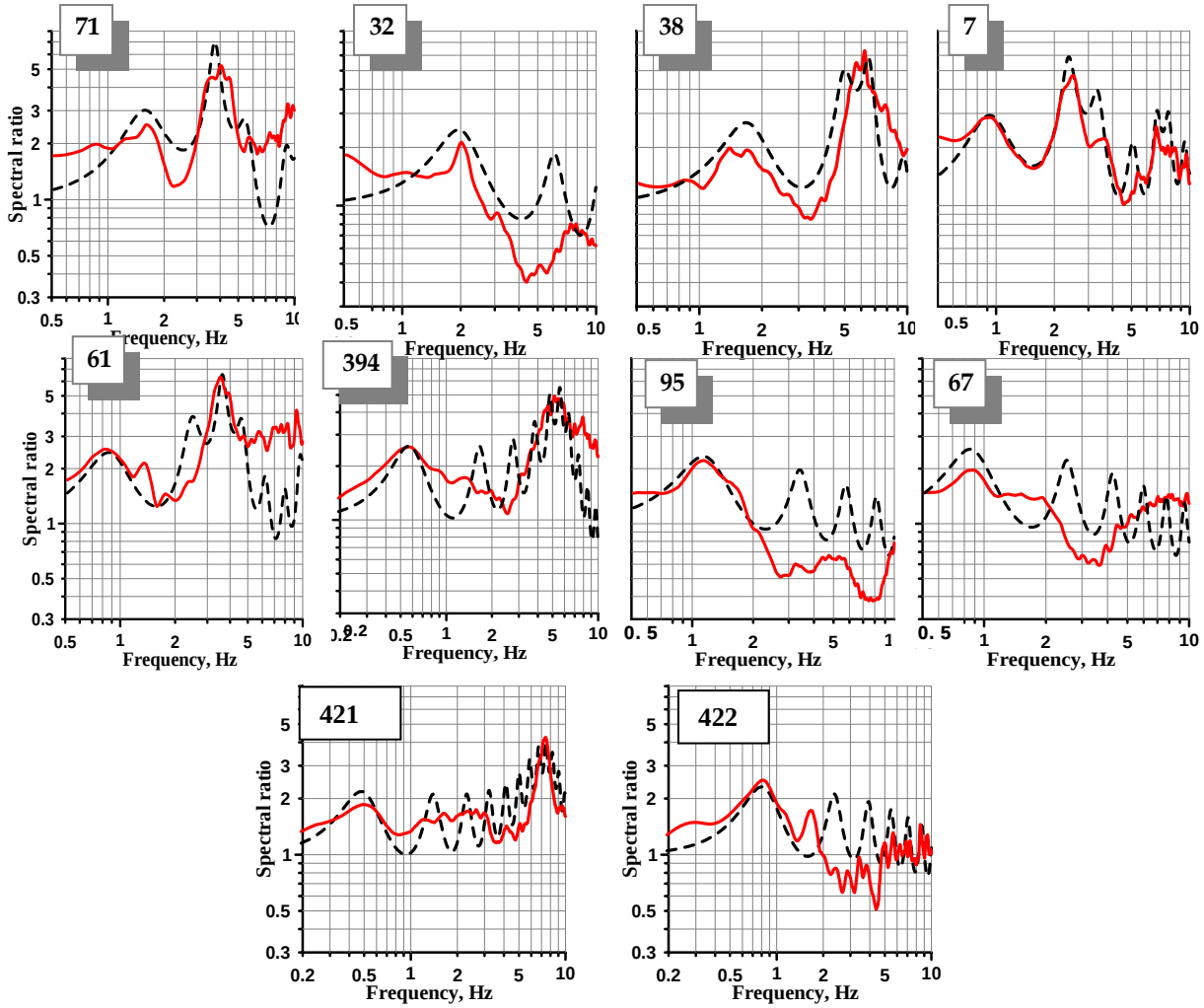

Figure 31. H/V spectral ratio and analytical transfer functions along profile 9.

9.5. Profile 10

Profile 10, cross section of which is depicted in Figure 32, passes through the zone characterized by the higher (up to 10) H/V amplitude. Such amplitude values we observe on profiles 5, 3 and 13 crossing this zone that are above described. It is also of interest to track the structural elements which are detected in profiles 8 and 9 passing parallel to profile 10 (see Fig. 18 for location). The following conclusions are made based on the analysis of the measurement results: the layer with Vs=160 m/sec is present along profile 10 with exception of points 59 to 467; three faults which are revealed below points 391, 36 and 57 are traced in the both profiles 8 and 9; at point 59 we observe decrease in the amplitude, the low velocity layer is tinning out and no indications of a fault. It means that the graben observed on profiles 8 and 9 is not

found in profile 10. It is limited by the fault directed south north and is identified in profile 3 (Fig.22).

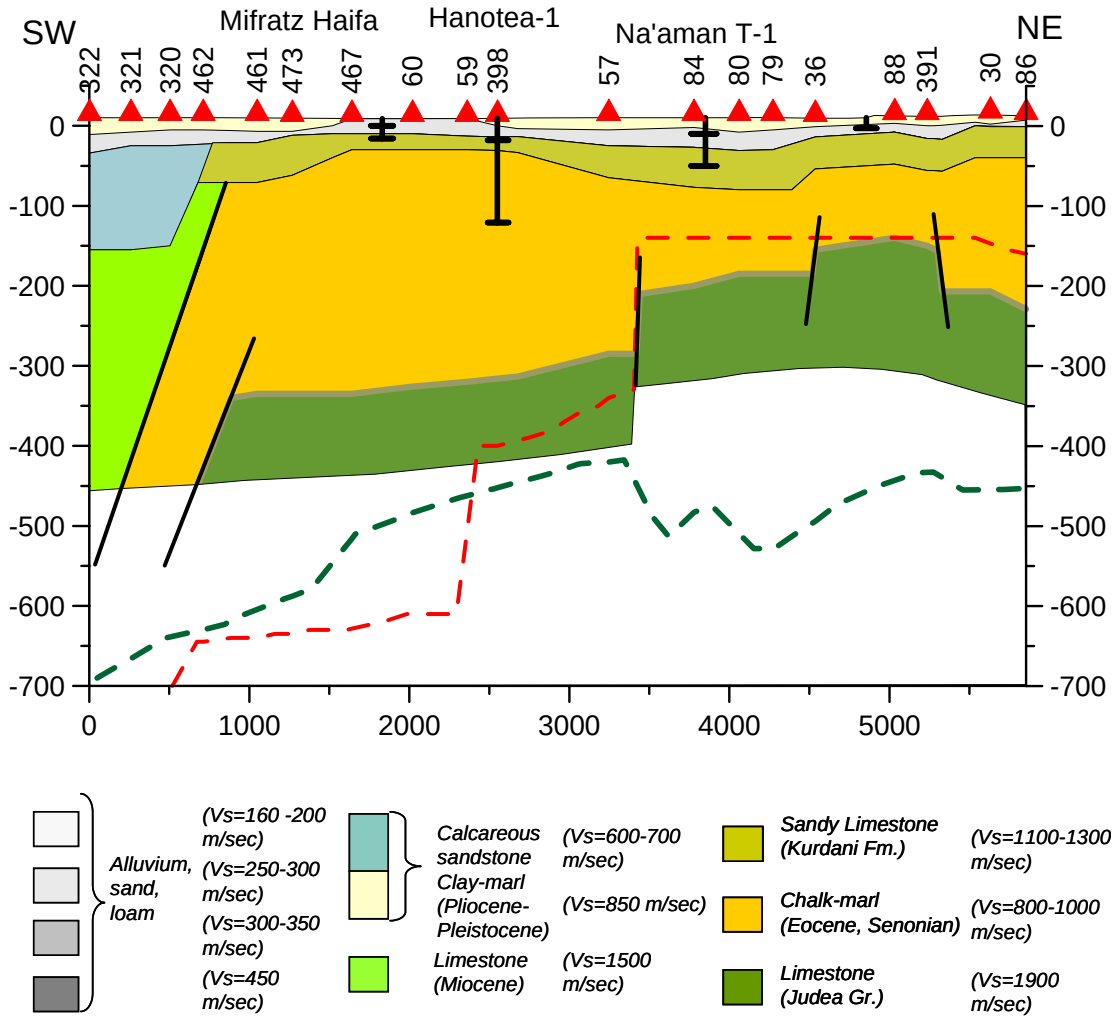

Figure 32. Cross section along profile 10.

H/V ratio for point 320 shows the first and second frequencies, which can be hardly separated one from the other and both form the wide area of resonance in the frequency range from 1 Hz up to 3 Hz. It indicates that geological conditions are different and this point is located within the Qishon graben.

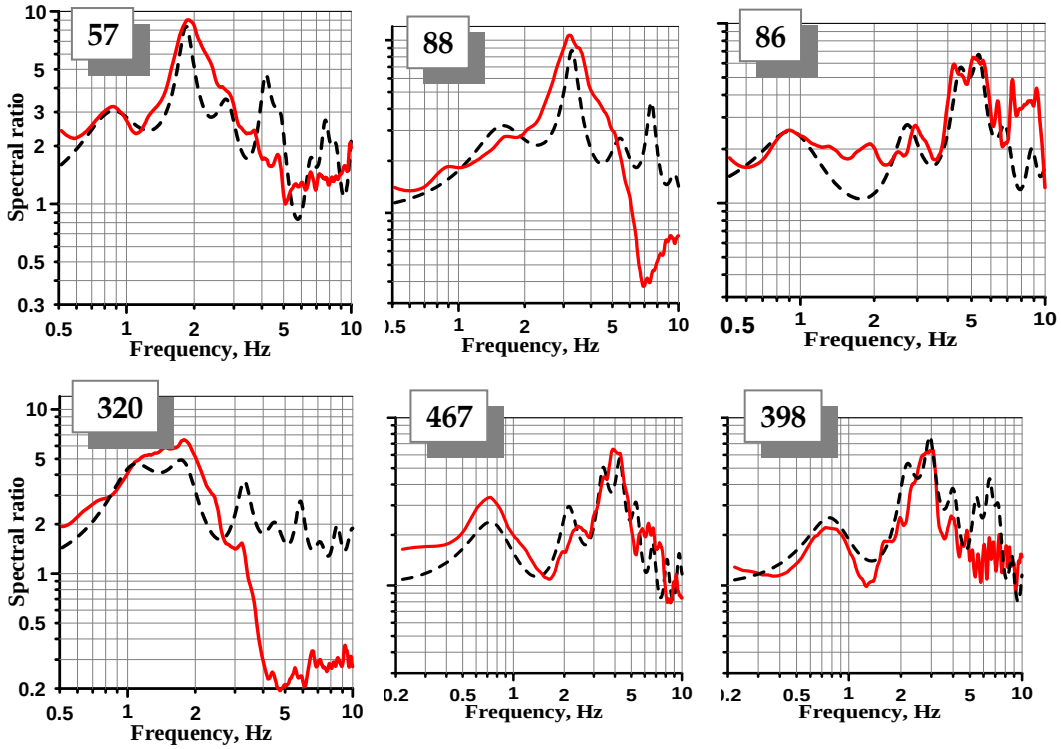

Figure 33. H/V spectral ratios (the red line) and theoretical transfer functions (the black dashed line) along profile 10.

9.6. Profile 2

Profile 2 (see Fig. 34), which is 18 km long, is one of two profiles designed at request of the Geological Survey. It crosses from the northeast to the southwest the main block structures known in this area: the Hillazon graben, the Central Horst and the Qishon Graben indicated in Fig. 3. H/V spectral ratios for points from 309 to 307 (Fig. 35) have amplitude of the first peak 2-2.5 typical for the lithological structure using Top Judea Gr. as a reflector. The H/V ratios for points 309-310 show the second peak at frequencies of 3.5 Hz and higher due to the alluvium layer overlying the Eocene chalk. Point 307 has a single peak at frequency 0.85 Hz, because the Eocene chalk crops out. Comparison between points 316 and 307 shows that though both points are characterized by a single peak, H/V amplitude level for point 316 is double the amplitude at point 307. It looks as if point 316 is located in the Hillazon graben. H/V ratios for points 316-255 demonstrate the single peak at frequencies from 1.1 Hz down to 0.9 Hz with amplitude of about 4 units. According to Acco T/1 well data, the alluvium layer of 70 meters thick overlays the 70 meters of Kurdani Fm., which is

underlain by limestone and chalk of Miocene age. The fault between two structural blocks (horst and graben) according to the geological maps must be 300 meters to the north. H/V ratio for point 296 in comparison with point 255 appears to be different. The first amplitude of about 2 indicates the deep reflector that is, probably, again the Top Judea Gr. and this point is at the Central Horst. From point 296 to 254 we observe H/V curves stable enough, i.e. the first peak at frequency 0.65-0.7 Hz with low amplitude and second peak at frequencies of 1.5-1.7 Hz and higher amplitude. Typical representatives of these points (296 and 313) are shown in Fig. 36. According to the both structural maps of Mero (1983) and Fleischer and Gafsou (2003), in the vicinity of points 381-384 several faults can be found. However, since the first resonance frequency at these points changes insignificantly, we do not have clear indications of these faults.

Point 253 is characterized by the first peak at frequency 0.55 Hz and the second peak at frequency 1.1 Hz. Point 253 is located close to the refraction line SL-7, S-wave velocity-depth section of which is shown in Fig. 37. The theoretical model for point 253 (see Fig. 38) is calculated considering the results of the refraction survey, which indicates a presence at a depth of 45-50 meters of a layer with Vs=650 m/sec. This velocity is associated with calcareous sandstone of the Kurkar Gr. and Pliocene clay that, in turn, is found in the Qishon graben. At points 253 to 169 variations in frequency and amplitude of both the first and second peaks are local and may be explained by variation in velocity of the upper layer and depth of the reflector (limestone of the Ziqlag Fm.). At points 169 and 212 the increase of the first resonance frequency corresponds to a decrease of the depth of Ziqlag Fm. We derive this horst also in Profile 11 (see next section). Here a series of faults is observed by Mero (1983) and Fleischer and Gafsou (2003). These faults are located near points 173, 142 and are confirmed by our measurements.

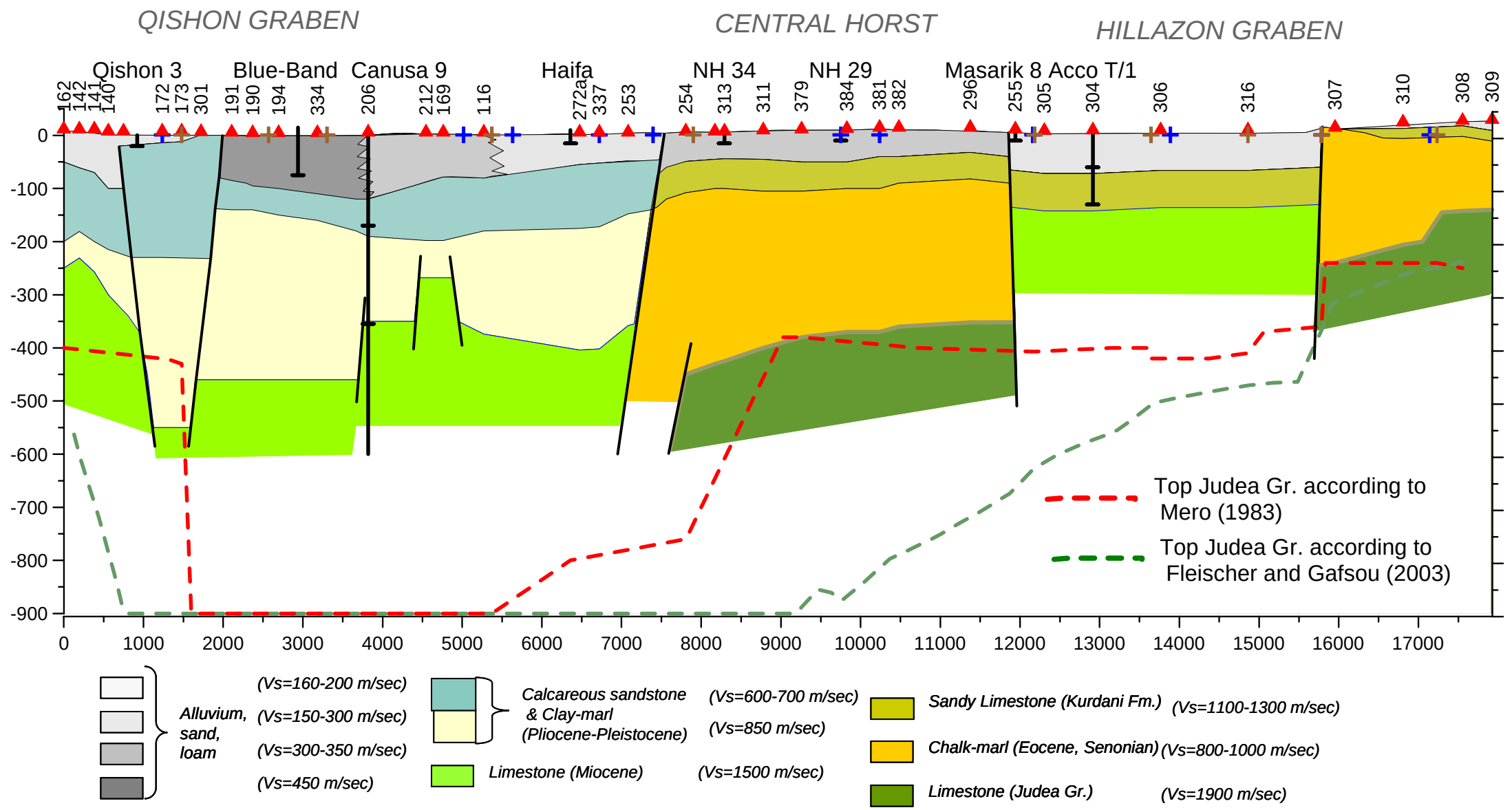

Figure 34. Cross section along profile 2.

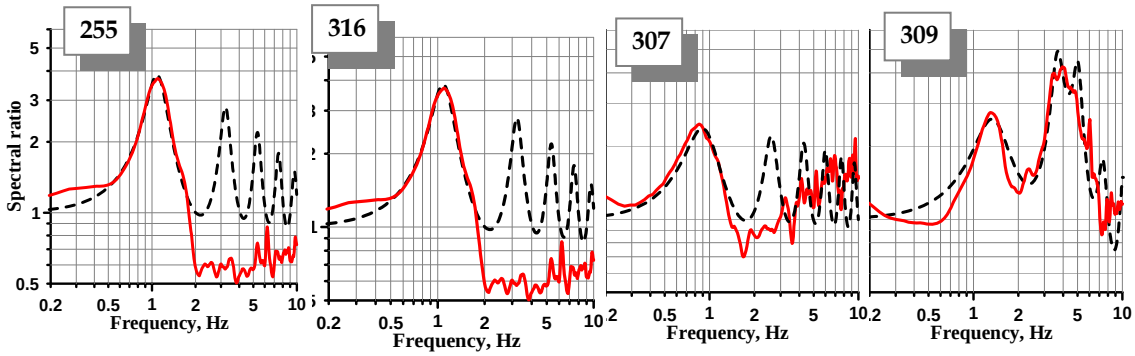

Figure 35. H/V spectral ratio and theoretical transfer functions.

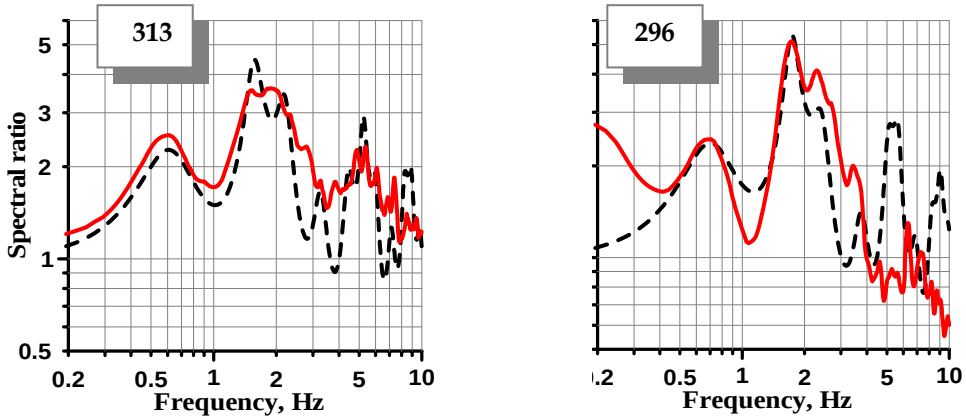

Figure 36. H/V spectral ratio and theoretical transfer functions for points 212 and 296 located at the Central Horst.

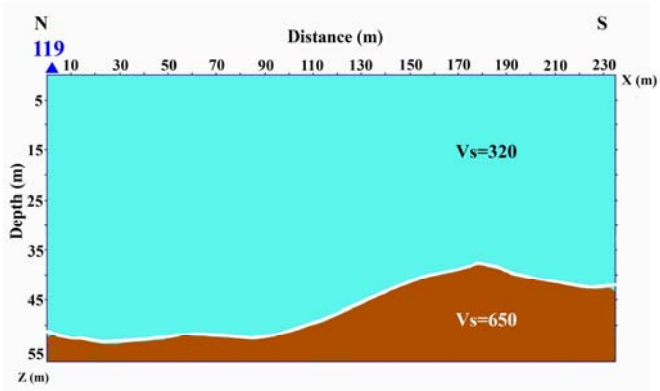

Figure 37. Velocity-depth section for S-wave along refraction line SL-7.

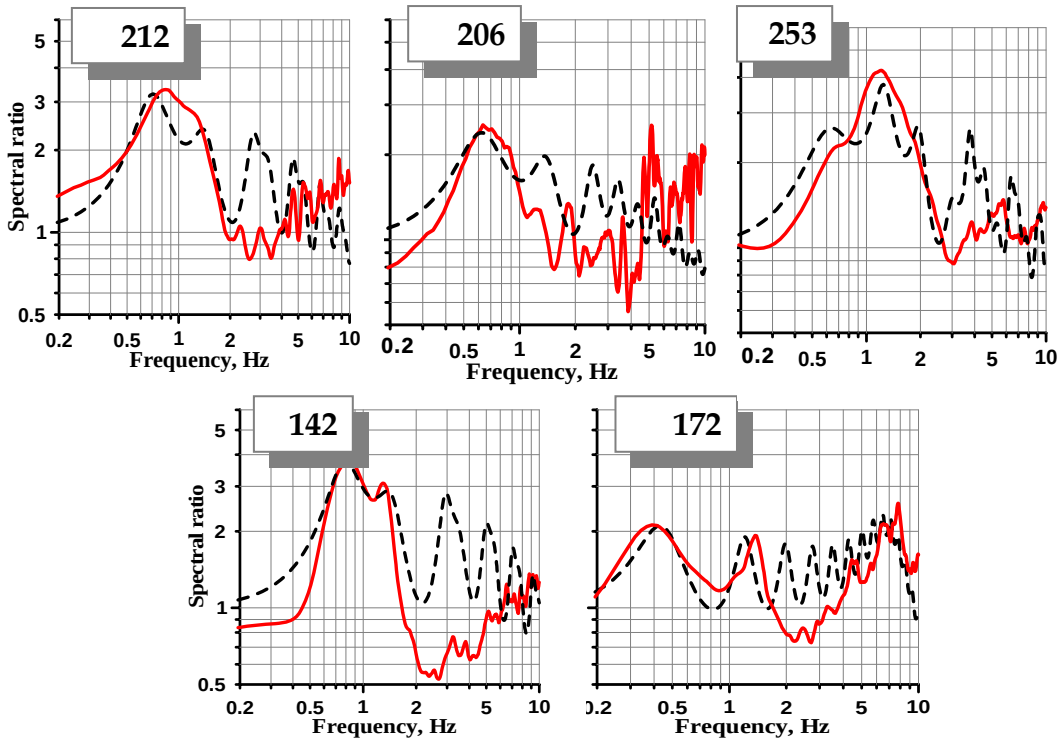

Figure 38. H/V ratios and theoretical transfer function for point located within Qishon graben.

9.7. Profile 11

The cross section along profile 11 (Fig. 39), which is constructed on the basis of measurements, agrees generally with the neighboring cross sections along profile 10 and 2. Therefore, from a number of measuring points located along the profile we can demonstrate only those that indicate discontinuities of subsurface model. Such situation we have in the transition from the Central Horst to the Qishon graben. For comparison, in Fig. 40 three points are depicted (295, 226 and 89) on the Central Horst and three points (111, M17 and 378) within the Qishon graben. The transition, we suppose, occurs between points 89 and 111. The characteristic indication of the model alteration is a change of balance between amplitudes of the first and second peaks that implies in turn a change of both deep and shallow impedance contrasts. The absolute amplitude level is varied as well. Point 378 is distinguished from points M17 and 111 by high amplitude of the second peak and different resonance frequencies (1 Hz and 1.8 Hz vs. 0.6 Hz and 1.3 Hz at point M17). It is explained by local decrease of Vs for upper layer and sharp slope of the top Ziqlag Fm. We note that due to sparse measurement grid in the eastern part of profile 11 (from 369 to 446) we suggest the existence of fault between M17 and M26 and do not show any local structures.

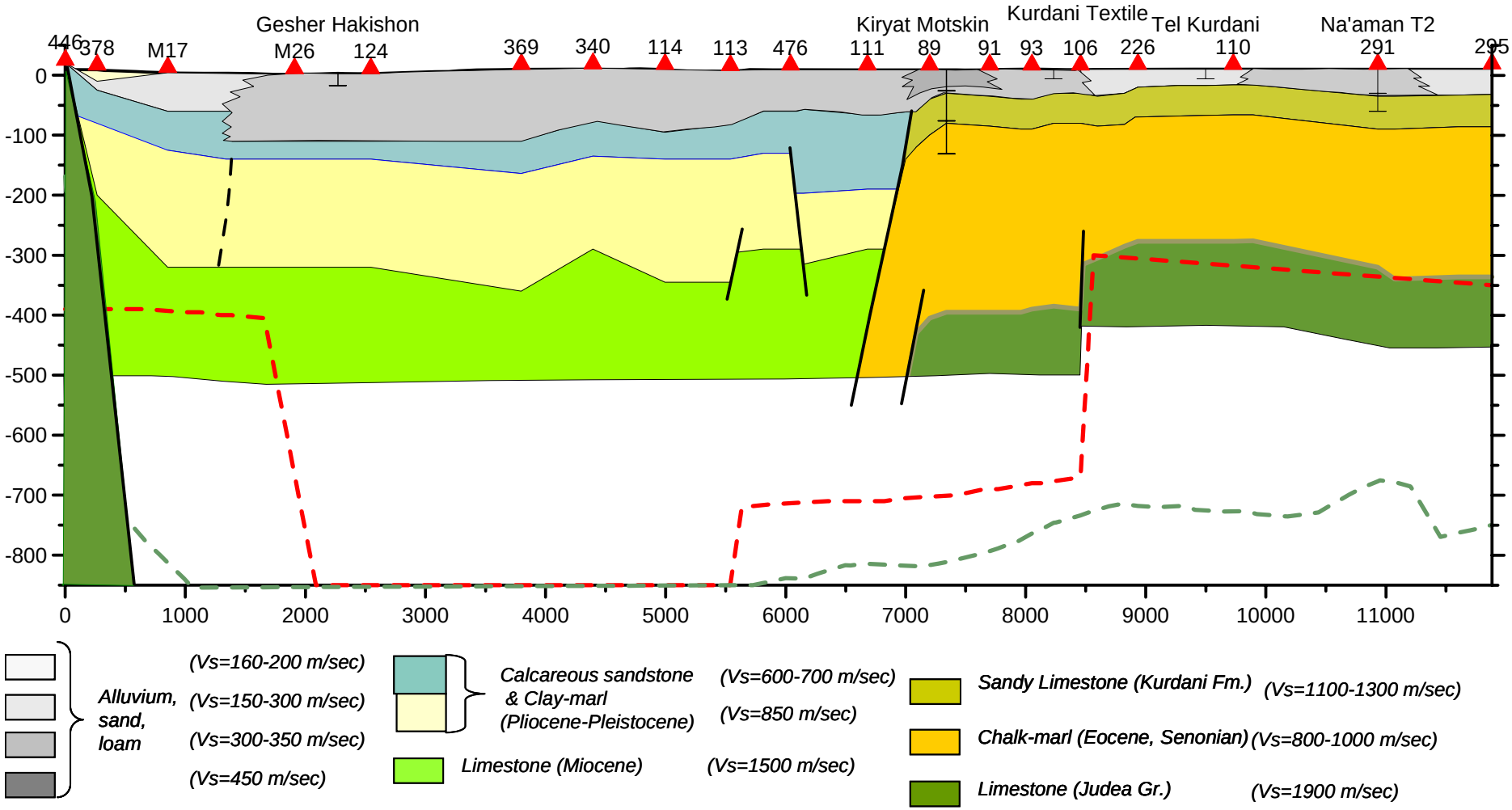

Figure 39. Cross section along profile 11

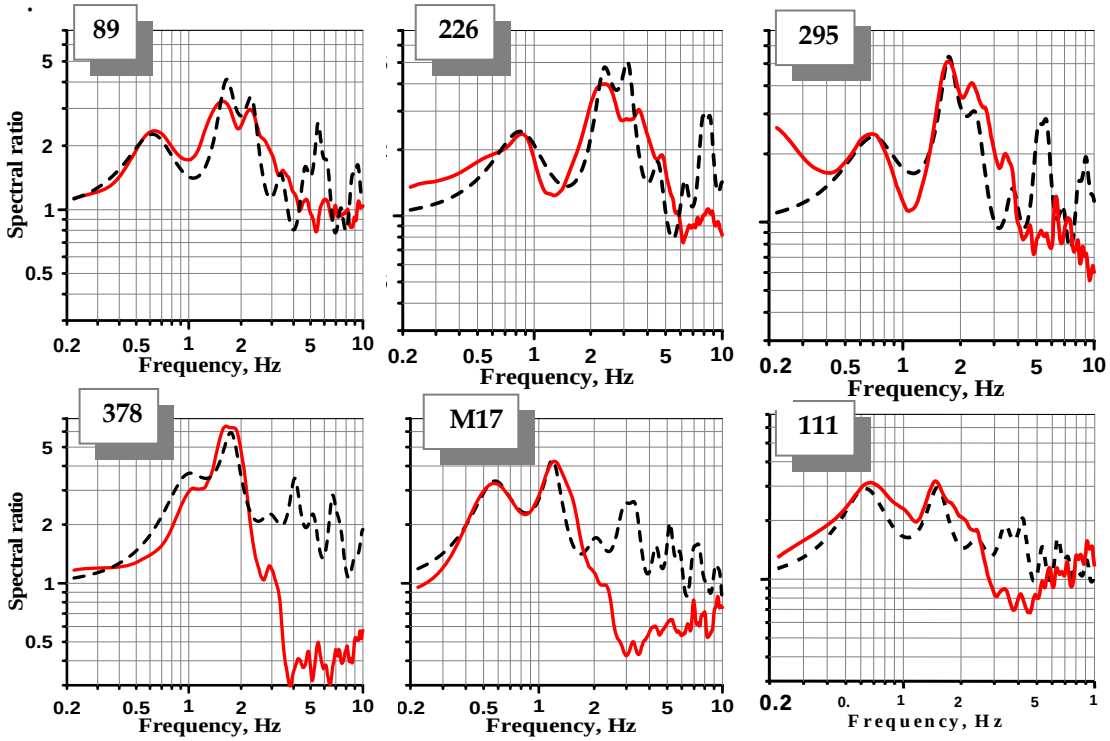

Figure 40. H/V ratios and theoretical transfer function for point located along profile 11.

9.8. Profile 1

The geological cross-section over Qishon Graben reconstructed using H/V microtremor measurements is displayed in Fig. 41. For comparison, the depth of the Top Judea Group according to the structural map of Fleischer and Gafsou (2003) (green line) is shown on the cross section. One can see that points 136-134 (Fig. 42, from the southwest to the northeast) are located on the outcropping Eocene chalk overlying the limestone of the Judea Group. The values of depth to reflector that is either calculated via modeling or taken from the structural map are in a good agreement. S-velocity for Eocene-Senonian rocks overlying the Judea Gr. is in accordance with the refraction survey along line SL-8, which was carried out close to points 260-262 (Fig. 43). The sharp increase in the fundamental frequency from 0.6 Hz up to 1.5 Hz that is observed between points Q134 and Q133 confirms the presence of a fault, marked in the structural map of the Judea Gr. (Fleischer and Gafsou, 2003). However, the vertical shift estimated by measurement data exceeds significantly the geological estimation.

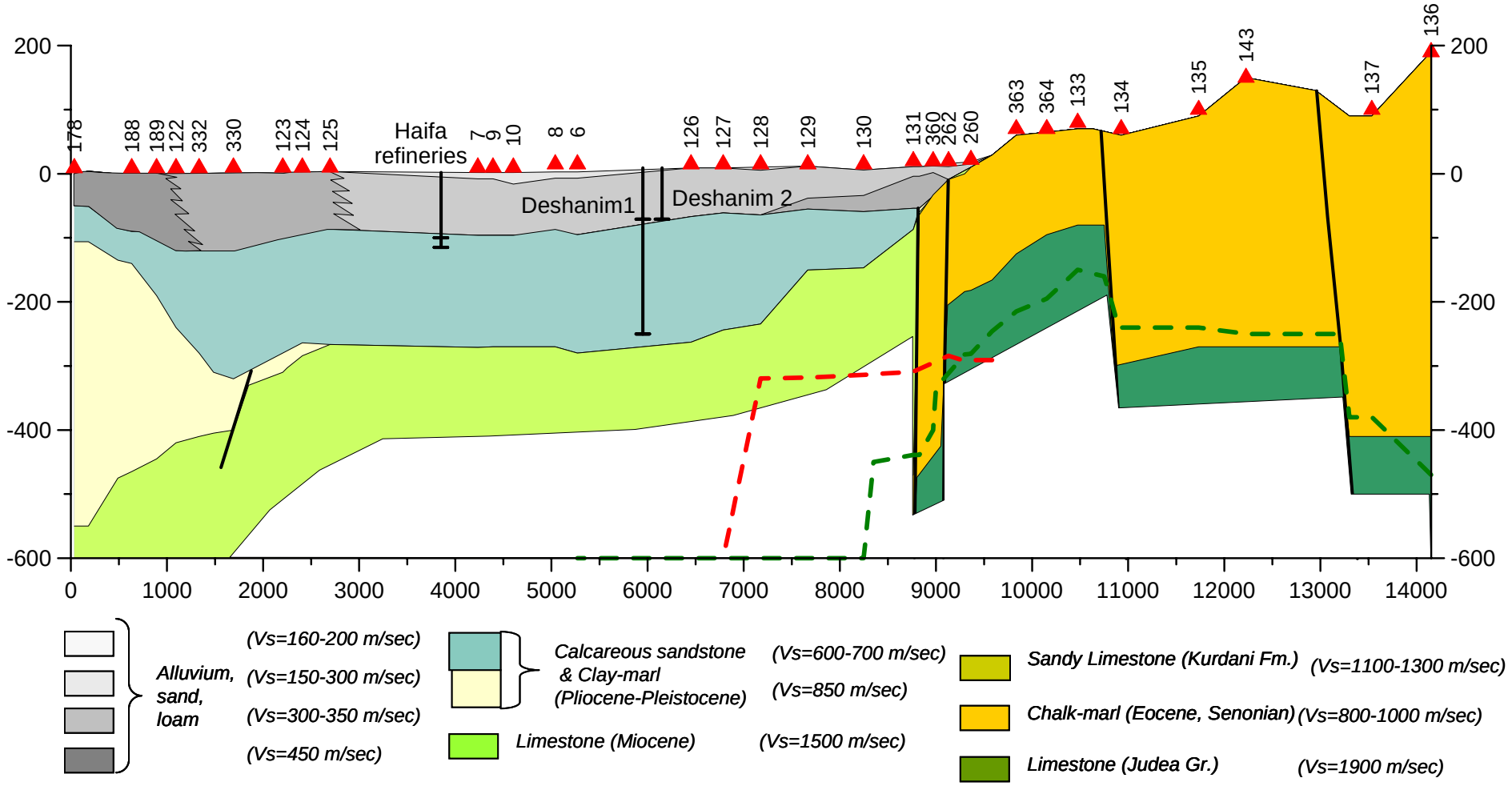

Figure 41. Cross section along profile 1

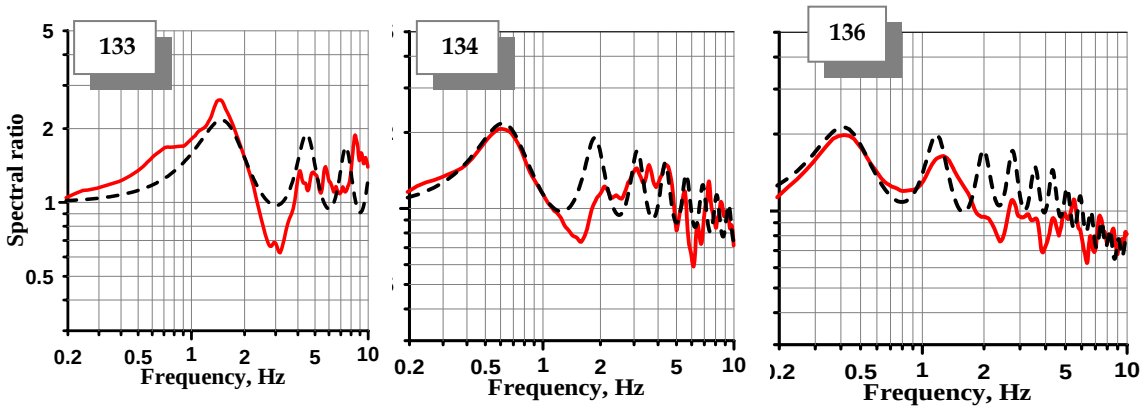

Figure 42. H/V ratios and analytical transfer functions for points 133, 134 and 136.

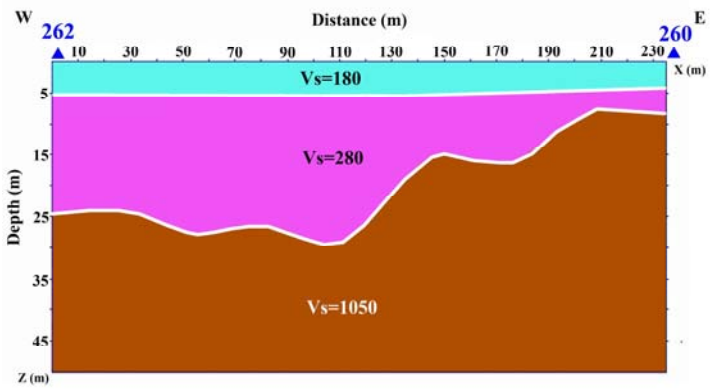

Figure 43. Velocity-depth section along refraction line SL-8.

Fig. 44 shows points 260-262 that are located along the refraction line SL-8. They are characterized by two peaks at frequencies of about 0.6 Hz and 1.2 Hz and a prominent high-frequency peak. The cause of the first peak is due to the reflection from Top Judea Group; the second, high-amplitude peak is associated with impedance contrast between soft alluvial layers (Vs=180 m/sec and Vs=280 m/sec) and the Senonian chalk (Vs=850-900 m/sec). Whereas H/V ratio for point 360 in Fig. 44 presents two resonance peaks with amplitudes close to the previous points but at lower frequencies, the H/V ratio at point 131 exhibits one clear peak at frequency of 1.2 Hz with an amplitude of 4. Point 130 has amplitude of the main peak like point 131 but smaller frequency of the main peak (0.9 Hz vs. 1.2 Hz) and slight additional peak at frequency 1.8 Hz. We suggest that points 130 and 131 are located within the Qishon graben. Using velocity structure for Canussa-9 well we match the analytical transfer functions to the H/V ratios.

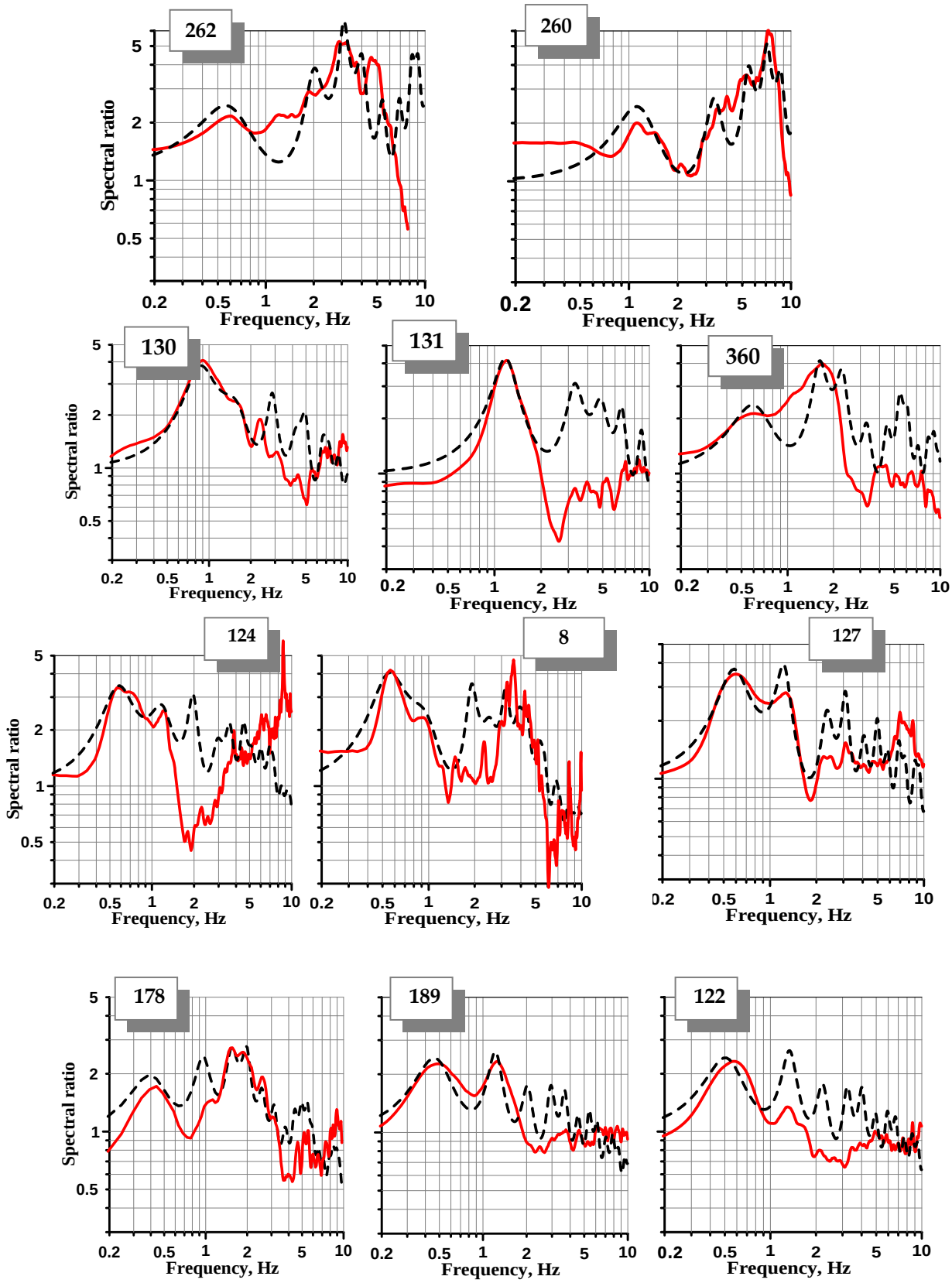

Figure 44. H/V spectral ratios obtained along profile 1 compared with the optimal analytical transfer function.

The structural map of Fleisher and Gafsou (2003) traces the fault delineating the southeastern edge of the Qishon graben between points 130 and 131 (see cross section in Fig. 41). Further analysis shows that the velocity model assumed for point Q131 is appropriate for the rest of the points within the Qishon graben. H/V spectral ratios for points 127, 8 and 124 are superimposed with analytical transfer functions calculated using velocity model for the Qishon graben in Fig. 44.

To provide a first approximation of the thickness of the Kurkar and Pliocene layers we use the 1-D models of nearby well sites. In the process of modeling a general increase in S-velocity of the upper soft layer from the central part of the Qishon graben toward the seacoast is revealed. This general trend is accompanied by local Vs variations.

We would like to draw the attention to the fact that reflection from the calcareous sandstone or/and clay of Yafo Fm. we detect practically within the whole Qishon graben as a second peak. While approaching to the sea coast we see that the second peak increases, and finally exceeds the fundamental low frequency peak. It occurs due to a combination of two factors influencing the site response: intensively dipping limestone of the Ziqlag Fm. and corresponding increasing the thickness of overlying sediments; and simultaneously local decrease of Vs of the upper layer. Thus, in this part of the cross section, at a distance of 0.5 km from the coastline, calcareous sandstone of the Kurkar Gr. may dominate the site response. The gradual reflector change is illustrated by three examples of H/V spectral ratios obtained at a distance 500 meters from each other. From point 122 to point 178 we observe diminution in amplitude of the fundamental peak caused by the Ziqlag Fm. and increase and, finally, predominance of the second "Kurkar" peak.

10. DISTRIBUTION OF RESONANCE FREQUENCY AND AMPLITUDE LEVEL FOR TWO H/V PEAKS

Analytical subsurface models constructed on the basis of the microtremor measurements facilitated understanding and interpretation of spatial distributions of the resonance frequency and its associated amplitude for two peaks characterizing H/V spectral ratios within the study area. The maps integrating 480 points of microtremor measurements are presented in Figs. 45 and 46. They are constructed within the limits of the area covered by a grid of measurements only, and those parts of the profiles 1 and 2 exceeding the bounds of this area are not included.

Analysis of the interpretation results shows that the area mapped can be divided into two zones characterized by different subsurface structure. The first zone extends over the Central Horst and the second one (the shaded area in the maps) occupies the Qishon Graben within the limits determined by interpretation of the microtremor data. As one can see from Figs. 45a,b, the maximum fundamental frequencies (3-5 Hz) and amplitude level (4.5-6.5) of the first peak are attained in the eastern part of the study area, where two geological structures are possible: alluvium overlies limestone of Judea Group or, alluvium overlies the Kurdani Fm. up to 20 meters thick, below the Senonian chalk and Judea Gr. Toward the west a gradual decrease is observed in the resonance frequency in agreement with the dipping of Top Judea Group. The H/V amplitude shows local variations reflecting changes in thickness and velocity of the upper layer. So, amplitudes of 2-2.5 are found at outcrops of the Kurdani Fm. or Senonian chalks. Amplitudes of 3-4.5 are attained at sites where low velocity layer (Vs=160 m/sec) of 10-15 m thick exists. We note that the amplitude does not exceed 2.5-3 at sites where the Top Judea Gr. occurs at a depth greater than 200 meters. Further variations of the first amplitude peaks are in the range of 2-3 while resonance frequency gradually decreases due to dipping of Judea Gr.

The distribution of the second resonance frequency and its amplitude (Figs. 46a,b) strongly depends on the geotechnical characteristics of the upper layer above the reflector and underlying rock, which is represented in the northeastern part of the study area by the Senonian chalk or sandy limestone of Kurdani Fm. The range of the second resonance frequency in this part of this area is 1.5-10 Hz and its associated amplitude level is 2.0-10. Sites with no resonance frequency are found at exposed Kurdani Fm. Zone of the highest amplitude values, mapped from the northeast to the southwest, are already mentioned with regard to the first peak and is directly connected with appearance of the low velocity layer. The tendency of the sedimentary thickness above the shallow reflector to increase from the Kurdani outcrop in the east of the area toward the west explains general decrease in the frequency of the second peak. Rise in frequency from 1.5 Hz to 3 Hz observed at the seacoast has a local nature and related to the velocity characteristics.

South of the fault crossing the study area from the north to the south (see Figs. 45 and 46), the geological situation in the region is drastically changed. This part of the study area (shaded area in the maps) is located, by our estimations, within the

Qishon graben. The Top Judea Group deepens down to a depth significantly greater than 800 meters, and the Miocene and Eocene limestone and chalk can be assumed as deep reflector. Calcareous sandstone of the Kurkar Group together with the Pliocene clay and marl are the shallow reflector. It is of interest to examine the behavior of the frequency and amplitude of the two peaks, which we observed at sites located in this part of the study area. The first and second resonance frequencies vary in the ranges of 0.3-1.2 Hz and 0.7-2 Hz, respectively. Regarding the first resonance frequency we can say that variations observed are related mainly to the relief of the basement. In most cases sharp changes in the reflector depth are associated with faults.

Analysis of microtremor data shows that H/V amplitude values of 2.0-3.5 correspond to limestone of the Ziqlag Fm. Increase in amplitude level up to 4.5 is connected with decrease of Vs for alluvium layer. Dipping of the Ziqlag Fm. close to the coastline is followed by an increase of Vs of the alluvium. This is indicated by a decrease in the H/V amplitude down to 2-2.5. The impedance contrast between alluvium layer and calcareous sandstone determines the second peak of H/V ratios in the Qishon graben. It should be taken into consideration; however, that variation of the Vs for the upper layer may be significant.

It is important to understand that in multilayer medium with intermediate hard layer the first and second peaks of H/V ratio are inseparably linked and variations in velocity of the upper layer are immediately reflected in amplitude of the second peak as well as amplitude of the first peak. Only joint interpretation of these parameters can clarify the spatial distribution of site response.

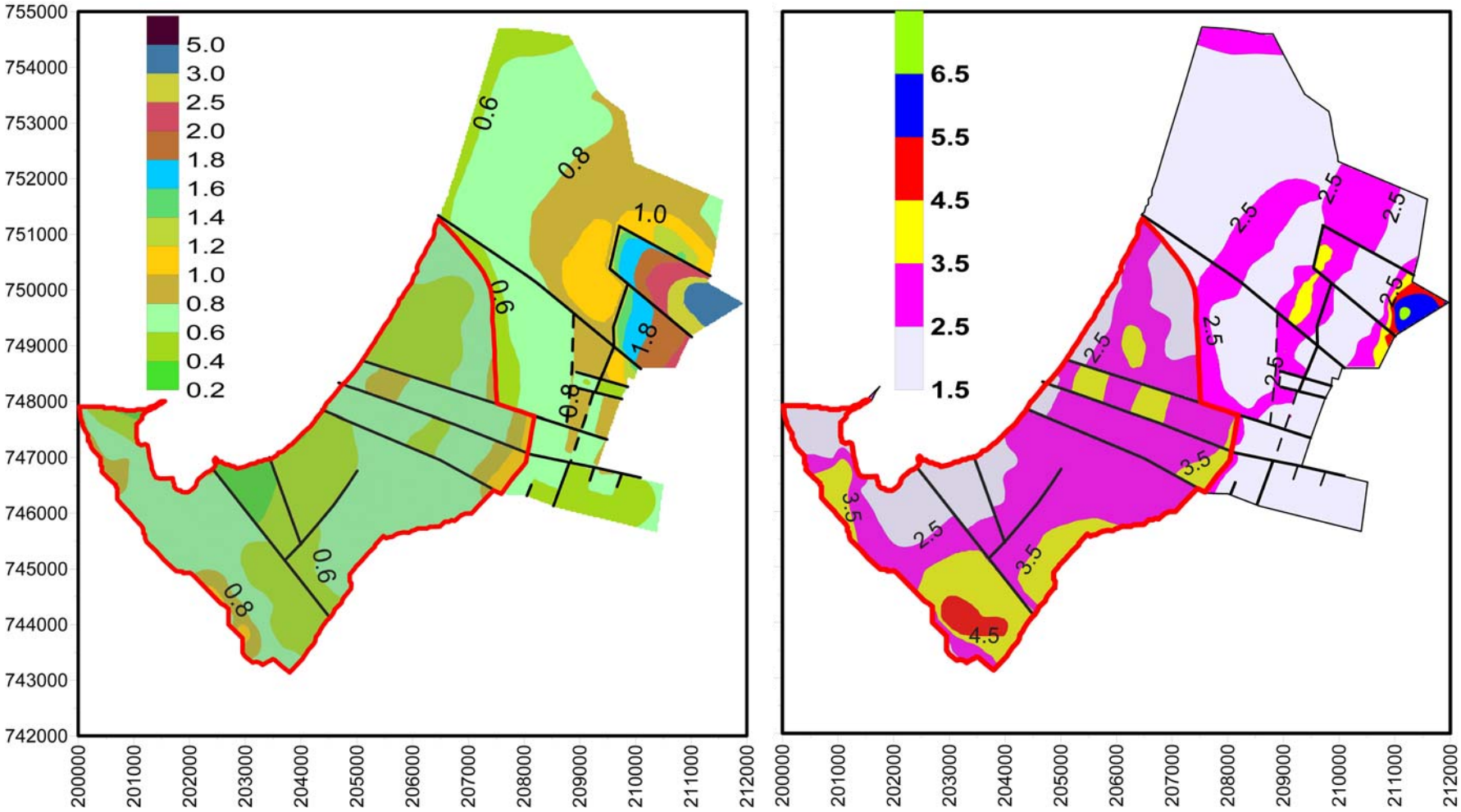

Figure 45. Distribution of the first H/V resonance frequency and its associated amplitude. The red line indicates the limits of the Qishon Graben determined by interpretation of the microtremor data.

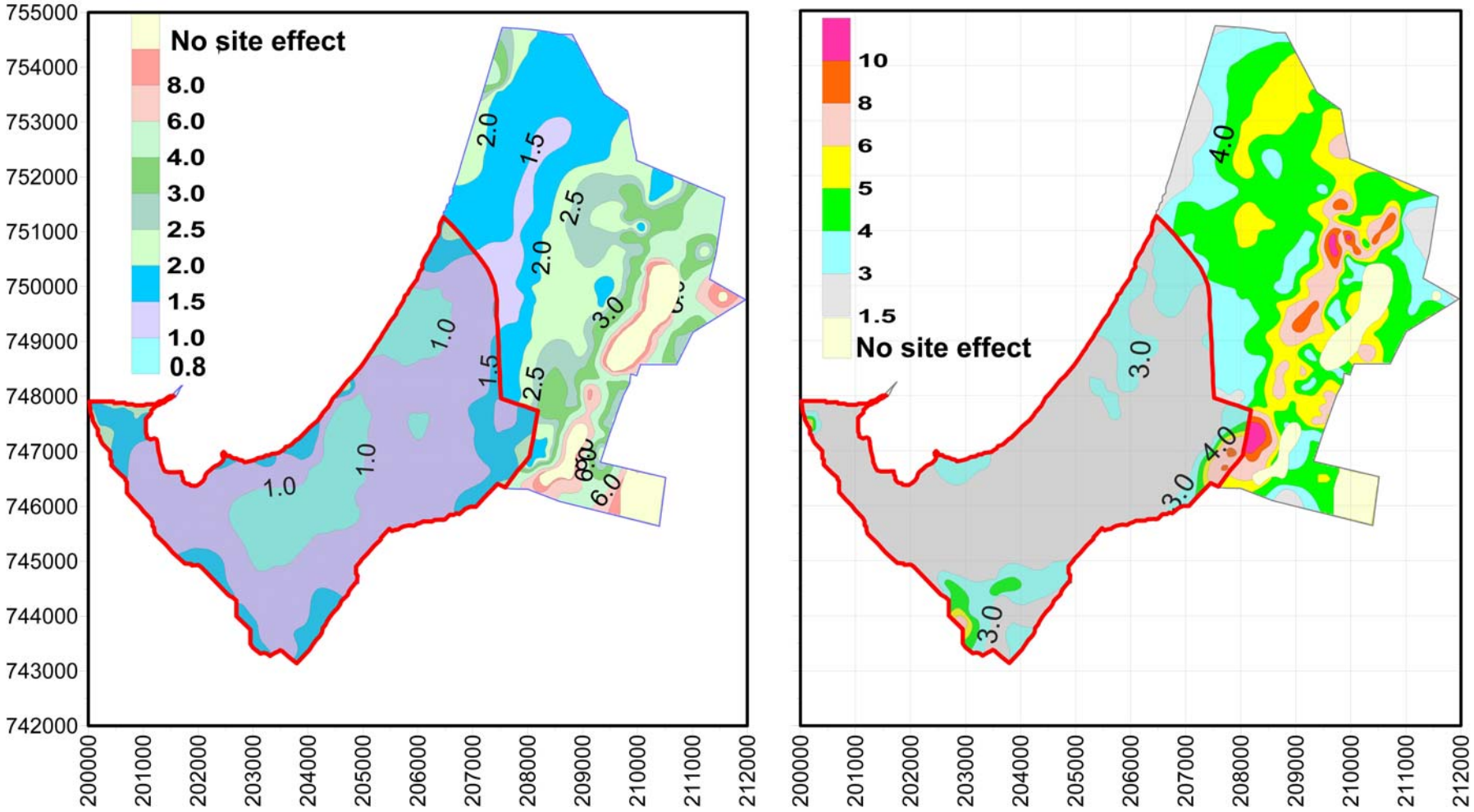

Figure 46. Distribution of the second H/V resonance frequency and its associated amplitude.

11. PREDICTION OF SITE-SPECIFIC ACCELERATION SPECTRA AND SEISMIC ZONATION IN THE QRAYOT - HAIFA BAY AND AREA

We use H/V measurements together with available geological and geophysical information to construct a subsurface model for the investigated region. This model, in turn, may be used for estimating the expected site effects during earthquakes. In the engineering practice, the aseismic building design and assessments of the earthquake risk refer to the site-specific acceleration (or displacement) spectrum. The design acceleration spectrum is essentially a representation of the maximum acceleration amplitudes for a prescribed probability of occurrence developed on a set of one degree of freedom oscillators with a given damping ratio. Since seismic activity in areas such as Israel is low, local acceleration data from strong earthquakes is insufficient to estimate directly the design acceleration spectrum; therefore, in areas covered by soft sediments, we must resort to the use of synthetic data. For this purpose Shapira and van Eck (1993) developed the SEEH method (Stochastic Estimation of the Earthquake Hazard). In brief; SEEH produces a number of synthetic earthquake catalogues that represent the possible future seismic activity within 200 km of the investigated site. These catalogues adhere to the available information about the seismogenic zones in the area and their associated seismicity. The Monte Carlo statistics are used to generate different catalogues which reflect the uncertainty associated with the spatial and temporal parameters of the seismicity. For each of the earthquakes in a catalogue, SEEH implements the stochastic simulation method (see Boore, 2000) to generate synthetic S waves accelerogram for the surface of the bedrock which then propagates through the soil column of the site (using Joyner, 1977; or Shnabel, 1972) to the surface. The synthetic free surface accelerogram is used to calculate the acceleration response spectrum for a predefined damping. Here again, the Monte Carlo statistics are used to select the values of the parameters used in the ground motion simulations. For example; we assume a unified distribution for locating the hypocenter within a defined seismogenic zone and within a 5-20 km depth, and the estimated seismic moment of the event (and thus the energy at the source) are log-normally distributed around the expected value with an uncertainty factor of 3 and so forth. The parameters used are based on studies done in the area and reflect our current knowledge (and uncertainty) about the seismic activity and the main parameters that control the spectra of expected ground motions at a given site. The ensemble of these hundreds

(sometimes thousands) of synthetic acceleration response spectra are statistically analyzed in order to assess the spectral amplitude level to be exceeded at least once in a certain exposure time (usually 50 years) and a certain probability (usually 10%). For more details see Shapira and van Eck (1993).

Based on the comparative analysis of the acceleration spectra computed, the Haifa Bay area is divided into seventeen zones (Fig. 47). Soil-column models, corresponding analytical functions and acceleration spectra generalized for each zone are given in Table 5, Figs. 48 and 49 respectively. We also plotted in Fig. 49 the acceleration spectra required by the current building code IS-413 for ground types S1-S4 corresponding to the model with the design horizontal Peak Ground Acceleration (PGA) value of 0.185. As was expected from the distribution of the frequencies and amplitude for both H/V peaks (see maps in Figs. 45 and 46) the most "variegated" part of the study area is the town of Qiryat Bialik and its surroundings, where the frequency gradient is high. The area adjacent to Qiryat Bialik in the northeast direction is characterized by the highest acceleration values. Zones 14, 15 and 17 located in the Haifa yield the lowest acceleration value less than 0.45 g for linear spectra and comparable with IS-413.

The calculated theoretical model can then be easily used to modify synthetic seismogram computed for rock (SEEH method) and predict also nonlinear site specific ground motion during large earthquakes at sites where the ground motions have not been recorded. For many years, the geotechnical engineering and seismology communities have had different approaches to significance of non-linear soil behavior during ground shaking. Thus the main question of the discussion is: when is soil amplification amplitude dependent? For example, Gutierrez and Singh (1992) described the character of strong motion on soft sites and assert that they did not found clear evidence of nonlinear behavior even then when peak horizontal acceleration exceeds 0.3 g.

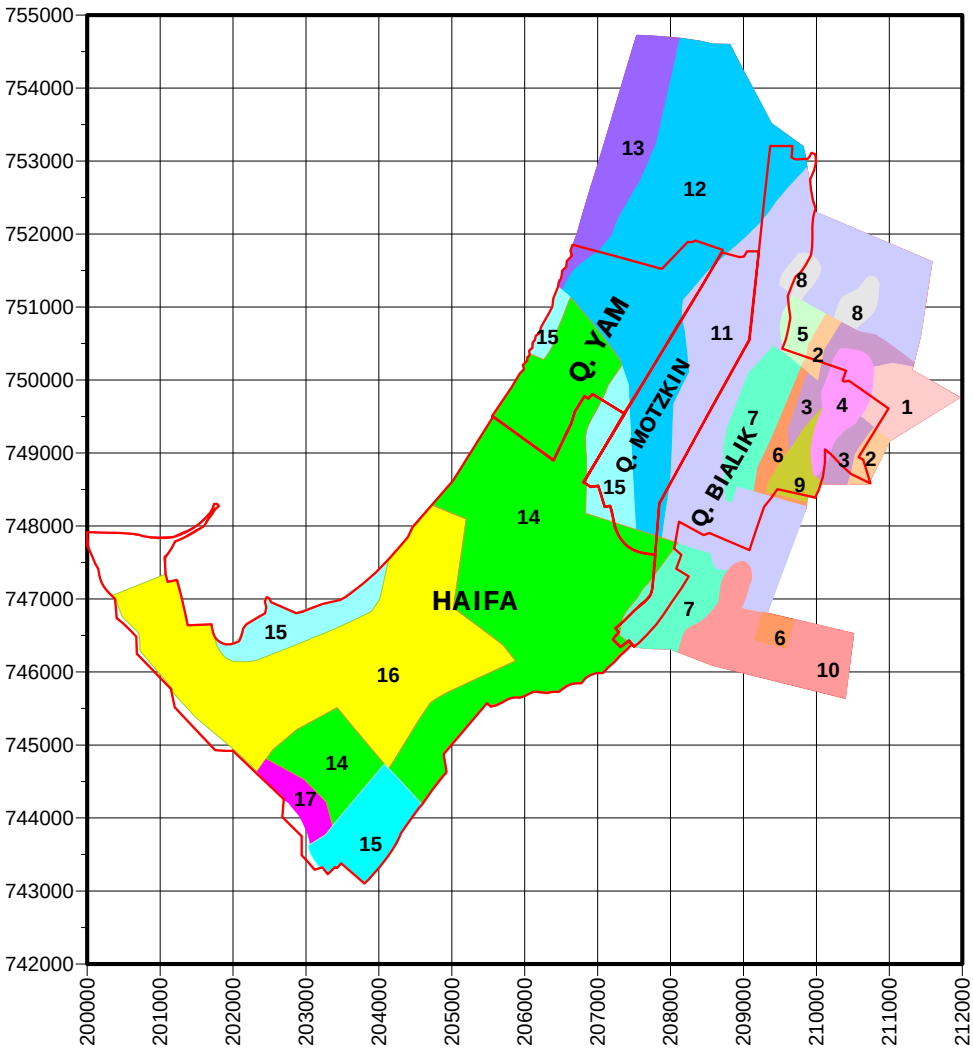

Figure 47. Map of seismic zonation in the Haifa Bay area.

Table 5. Soil column models for representative sites of zones.

Zone's number	Thickness m	Density gr/cm^3	Vs m/sec	Damping %
1	5	1.6	160	4
	10	1.7	250	3
	16	2.0	1200	1
	27	1.9	800	2
	Half space	2.3	1900	
2	20	1.7	250	4
	15	2.0	1200	1
	65	1.9	750	2
	Half space	2.3	1900	
3	15	1.7	250	3
	20	2.0	1200	1
	100	2.0	900	2
	Half space	2.3	1900	
4	30	2.0	1200	1
	80	2.0	850	2
	Half space	2.3	1900	

5	12	1.6	160	4
	13	1.7	250	3
	30	2.0	1200	1
	130	1.9	900	2
	Half space	2.3	1900	
6	10	1.7	270	3
	12	1.7	350	3
	20	2.0	1200	1
	190	2.0	900	2
	Half space	2.3	1900	
7	13	1.6	160	4
	23	1.7	280	3
	45	2.0	1200	1
	150	2.0	900	2
	Half space	2.3	1900	
8	10	1.6	130	4
	7	1.7	300	3
	10	2.0	1200	1
	175	2.0	850	2
	Half space	2.3	1900	
9	30	2.0	1200	1
	135	1.9	850	2
	Half space	2.3	1900	
10	10	1.7	350	3
	30	2.0	1200	1
	275	2.0	950	2
	Half space	2.3	1900	
11	25	1.7	270	3
	50	2.0	1100	1
	250	2.0	950	2
	Half space	2.3	1900	
12	40	1.7	290	3
	50	2.0	1100	1
	280	2.0	950	2
	Half space	2.3	1900	
13	15	1.7	270	3
	60	1.8	600	2
	60	2.0	1100	1
	360	2.0	1000	1
	Half space	2.3	1900	
14	60	1.7	260	3
	110	1.8	600	2
	130	2.0	850	2
	Half space	2.1	1500	
15	45	1.7	300	3
	115	1.8	600	2
	160	2.0	850	2
	Half space	2.1	1500	
16	65	1.7	290	3
	140	1.8	600	2
	150	1.9	850	2
	Half space	2.1	1500	
17	18	1.6	150	4
	35	1.7	250	3
	190	1.9	750	2
	Half space	2.1	1500	

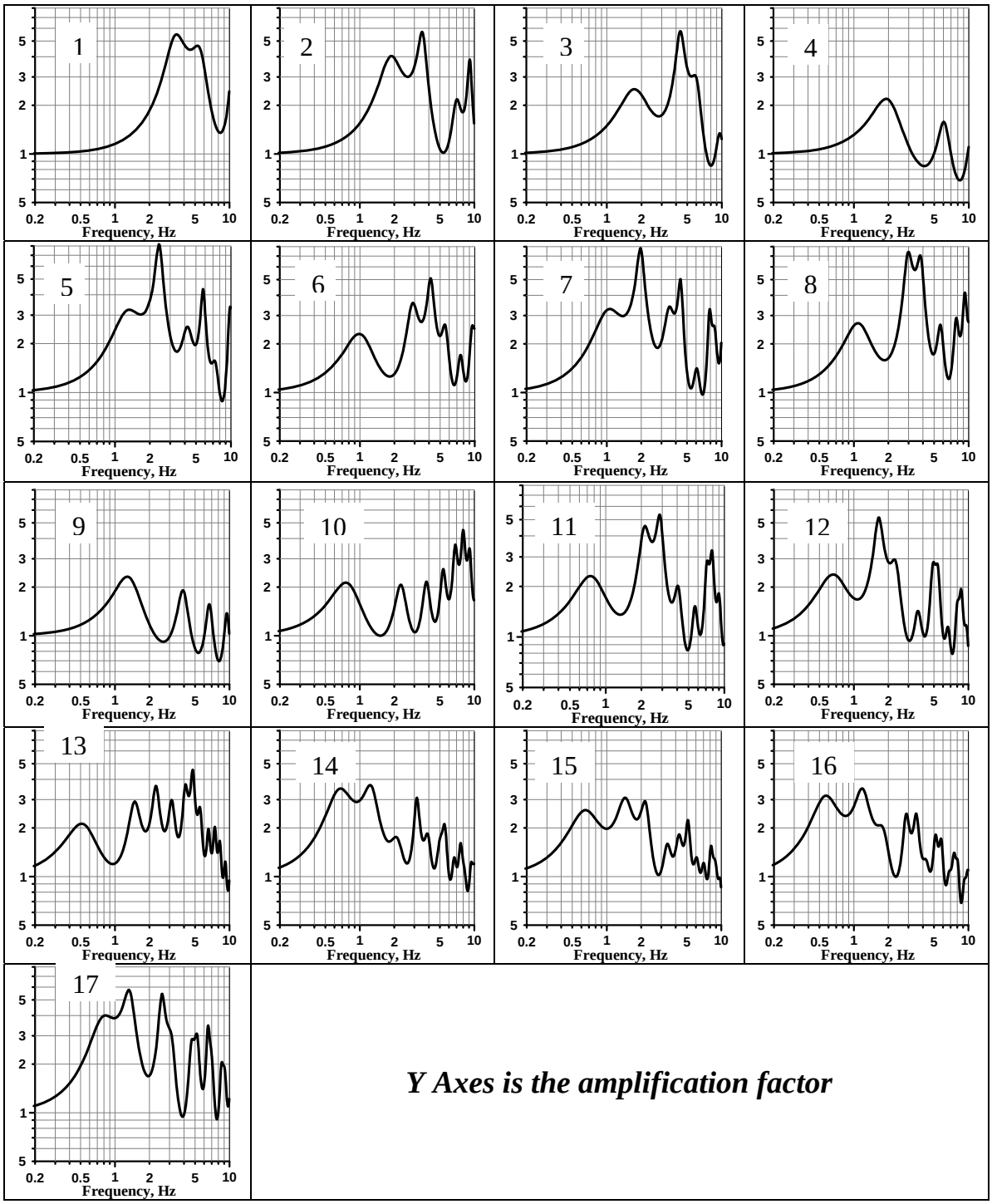

Figure 48. Analytical transfer functions for each zone.

In accordance with Su et al. (1998) the difference between weak-and strong-motion site responses becomes significant when the peak acceleration is above 0.3 g. At lakebed sites in Mexico city, the ground motions were amplified as much as several tens times relative to hill zone during the 1985 Michoacan earthquake, however only at Station Central de Abastos (Reinoso and Ordas, 1999) little non-linear behavior was observed.

The identification of nonlinearity in site response is challenging because the classical spectral technique with reference station only partly relieves this problem. Perhaps, nonlinear soil response could be completely hypothetical a decade ago. The field observation of recent earthquakes by modern surface and downhole vertical arrays of seismometers indicated that soil non-linearity influenced the ground motion (Field et al., 1997; Trifunac and Todoravska, 1998; Frankel et al., 2002; Pavlenko and Irikura, 2002; and others) and its correct prediction have major importance for seismic hazard assessment and building design requirements. In USA, the National Earthquake Hazard Reduction Program (NEHRP, 1994) soil classification scheme is used to consider the effect of different soil types. Site categories E, B, C and D for Qrayot and Haifa bay areas as given in Table 6.

Numerous methods and programs developed for calculating the ground response in strong motion in various conditions of stress-strain relations. Hartzell et al. (2004) compared different nonlinear soil models for wide range of site condition from rock to soft soil in terms of the Fourier spectral ratio of ground motion at the surface with respect to the input motion at the base of velocity profile. In this study we used an algorithm elaborated by Joyner and Chen (1975) and a program of Joyner (1977), kindly provided by Prof. Sam Friedman (Technion, Haifa) designed for calculating the nonlinear seismic response of a system of horizontal soil layers underlain the medium. The physical properties of the soil layers are specified following the values: thickness density, shear wave velocity and dynamical shear strength. To estimate the dynamical shear strength for different class of soils we use method of "trial and error" to find best agreement between our calculation and result obtained by Hartzell et al. (2004). Optimal values of dynamical shear strength are summarized in Table 6.

Table 6. Site classification and optimal dynamic shear strength (DSS) used to calculate nonlinear response spectra.

Site Class	V_S m/sec	DSS $(dyne/cm^2)*10^5$
E	150-200	6
D	250-300	10-12
D	350	15
C	600-750	20-30
B	750-800	30-35
B	900	45
B	1100-1200	95-100

The results of our computations are shown in Fig. 49. We can see that for Zones 1, 3 and 6 there are no significant differences between linear and non linear approaches, while for zones 5, 8, and 12 the linear response spectrum is twice as much as the nonlinear spectrum in the frequency range 1.5-5 Hz. It must be mentioned that the problem of predicting the nonlinear ground motion forecast is very complex, since such components of the site response analysis as input motion, site characterization, soil model and numerical analysis influence significantly the calculated result. Therefore, our computations of nonlinear behavior of soil sediments have only illustrative character.

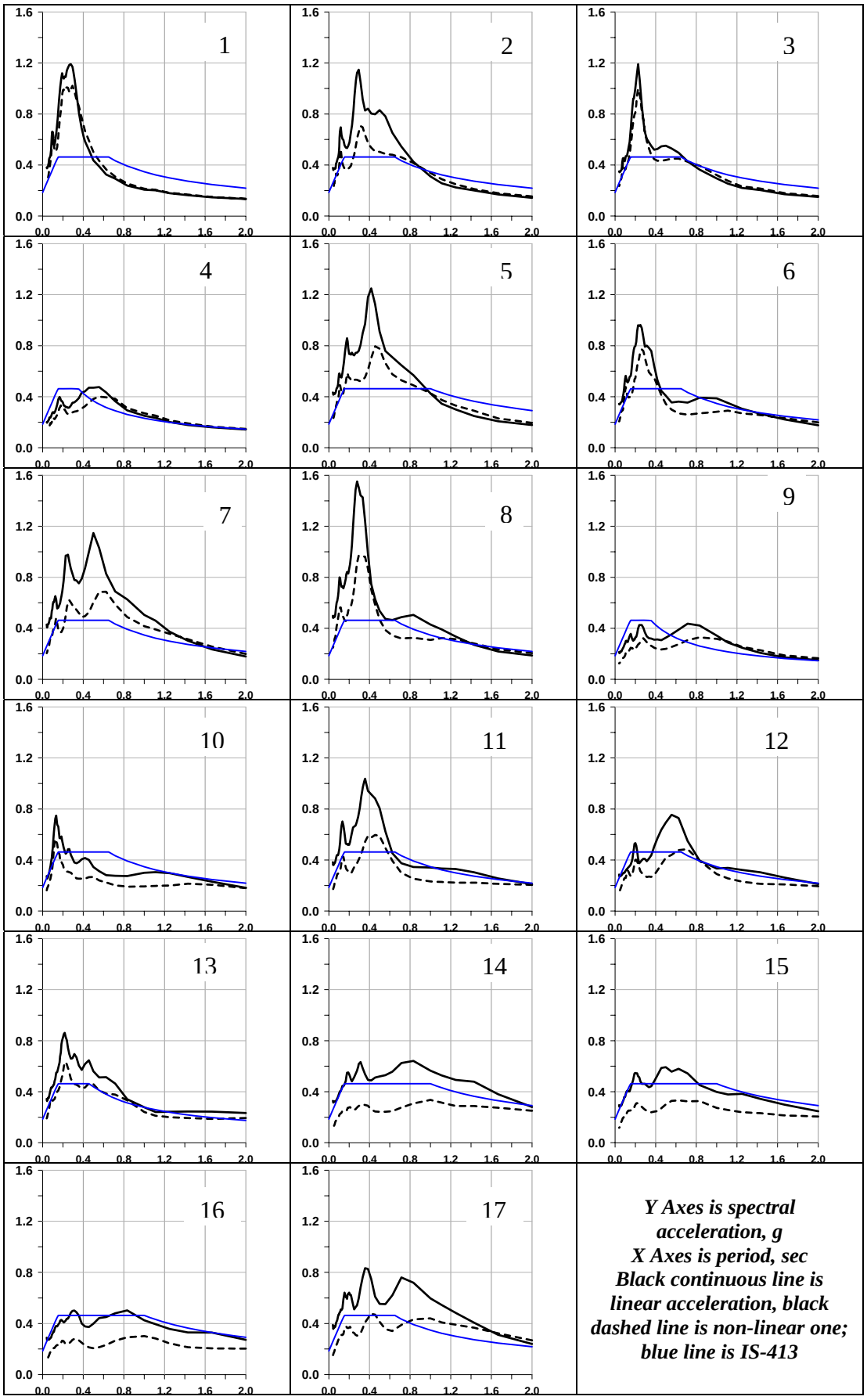

Figure 49. Linear and nonlinear spectral accelerations for each zone.

12. CONCLUSIONS

The present report describes the seismic microzoning study in the Haifa Bay and Qrayot areas. The main objectives of this study are:

- Obtaining H/V spectral ratios from microtremor observations and mapping of fundamental frequency and its corresponding amplitude;
- Deriving shear-velocity structure by combining H/V spectral ratios from microtremor with geophysical survey results and borehole data at corresponding locations;
- Using the velocity models for constructing the subsurface structure along selected profiles;
- Extrapolating the derived theoretical models over the study area and integrating them into computing the uniform hazard site specific acceleration response spectra for 10% probability during an exposure time of 50 years and damping ratio of 5%;
- Dividing the study area into zones based on the comparative analysis of the acceleration spectra.

Based on our observations discussed in this report we may conclude:

- Only by observance of numerous proper field work conditions, such as qualitative visual control over the microtremor waveforms and quantitative Fourier spectra and H/V spectral ratio inspection during data acquisition, Nakamura's method is feasible;
- Data processing of ambient vibration (microtremors) and interpretation of the H/V spectral ratio technique requires a good knowledge about different method of random data analysis and its application to estimation of frequency response function from input-output data measured during exposure of the physical system to its natural environment;
- Site response variations in the study area are significant over short distances, thus it is recommended that prediction of the seismic characteristics during large earthquakes should be based on the H/V ratios obtained over a relatively dense grid of the measuring sites;
- H/V spectral ratios obtained at 480 locations in an area of about 50 km^2 show two peaks at frequencies related to resonances of deep and shallow structures. Spatial variations of the frequency (0.5-5 Hz for the first peak and 0.8-10 Hz

for the second peak) and H/V amplitude level (2-6 for the first peak and 2-12 for the second peak) reflecting the geological complexity are shown in four distribution maps;

- Results of modeling carried out at locations of borehole and refraction surveys indicate that there is a good agreement between H/V ratios and 1-D multi layers analytical models. Thus such a comparison may be used for improvement of models assumed;
- Geological interpretation of the results and matching the frequency and amplitude patterns the available geological data became possible only after a number of the cross sections were constructed. In some cases, it is suggested a revision of existing concepts as regards the subsurface structure in the region;
- Map of zones presented in the report in terms of the Uniform Hazard Site-specific Acceleration Spectra for a probability of exceedence of 10% during an exposure time of 50 years and a damping ratio of 5%, computed using SEEH procedure by applying the evaluated subsurface models may be useful for land use planning or making regional hazard decisions;
- Comparison of the predicted linear and nonlinear Uniform Hazard Site-Specific Acceleration Spectra shows significant differences between two approaches. The problem predicting the ground motion forecast is very complex, since such components of the site response analysis as input motion, site characterization, soil model and numerical analysis influence significantly the calculated result. Therefore, our computations of nonlinear behavior of soil sediments have only illustrative character;
- Our results point out that H/V spectral ratio technique, using microtremors, is useful in earthquake engineering, and has been frequently adopted in seismic microzonation investigations. The application of this technique is very important in Israel, where big earthquakes present a long return period, but might exhibit a high seismic risk, according to historical reports.

ACKNOWLEDGEMENTS

Our cordial thanks to the Steering Committee for the National Earthquake Preparedness and Mitigation for the financial support. We are very grateful to Dr V. Pinsky for his useful comments. We thank Y. Menahem for his assistance in preparing this report.

REFERENCES

Alva Hurtado, J. E., Meneses Loja, J.F., Martinez Del Rosario J.A., and Human-Egoavil, C.E., 1991. Advances on the seismic microzonation of Lima City, Peru. Proceedings Fourth International Conference on Seismic Zonation, Stanford University, August, III, 65-72.

Amiran, D.H.K., Arieh, E., and Turcotte, T., 1994. Earthquakes in Israel and Adjacent Areas: Macroseismic Observations since 100 B.C.E. Israel Exploration J., 2: 261-305.

Bar Yossef, Y., Michaeli, A., Zah-Dvori, N., and Wolman, S., 2003. Hydrological model (prediction) for testing producing scenarios in Naaman and Kurdani Aquifers. Natural Resources Department LTD, Report NR/389/03.

Borcherdt, R., Glassmoyer, G., Andrews, M., and Cranswick, E., 1989. Effect of site conditions on ground motion and damage. Earthquake Spectra, Special supplement: 23-42.

Boore, D.M., 2000. SMSIM – Fortran programs for simulating ground motions from earthquakes: Version 2.0 – a revision of OFR 96-8-A, U.S. Geological Survey Open-File Report OF 00-59, 55pp.

Bounden-Romdhane, N., Mechler, P., Duval, A. M., Meneroud, P., and Vidal, S., 2000. Microzoning the city of Tunis both background noise and weak motion. Proc. of 12th World Conference on Earthquake Engineering, Auckland, New Zealand, 2000, No.0343, pp 8.

Cardona, O.D., and Yamín, L. E., 1997. Seismic microzonation and estimation of earthquake loss scenarios: integrated risk mitigation project of Bogotá, Colombia. Earthquake Spectra, 13, 795-814.

Chávez-Garcia, F. J., Cuenca J., Lermo J., and Mijares, H., 1995. Seismic microzonation of the city of Puebla, Mexico. Third International Conference on Recent Advances in Geotechnical Earthquake Engineering and Soil Dynamics, St. Luis, Missouri, April, 2, 545-548.

Chávez-García, F. J., and Cuenca, J., 1998. Site effects and microzonation in Acapulco. Earthquake Spectra, 14(1): 75-93.

Darragh, R. B., and Shakal, A. F., 1991. The site response of two rock and soil station pairs to strong and weak motion. Bull. Seism. Soc. Am., 81: 1885-1889.

Enomoto T., Kuriyama, T., Abeki, N., Iwatate, T., Navarro, M., and Nagumo, M., 2000. Study on microtremor characteristics based on simultaneous measurements between basement and surface using borehole. Proc. of 12th World Conference on Earthquake Engineering, Auckland, New Zealand, 2000, No 1522, pp 8.

Field, E. H., and Jacob, K. H., 1995. A comparison and test of various site-response estimation techniques, including three that are not reference-site dependent. Bull. Seism. Soc. Am., 85: 1127-1143.

Field, E. H., Hough, S. E., and Jacob, K. H., 1990. Using microtremors to assess potential earthquake site response: a case study in flushing meadows. New York City, Bull. Seism. Soc. Am., 80: 1456-1480.

Field, E. H., Johnson, P. A., Beresnev, I. A., and Zeng, Y., 1997. Nonlinear ground motion amplification by sediments during the 1994 Northridge earthquake. Nature, 390: 599-602.

Fleischer, L., and Gafsou, R., 2003. Top Judea Group - digital structural map of Israel. The Geophysical Institute of Israel, Report 753/312/03.

Frankel, A. D., Carver, D. L, and Williams, R. A., 2002. Nonlinear and linear site response and basin effects in Seattle for the M 6.8 Nisqually, Washington, earthquake, Bull. Seism. Soc. Am., 92: 2090-2109.

Gaull, B. A., Kagami, H., and Taniguchi H., 1995. The microzonation of Perth, Western Australia, using microtremor spectral ratio, Earthquake Spectra, 11: 173-191.

Ghayamghamian M.R., Kawakami H., and H. Mogi, 1995. Microtremor data analysis for seismic microzonation in north of Tehran. Proceedings of IS-Tokyo '95. The First International Conference on Earthquake Geotechnical Engineering, Tokyo, November, 1, 561-566.

Gitterman, Y., Zaslavsky, Y., and Shapira, A., 1995. Analytical evaluation of the site response. Annual meeting of Israel Geological Society.

Goulá X., Susagna T., Figueras S., Cid J., Alfaro A., and Barchiesi, 1988. Comparison of the numerical simulation and microtremor measurement for the analysis of the site effects in the city of Barcelona, Spain. Proc. of 11th European Conference Engineering, Balkema, Rotterdam.

Gutierrez, C., and Singh, S. K., 1992. A site effect study in Acapulco, Guerrero, Mexico: Comparison of results from strong-motion and microtremor data. Bull. Seism. Soc. Am., 82: 642-659.

Hamdache, M., Peláez, J.A., and Yelles-Chauche, A. K., 2004. The Algiers, Algeria earthquake (M_W 6.8) of 21 May 2003: preliminary report. Seismo. Res. Lett., 75: 360-367.

Hartzell, S. H., Leeds, A., Frankel, A., and Michael, J., 1996. Site response for urban Los Angeles using aftershocks of the Northridge earthquake. Bull. Seism. Soc., Am. 86: S168-192.

Hartzell, S., 1998. Variability in nonlinear sediment response during the 1994 Northridge, California, Earthquake. Bull. Seism. Soc. Am., 88; 1426-1437.

Hartzell, S., Bonilla, L. F., and Williams R. A., 2004. Prediction of nonlinear soil effects. Bull. Seism. Soc. Am., 94: 1609-1629.

Horike, M., Zhao, B., and Kawase, H., 2001. Comparison of site response characteristics inferred from microtremors and earthquake shear wave. Bull. Seism. Soc. Am., 91; 1526-1536.

Hough, S. E., Friberg, P.A., Busby, R., Field, E. F., Jacob K.H, and Borcherdt, R.D., 1990. Sediment-induced amplification and the collapse of the Nimitz Freeway. Nature, 344: 853-855.

Iwata, T., Hatayama, K., Kawase H., and Irikura K., 1996. Site amplification of ground motions during aftershocks of the 1995 Hyogo-ken Nanbu Earthquake in several damaged zone – array observation of ground motions at Higashinada ward, Kobe city, Japan. Journal of Physics of the Earth, 44(5):553-61.

Jarpe, S. P., Cramer, C. H., Tucker, B. E., and Shakal, A. F., 1988. A comparison of observations of ground response to weak and strong motion at Coalinga, California. Bull. Seism. Soc. Am., 78: 421-435.

Jarpe, S. P., Hutchings, L. J., Hauk, T. F., and Shakal, A. F., 1989. Selected strong- and weak-motion data from the Loma Prieta earthquake sequence Seism. Research Letters, 60(4): 167-176.

Jimenez, M.J., Garcia-Fernandez, M., Zonno, G., and Cella, F., 2000. Mapping soil effects in Barcelona, Spain, through an integrated GIS environment. Soil Dynamics and earthquake Engineering 19 (2000) 289-301.

Joyner, W. B., 1977. A Fortran program for calculating nonlinear seismic response. U. S. Geological Survey, Open File Report 77-671.

Joyner, W. B., and Chen, A. T. F., 1975. Calculation of nonlinear ground response in earthquakes. Bull. Seism. Soc. Am., 65: 1315-1356.

Kafri, U., and Ecker A., 1964. Neogene and Quaternary subsurface geology and hydrogeology of the Zevulun Plain. Geology Survey of Israel, Bull. No 37.

Kobayashi, H., Seo, K., Midorikawa S., Samano T., and Y. Yamazaki, 1991. Seismic microzoning study of Mexico City by means of microtremor measurements. Proceedings [of the] Fourth International Conference on seismic Zonation, Stanford Univercity, August, II, 557-564.

Kudo, K., 1995. Practical estimates of site response. State-of-art Report. Proceedings of 5th International Conference on Seismic Zonation, Nice, France, October 17-19, 1878-1907.

Lachet, C., Hatzfeld, D., Bard, P-Y., Theodulidis, N., Papaioannou, Ch., and Savvaidis, A., 1996. Site effects and microzonation in the City of Thessaloniki (Greece). Comparison of different approaches. Bull. Seismol. Soc. Am., 86 (6):1692-1703.

Lebrun, B., Duvall, A-M., Bard, P-Y., Monge, O., Bour, M., Vidal, S., and Fabriol H., 2004. Seismic microzonation: a comparison between geotechnical and seismological approaches in Pointe-á-Pitre (French West Indies), Bull. Earth. Eng. 2: 27-50.

Lermo, J., and Chávez-García, F. J., 1994. Are microtremors useful in site response evaluation?, Bull. Seism. Soc. Am., 84: 1350-1364.

Love, D. N. Bierbaum S.J., Poulos H., and S.A. Greenhalgh, 1995. Seismic risk analysis and microzonation of Adelaide, Proceedings [of the] Pacific Conference on Earthquake Engineering, Melbourne, Australia, November, 2, 59-67.

Malagnini, L., Tricarico, P., Rovelli, A., Herrmann, R. B., Opice, S., Biella G., and de Franco, R., 1996. Explosion, earthquake, and ambient noise recording in a pliocene sediment-filled valley: inferences on seismic response properties by reference- and non-reference-site techniques, Bull. Seism. Soc. Am., 86: 670-682.

Marcellini, A., Bard, P-Y., Iannaccone, G., Meneroud, P, J., Mouroux, P., Romeo, R.W., Silvestri, F., Duval, A-M., Martin, C., and Tento, A., 1995. The Benevento seismic risk project: II-The microzonation. Proceedings of 5th International Conference on Seismic Zonation, Nice, France, October 17-19, 810-817

Mero, D., 1983. Subsurface geology of Western Galilee and Zevulun. Plain. TAHAL, Tel-Aviv, Internal Report No. 04/83/48: 36 pp.

Midorikawa S., 1998. Seismic microzoning of Odawara City, Japan, based on dense strong-motion observation and microtremor measurement. Proceedings of Second International Symposium on the Effects of Surface Geology on Seismic Motion, Yokohama, Japan, December, 1, 161-170.

Mirzaoglu, M., and Dýkmen, Ü., 2003. Application of microtremors to seismic microzoning procedure. J. Balkan Geophys. Soc., 6: 143-156.

Motamed and Ghalandarzadeh, 2005. Seismic Microzonation and Damage Assessment of Bam City, Southeast of Iran, Proceeding of International Conference of Earthquake Engineering in the 21st Century (EE-21C), Skopje, 27 August-1 September.

Mucciarelli, M., 1998. Reliability and applicability of Nakamura's technique using microtremors: an experimental approach. Journal of Earthquake Engineering, 4: 625-638.

Mucciarelli, M., and Monachesi, G., 1998. A quick survey of local amplifications and their correlation with damage observed during the Umbro-Marchesan (Italy) earthquake of September 26, 1997. Journal of Earthquake Engineering, 2 (2): 325-337.

Mucciarelli M., and Gallipoli, M. R., 2004. The HVSR technique from microtremor to strong motion: empirical and statistical considerations. Proc. of 13th World Conference of Earthquake Engineering, Vancouver, B.C., Canada, Paper No. 45.

Mukhopadhyay, S., Pandey, Y., Dharmaraju, R., Chauhan, P.K.S., Singh, P., and Dev., A., 2002. Seismic microzonation of Dehli for ground-shaking effects. Current Science, Vol. 82 (7), April, 877-81.

Nakamura, Y., 1989. A method for dynamic characteristics estimation of subsurface using microtremor on the ground surface. Quarterly Report of Railway Technical Research 30(1): 25-33.

National Earthquake Hazard Reduction Program (NEHRP), 1994. Recommended provisions for seismic regulations for new buildings, Federal Emergency Management Agency Report FEMA 368 and 369, Washington, D.C., 290 pp.

Navarro, M., Sanchez, F.J., Posadas, A.M., Luzos, F., Enomoto, T., Matsuda, I., Vidal, F., and Seo, K., 1998. Microtremor measurements and its application to seismic microzoning of Almeria City, Southern Spain, Proc. of 11th Conference on Earthquake, Balkema, Rotterdam No 2, 325-337.

Ohmachi, T., Nakamura, Y., Toshinawa, T., 1991. Ground motion characteristics of the San Francisco bay area detected by microtremor measurements. Second International conference on recent advances in geotechnical earthquake engineering and soil dynamics, St. Louis, Missouri, 1643-1648.

Ojeda, A., and Escallon, J., 2000. Comparison between different techniques for evaluation of predominant periods using strong ground motion records and microtremors in Pereira Colombia, Soil Dynamics and Earthquake Engineering, 20:147-143.

Ozel, O., Cranswick, E., Meremonte, M., Erdik, M., and Safak, E., 2002, Site effects in Avcilar, west of Istanbul, Turkey, from strong-and weak-motion. Bull. Seism. Soc. Am., (Special Issue) 92(1): 499-508.

Pavlenko, O., and Irikura, K., 2002. Nonlinearity in the response of soils in the 1995 Kobe earthquake in vertical components of records. Soil Dynamics and Earthquake Engineering 22, 967-975.

Ramirez-Centeno, M., and Martin del Campo, R., 1998. Seismic Zonation of the metropolitan area of Guadalajara, Mexico. Proceedings of the Second International Symposium on the Effects of Surface Geology on Seismic Motion, Yokohama, Japan, December 1-3, 2 1207-1214.

Reinoso, E., and Ordaz, M., 1999. Spectral amplification for Mexico City from free-field recordings. Earthquake Spectra, Vol. 15 No. 2, p. 273-295.

Rovelli, A., Singh S. K., Malagnini, L., Amato, A., and Cocco, M., 1991. Feasibility of the use microtremors in estimating site response during earthquakes: some test in Italy. Earthquake Spectra, 7: 551-561.

Satoh, T., Sato, T., and Kawase H., 1995. Nonlinear behavior of soil sediments identified by using borehole records observed at the Ashigara valley, Japan. Bull. Seism. Soc. Am., 85: 1821-1834.

Satoh, T., Kawase, H., Matsushima, S., 2001. Difference between site characteristics obtained from microtremors, S-wave, P-waves, and codas. Bull. Seism. Soc. Am., 91: 313-334.

Schnabel, P.B., Lysmer, J., and Seed, H.B., 1972. SHAKE – a computer program for earthquake response analysis of horizontal layered sites. Rpt. No. EERC 71-12, Earthquake Engineering Research Center, Berkeley, CA.

Seekins, L. C., Wennerberg, L., Margheriti, L. and Liu, Hsi-Ping, 1996. Site amplification at fife locations in San Francisco, California: a comparison of S waves, codas and microtremors. Bull. Seism. Soc. Am., 86: 627-635.

Shapira, A., and van Eck, T., 1993. Synthetic uniform hazard site specific response spectrum, Natural Hazard, 8, 201-215.

Shapira, A., and Avirav, V., 1995. PS-SDA Operation Manual, IPRG Report Z1/567/79, p.24.

Shapira, A., Feldman, L., Zaslavsky, Y., and Malitzky, A., 2001. Application of a stochastic method for the development of earthquake damage scenarios: Eilat, Israel test case. The Problems of Lithosphere Dynamics and Seismicity, Computational Seismology, V.32, 58-73.

Shapira, A., and Hofstetter, A., 2002. Seismicity parameters of seismogenic zones. http://www.gii.co.il/

Singh, S. K., Lermo, J., Dominguez, T., Ordaz, M., Espinosa, J. M., Mena, E. and Quaas, R., 1988. A study of amplification of seismic waves in the Valley of Mexico with respect to a hill zone site, Earthquake spectra 4: 653-673.

Storn R., and Price, K., 1995. Differential evolution: A simple and efficient adaptive scheme for global optimization over continuous spaces. Technical Report TR-95-012, International Computer Science Institute, Berkeley.

Su, F., Anderson, J. G., and Zeng, Y., 1998. Study of week and strong ground motion including nonlinearity from the Northridge, California. Earthquake Sequence, Bull. Seism. Soc. Am., 88, 1411-1425.

Teves-Costa, P., and Senos, M.L., 2000. Estimating site effects using microtremor measurements and analytical modeling – application to the Lower Tagus valley, Portugal. Proc. of 12th World Conference on Earthquake Engineering, Auckland, New Zeeland, 2000, No 1250, pp 8.

Toshinawa, T., Taber, J.J., and Berrill, J.B., 1997. Distribution of ground motion intensity inferred from questionnaire survey, earthquake recordings, and microtremor measurements - a case study in Christchurch, New Zealand during 1994 Arthur's Pass earthquake. Bull. Seism. Soc. Am., 87, 356-369.

Trifunac, M. D., and Todoravska, M. I., 1998. Nonlinear site response as a natural passive isolation mechanism – the 1994 Northridge, California, earthquake. Soil Dynamics and Earthquake Engineering 17, 41-51.

Zaslavsky, Y., Gitterman, Y., and Shapira, A., 1995. Site response estimations using week motion measurements. Proceedings of 5th International Conference on Seismic Zonation, Nice, France, October 17-19, 1713-1722.

Zaslavsky, Y., Shapira, A., and Leonov, J., 1998. Site effect estimates and seismic hazard assessment for the Haifa port extension project area, GII Final Report 521/54/98(3).

Zaslavsky, Y., Shapira, A., Leonov, J., and Peled, U., 2000a. Site response and seismic hazard assessment for Nesher Israel Cement Enterprises, Haifa. GII Report No. 548/30/00.

Zaslavsky, Y., Shapira, A., and Arzi, A.A., 2000b. Amplification effects from earthquakes and ambient noise in Dead Sea Rift (Israel). Soil Dynamics and Earthquake Engineering, V. 20/1-4, 187-207.

Zaslavsky, Y., Shapira, A., and Arzi, A. A., 2002. Earthquake site response on hard rock – empirical study. Proceeding of 5 th International Conference on analysis

of Discontinuous Deformation, ICADD, 6-10 October 2002, Beer-Sheva, Israel 133-144.

Zaslavsky, Y., Shapira, A., and Leonov, J., 2003c. Empirical evaluation of site effects by means of H/V spectral ratios at the locations of strong motion accelerometers in Israel. Journal of Earthquake Engineering, Vol. 7, No. 4, 655-677.

Zaslavsky, Y., Shapira, A., Gorstein, M., Aksinenko, T., Kalmanovich, M., Ataev, G., Giller, V., Perelman, N., Livshits, I., Giller, D., and Dan H., 2003d. Local site effect of Hashefela and Hasharon regions based on ambient vibration measurements. GII Progress Report No 569/313/03.

Zaslavsky, Y., Gorstein, M., Kalmanovich, M., Giller, D., Peled, U., 2004a. Experimental study of site effects and local seismic hazard assessment for the Carmel Olefins area. Haifa, GII Report No 547/037/04.

Zaslavsky, Y., Shapira, A., Gorstein, M., Aksinenko, T., Kalmanovich, M., Ataev, G., Giller, V., Perelman, N., Livshits, I., Giller, D., and Dan, H., 2005a. Expected site amplifications in the Coastal Plane of Israel. Proceeding of International Conference of Earthquake Engineering in the 21st Century (EE-21C), Skopje, 27 August-1 September.

Zaslavsky, Y., Ataev, G., Kalmanovich, M., Gorstein, M., Mikenberg,M., Aksinenko, T., Giller, V., Perelman, N., Livshits, I., Giller, D., Dan, H., and Shapira, A., 2005b. Seismic hazard microzonation in Qiryat Shemona, northern Israel, Proceeding of International Conference of Earthquake Engineering in the 21st Century (EE-21C), Skopje, 27 August-1 September.

Zaslavsky, Y., Shapira, A., Gorstein, M., Kolmanovich, M., Giller, V., Perelman, N., Livshits, I., Giller D., and Dan, I., 2005c. Site response from ambient vibrations in the towns Lod and Ramle (Israel) and earthquake hazard assessment, Bull. Earthq. Engin., Volume 3 No. 3.

יזרסקי, מ., 2003. סקר רפרקציה סייסמית בתחנת כוח, חיפה. דו״ח מג״י 319/298/03. הוכן עבור חברת החשמל.

יזרסקי מ., 2004. סקר רפרקציה סייסמית בעמק הזבולון, אזור קרית מוצקין. דו״ח מג״י 221/097/04. הוכן עבור ועדת ההיגוי להיערכות לטיפול ברעידות אדמה (משרד השיכון)

מדבדייב ב., 2005. איתור העתקים חשודים כפעילים בעמק זבולון. דו״ח מג״י 351/081/04.

זסלבסקי, י., שפירא, א., פלד, א., 1997. הערכת ספקטרום תאוצות במחלף צ׳ק פוסט, דו״ח מס׳ 579/144/96.

זסלבסקי, י., גורשטיין, .מ., פלד, א., קלמנוביץ׳, מ., 2003a. קביעה ניסיונית של תגובת האתר והערכת סיכוני רעידות אדמה בדרך הקישון (חיפה). דו״ח מג״י מס׳ 513/287/2003.

זסלבסקי, י., פלד, א., קלמנוביץ׳, מ., אטייב, ג., 2003b. קביעה ניסיונית של תגובת אתר והערכת סיכוני רעידות אדמה באתר תחנת הכוח – חיפה. דו״ח מג״י מס׳ 527/292/2003.

זסלבסקי, י., קלמנוביץ׳, מ., פרלמן, נ., גורשטיין, מ., גילר, ד., אטייב, ג., דן, א., גילר ו., ליבשיץ, י., שווצבורג, א., 2004b. הערכה נקודתית של סיכוני רעידת אדמה בארבעה אתרי גשרים. דו״ח מג״י מס׳ 552/058/2004.